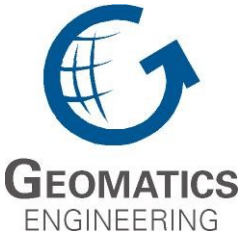

UCGE Reports
Number 20315

Department of Geomatics Engineering

Practical Consideration of Temporal Correlation in RTK GPS Surveying using a Modified Kalman Filter

(URL: http://www.geomatics.ucalgary.ca/graduatetheses)

by

Charles Miller

September 2010

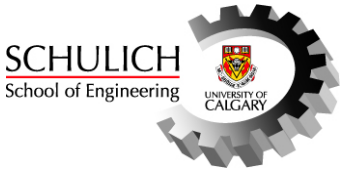

UNIVERSITY OF CALGARY

Practical Consideration of Temporal Correlation in RTK GPS Surveying using a Modified Kalman Filter

by

Charles Miller

A THESIS

SUBMITTED TO THE FACULTY OF GRADUATE STUDIES

IN PARTIAL FULFILMENT OF THE REQUIREMENTS FOR THE

DEGREE OF MASTER OF SCIENCE

DEPARTMENT OF GEOMATICS ENGINEERING

CALGARY, ALBERTA

SEPTEMBER, 2010

Abstract

Many manufacturers of Real-Time Kinematic (RTK) Global Positioning System (GPS) positioning software ignore the temporal correlations found in GPS measurement errors. To understand the statistical value of GPS positions, temporal correlations must be accounted for. A time-differencing Kalman filter is implemented which uses time-differencing to account for temporally correlated errors.

A 3-dimensional survey network was formed on the University of Calgary campus using traditional survey methods. The adjusted network was surveyed repeatedly using commercial RTK equipment using baselines up to 10km. Positions were processed using both commercial RTK software and the modified Kalman filter.

Error ellipses (95% probability) are formed and analyzed in the local coordinate system. When temporal correlation is ignored, far more than 5% of the results produce error ellipses that do not contain the true coordinates. Using the time-differencing modified Kalman filter, the resulting 95% probability error ellipses included the truth position approximately 95 percent of the time without becoming over-pessimistic.

Preface

This is an unaltered version of the author's Master of Science thesis. The thesis was accepted by the Faculty of Graduate Studies in September, 2010. The faculty supervisor for this work was Dr. Kyle O'Keefe. The co-supervisor was Dr. Yang Gao. Other members of the examining committee were Dr. Mark Petovello, Dr. William Teskey, and Dr. John Nielson.

Acknowledgements

This research would not have been possible without the generous encouragements and contributions of others over the past few years.

First I would like to express gratitude to my supervisor Dr. Kyle O'Keefe, for giving me the opportunity to come to Canada and further my education, and trusting that my abilities and motivations were enough to get the job done. He mentored and guided me in the right direction regarding this research and life. Special thanks to both him and my co-supervisor, Dr. Yang Gao, for granting me sufficient funds to be able to focus on my research.

This work would have been dramatically more difficult without the contributions of Dr. Glenn MacGougan and Dr. Mark Petovello. Dr. MacGougan, in addition to being a great friend, provided fully functional C++ GPS positioning software in which the modified Kalman filter was implemented. Dr. Mark Petovello, in addition to work performed Dr. O'Keefe, was the researcher responsible for the original derivation of the modified Kalman filter used in the work.

I would like to thank my parents for always setting high expectations for me, and instilling an understanding in me regarding the value of an education. None of this work would have occured without them.

Above all, I would like to thank my wife Alyssa, for constantly encouraging me during difficult times, giving me the confidence required to get it done, and for sacrificing everything to follow me up to a new place, to start a new life.

Contents

List of Figures

List of Tables

Notation

α	Scale Factor for the VCV Matrix
χ	Time-Correlated Design Matrix from Previous Epoch
λ	Signal Wavelength
∇	Between Satellite Difference Operator
$\bar{x}$	Mean Value of Variable x
Φ	Carrier Phase Observable
ϕ	Transition Matrix
σ	Standard Deviation (1-Sigma)
τ	Time Lag
$\triangle$	Between Receiver Difference Operator
ε	Nominal GPS Errors
Q_x	Cofactor Matrix
R_{xx}	Correlation Coefficient (Calculated)
A	Design Matrix
ADR	Accumlated Doppler Range
C	Correlation Matrix
c	Speed of Light
CI	Confidence Interval
DGPS	Differential Global Positioning System

DOP Dilution of Precision

dT Elapsed Time

dT Satellite Clock Bias

dt Receiver Clock Bias

ECEF Earth Centered Earth Fixed

EDM Electronic Distance Measurement

ENU East, North, Up

EPE Estimated Position Error

f Correlation Coefficient (Estimated)

GDOP Geometric Dilution of Precision

GNSS Global Navigation Satellite System

GPS Global Positioning System

H Design Matrix for Time-Differenced Observations

HDOP Horizontal Dilution of Precision

I Ionospheric Error

ICF Incorrect Fix

INS Inertial Navigation System

K Kalman Gain Matrix

l Observation Vector

M Variance-Covariance Matrix for Correlated Errors

MKF Modified Kalman Filter

MN Measurement Noise

N Integer Ambiguities

N Number of Samples

N Variance-Covariance Matrix for Random Errors

n Random Error Vector

P Observed Pseudorange

P Variance-Covariance Matrix describing Estimated States

p Geometric Range

PCF Probability of Correct Fix

PDOP Position Dilution of Precision

PN Process Noise

ppm Parts per million

PRN Pseudo-Random

Q Process Noise Variance-Covariance Matrix

R Measurement Noise Variance-Covariance Matrix

RINEX Receiver Independent Exchange

RMS Root Mean Square

RSS Root Sum Square

RTK Real Time Kinematic

S Transition Matrix for the Time Correlated Errors

SOS Sum of Squares

T Temporal Correlation used to Estimate Correlation Coefficient

TEC Total Electron Content

u Time-Correlated Error Vector

URE User Range Error

v Measurement Noise Vector

VCV Variance Co-Variance

VDOP Vertical Dilution of Precision

w Process Noise Vector

WGS World Geodetic System

x State Vector

z Measurement Vector

Chapter 1

Introduction

1.1 Motivation

One of the most accurate forms of Global Positioning System (GPS) positioning is real-time kinematic (RTK), utilized by land surveyors and others on a daily basis around the world. Most manufacturers of RTK systems proclaim an accuracy of 2 centimetres. The GPS measurements that receivers use to establish a position are riddled with a number of complex errors. These include ionospheric error, tropospheric error, multipath, orbital errors, clock errors, antenna phase center errors, and receiver noise. To realistically estimate the accuracy of a GPS position, the characteristics of these errors, including their variance and any correlations that they might contain, must be modeled.

According to Merriam Webster's On-line Dictionary (2009), correlation means that "two mathematical or statistical variables which tend to vary are associated in a way not ex-

pected to occur by chance alone." Various types of correlation occur in GPS positioning, including spatial correlations, mathematical correlations, and temporal correlations. In GPS positioning, spatially correlated errors occur when the magnitude of a specific error is similar at two different locations. By differencing observations collected by two simultaneously operating receivers, any spatially correlated errors are eliminated leaving only the small difference between the observations to affect the estimated position. This technique, known as double differencing, is extremely common and is important for the high-accuracy positioning required by land surveying and other applications (see Van Sickle, 2001; Leick, 2004). Mathematical correlation, expained in detail in Section 2.1.2.4, is the result of two observables becoming correlated through the differencing of the same reference satellite measurement. Mathematical correlation is accounted for in the measurement variance-covariance (VCV) matrix (VCV matrices are described in Section 2.1.0.1). As important as it is to recognize both spatial and mathematical correlations during the estimation process, it is equally important to recognize the temporal correlations found within the observation errors.

Temporally correlated errors occur when the magnitude of an error is similar over time. The errors within GPS observations are not purely random (white) with time. Coloured noise is very apparent in the carrier phase and code residuals (see Olynik, 2002; Raziq and Collier, 2006; El-Rabbany, 1994). A key assumption in the least squares and Kalman filtering is that each measurement is completely independent from the others, and if they are not independent, any error correlation must be accounted for (Ghilani and Wolf, 2006; Brown and Hwang, 1997)). Treating correlated measurements as independent results in an over-optimistic VCV matrix of the estimated states, which may result in an over optimistic probability of correct fix (PCF) when fixing the ambiguities to their integer values. Unlike spatial and mathematical correlations, temporal correlations are not dealt with properly in most of today's RTK software. By ignoring temporal correlations, the estimated accu-

racy of the position solutions proclaimed by many of the manufacturers are likely over-optimistic.

Simply told, the motivation of this research is to determine two things. First, it is to determine the accuracy of modern single-baseline RTK hardware and software that is trusted and used throughout the current surveying industry. Many of today's surveyors place a great deal of trust in the advertised accuracy of their RTK systems and an up-to-date analysis needs to be made on the modern equipment to determine whether or not the stochastic models used in the software realistically reflect the errors and correlations found within the observations. Second, it is to determine how the consideration of temporal correlation within the stochastic model influences the VCV matrix of the estimated positions, and whether or not it is critical that temporal correlation be included in the stochastic model to receive a realistic estimate of the accuracy of a position.

1.2 Methodology

The first task was to determine the accuracy of modern RTK GPS, and if estimated accuracy found in the VCV matrix reflects the true accuracy. A high precision network of points was formed for comparing the RTK estimated coordinates to known network coordinates. The survey network was surveyed repeatedly with RTK GPS, using survey procedures common within the industry. Baselines lengths were limited to 10 km. The accuracy of modern RTK GPS was analyzed relative to baseline length, various dilution of precision values (DOP), number of satellites, etc. GPS observations we made over a period of weeks at various times of day. By comparing the estimated accuracy to the absolute position error, conclusions could be made regarding whether or not the VCV matrix of the estimated states was over optimistic or pessimistic.

The second task was to determine how temporally correlated errors influence the magnitude of the VCV matrix of the estimated states, and whether or not modeling the temporal correlation provides a more realistic accuracy estimate. Since, to the author's knowledge, commercial software does not attempt to model temporal correlation, new software was written. This software implemented previously published equations that accounts for the temporal correlation within a Kalman filter (Petovello et al., 2009). These equations will be discussed in great detail in Chapter 3. Using raw data that was collected during the RTK surveys, positions were post-processed using the new software. These positions and their estimated accuracy were again compared to the network coordinates to determine whether the filter is an improvement over the current commercial software.

1.3 Thesis Outline

Chapter 2 introduces the theory and mathematical models used in GPS positioning, and describes its error sources. Previously published research related to the accuracy of single-baseline RTK is shared along with any relevant published studies on dealing with temporal correlation found within GPS measurements.

In Chapter 3, previously published equations (Petovello et al., 2009) for dealing with temporal correlation through a time differencing Kalman filter are shared. The issues encountered during filter tuning and the effect of each stochastic parameter on the positioning results are discussed, along with the difficulties of utilizing actual GPS data and the modifications to the equations that had to be made to allow for changes in the visible satellite constellation.

Chapter 4 describes the process used to determine how long the L1 carrier phase signal remains temporally correlated. Potential factors that could influence the length of temporal

correlation are considered such as receiver multipath environment, satellite elevation angle, and baseline length.

Chapter 5 describes the creation of a survey testing network used to determine whether or not RTK GPS is repeatable when the temporal correlation is considered or ignored.

Chapter 6 discusses the results. First, the results from the survey using commercial RTK software and equipment are analyzed. The accuracy and precision of the resulting positions are compared to various influencing factors such as receiver environment, baseline length, number of satellites, and DOP values. Results from the time-differencing Kalman filter are then analyzed in the same way.

Chapter 7 shares the conclusions that can be made from the results and any future work that can be completed to further advance this research topic.

1.4 Summary of Contributions

Over the course of this research, the following contributions have been made:

- This is the first application of a previously published (Petovello et al., 2009) time-differencing Kalman filter using real carrier phase data.
- In order to use real data within the filter, a method had to be created which would allow for changes in the visible satellite constellation or cycle slips, which are common in real world data collection.
- An independent assessment was made to determine how long the L1 carrier phase signal remains correlated considering a variety of environmental variables.

- An assessment is made on the practicality of using the time-differencing Kalman filter in survey applications.
- An independent analysis was made of the repeatability of RTK GPS using modern, state-of-the-art, GPS equipment using procedures typical of every day surveyors in typical survey site conditions, over baselines considered acceptable by the surveying community.
- The results presented in this thesis have been submitted for publication in the ASCE's Journal of Surveying Engineering and accepted for presentation at ION GNSS 2010.

Chapter 2

Background Information

2.1 GPS Theory and Observed Errors

In today's world, land surveyors rely on GPS technology everyday for precise relative positioning. GPS positioning functions using a very simple principle. Satellites, which have known positions, orbit the earth while broadcasting signals which the user can use to calculate their distance (range) from each individual satellite. With as few as 4 ranges, the user can trilaterate their position anywhere on the earth's surface. Using more than 4 satellites provides a good chance at obtaining a higher accuracy due to greater redundancy in the observations.

The GPS satellite constellation is made up of 32 satellites orbiting above the earth at an altitude of approximately 20,200 km. The satellites, distributed within 6 orbital planes around the earth, provide positioning capabilities 24 hours per day (Hofmann-Wellenhof et al., 2001). Each satellite broadcasts a variety of signals, depending on era that the satellite was launched. Block II/IIA/IIR satellites (U.S. Naval Observatory, 2010), launched between the

years 1989 and 2004, each broadcast at L1 (1575.42 MHz) and L2 (1227.6 MHz) frequencies (Leick, 2004) and a navigation message which contains the position of each satellite as a function of time, as well as the health of each satellite. The L1 frequency is modulated with a C/A code (coarse acquisition) as well as a P-Code (P = precise). The L2 signal is modulated only by the P-Code. The launches of Block IIR-M satellites began in 2005 and continues today. Launching of Block II-F satellites began in 2010 and Block III satellites are scheduled to begin launch in 2014, both of which include enhancements over previous satellite generations. In addition to all of the above signals, Block IIR-M satellites will broadcast an additional civil signal on the L2 frequency (L2C), and the newest satellites will also broadcast a civil signal on a new L5 signal (1176.45 MHz)(U.S. Naval Observatory, 2010; Kowoma, 2009). Contained within these broadcasted signals are 2 observables that are very useful for positioning.

The pseudorange observable is simply the range from the receiver to the satellite. The pseudorange is calculated from the signal travel time, requiring that both the time of the signal's departure and arrival be known. To determine the signal travel time, the satellites and the receiver simultaneously generate identical lines of pseudorandom (PRN) code. When the code from the satellite reaches the receiver, the receiver searches for a correlated match in its own PRN code to determine the length of elapsed time (Leick, 2004). This elapsed time is biased due to a mis-synchronization between the satellite and receiver clocks. Since the pseudorange is determined by multiplying the signals travel time by the speed of light, a time bias would result in extremely large errors unless dealt with properly. The clock bias must be accounted for in the mathematical model, and either estimated, or eliminated through measurement differencing. The observed pseudorange can be modeled as follows:

$$P = p + c(dT - dt) + I + T + \varepsilon_P \tag{2.1}$$

In Equation 2.1, P represents the pseudorange as observed by the receiver, p represents the desired geometric distance between the satellite and the receiver, c is the speed of light, dT and dt are the biases of the satellite and receiver clocks from GPS time, I and T represent the ionospheric and tropospheric errors to be described later, and ε_P represents other nominal errors which effect the pseudorange observable. These nominal errors include ephemeris errors, orbital errors, multipath, and system noise. Depending on the atmospheric conditions as the time of observation, the accuracy of the pseudorange measurements is about a metre (Hofmann-Wellenhof et al., 2001). The pseudorange observable is limited by the width of cycles generated in the PRN code. Even if the satellite and receiver generated PRN code is lined up precisely to determine the travel time of the signal, the bits of code that are lined up are so wide that a precise measurement is not possible. At the speed of light, a bit of code that has a cycle width of nearly a microsecond results in a large error.

With the limited accuracy of the pseudorange, high precision GPS surveying is greatly enhanced by use of the carrier phase observable, the number of fractional cycles of the carrier frequency. The carrier frequencies, L1 and L2, have wavelengths approximately 19.05 cm and 24.45 cm (Kowoma, 2009). When turned on, survey quality receivers measure the fractional beat phase the incoming phase signal. As long as the signal is continuously tracked, and lock is not lost through a cycle slip, the receiver sums up the incoming fractional cycles. The difficulty of using carrier phase measurements is that the receiver can only measure the change in the satellite range from the moment the satellite is first tracked. The number of complete cycles during the first epoch is an ambiguous term and must be solved for through an ambiguity resolution. If the receiver can correctly resolve how many complete cycles there were between the satellite and the receiver on that first epoch, the positioning solution will then benefit from a measurement that is accurate to a few millimetres (Hofmann-Wellenhof et al., 2001). The carrier phase observable can be modeled as follows:

$$\Phi = p + c(dT - dt) - I + T + N\lambda + e_\Phi \tag{2.2}$$

In Equation 2.2, Φ represents the carrier phase observable, N is the ambiguity term, λ is the signal wavelength, and ε_Φ represents other nominal errors which effect the carrier phase observable. These nominal errors, like the pseudorange observable, include ephemeris errors, orbital errors, multipath, and system noise. Carrier phase noise is drastically smaller than the noise found within pseudorange observable. All of the other variables are identical to those found within Equation 2.1. The carrier phase observable, like the pseudorange observable, is affected by atmospheric errors, clock errors, and other nominal errors. The key to using carrier phase measurements is to reduce the magnitude of these errors so that the ambiguities can be resolved to their correct integer values. The most common way of accomplishing this is through differencing the observables, see Section 2.1.2.

2.1.0.1 Stochastic Modeling of GPS Observations

GPS observations are riddled with complex errors that are impossible to meticulously model. The remaining errors, those that cannot be modeled deterministically, must be modeled stochastically. A stochastic model strives to model a random process in terms of the probability of where a process might lead. The stochastic process is modeled using the VCV matrix of the observations. Within the VCV matrix, the values along the diagonal describe the variance of the observations, or the distribution of the observations from their mean value. The off diagonal elements of the VCV matrix describe the correlation between the observations. Typically, GPS software simplifies the potentially complex stochastic model by assuming zero correlation between the observations and assuming that all observations have the same variance. By oversimplifying the stochastic model, the resulting VCV matrix of the estimated states fails to realistically describe the true statistical

value of estimated parameters. For more information regarding stochastic modeling of GPS observations, see Barnes et al. (1998).

Two VCV matrices of particular interest to this research are the measurement VCV matrix and the state VCV matrix. The measurement VCV matrix describes the statistical value of the observables used to establish the position. In the measurement VCV matrix, any correlations (see 2.1.2.4) should to be accounted for. The state VCV matrix describes the statistical quality of the estimated parameters, or in the case of GPS, the estimated position. If the measurement VCV matrix approximates the observed errors to be smaller than they actually are, the likely result will be a state VCV matrix that is over-optimistic, that provides an estimated positional accuracy that is better than it truely is. If correlations are ignored in the measurement VCV matrix, the state VCV matrix will be over-optimistic.

2.1.0.2 Ambiguity Resolution

An important aspect to consider when analyzing the repeatability of GPS is the resolution of the ambiguities to their integer values. During the estimation process, the ambiguities are estimated as real numbers, often called float ambiguities. In order to realize the centimetre-level accuracy that relative carrier phase positioning is capable of, the integer number of cycles has to be determined (resolved) from the float ambiguities. This is possible through a variety of methods including rounding, bootstrapping, and integer least squares (Teunissen and Kleusberg, 1998). The longer a satellite is tracked before resolving the ambiguity, the greater the possibility that it will be resolved correctly. This is explained very clearly within Misra and Enge (2001). One of the most popular and efficient methods is least squares ambiguity decorrelation adjustment (LAMBDA), see Teunissen (1994). Once a set of integer ambiguities are selected, they must be validated in a series of tests to ensure correctness. The two validation tests used within this research is the ratio test and the

probability of correct fix (PCF) (O'Keefe et al., 2006). In the ratio test, the ratio between the two lowest sum-of-squared residuals (SOS) (Lachapelle, 2008), or the difference between the estimated float ambiguities and selected integer set, are compared to a user selected threshold value. The ratio of the smallest set of SOS residuals to the second smallest set is determined, and if it meets the threshold value then the ambiguities are fixed using those in the smallest set. Based on a lack of proven methods to select the threshold value, and an incorrect assumption used in the derivation of the ration test, some question the effectiveness of the ratio test (see Teunissen and Verhagen (2004). The PCF uses the float ambiguity VCV matrix to determine the amount of confidence that can be had when fixing ambiguities at a certain epoch. This value is of particular interest to this study because by accounting for the temporal correlation, the VCV matrix theoretically becomes larger, directly affecting the PCF (O'Keefe et al., 2006).

2.1.1 Observed Errors in GPS Positioning

GPS is affected by a variety of errors which are well explained in a variety of textbooks, see(Hofmann-Wellenhof et al., 2001; Leick, 2004; Misra and Enge, 2001; Van Sickle, 2001), the following are most relevant to this research:

2.1.1.1 Multipath Error

In surveying applications, where many error sources are mitigated through observation differencing, multipath error is one of the most significant sources of temporal correlation. Multipath error is caused by signals being reflected off surfaces near the receiver. A variety of surfaces can cause reflections including trees, buildings, windows, cars, etc. Since reflective signals always travel further than direct signals, this causes an error in the positioning

solution which is modeled for signal traveling directly from the satellite to the receiver. Every location has multipath characteristics that are unique. This uniqueness to receiver environment means that multipath is not spatially correlated and cannot be reduced through differencing observables. Satellites at lower elevation angles are more prone to multipath, leading to an error magnitude that varies with time as satellites move across the sky. This is an issue in RTK surveying where a point is occupied only briefly (after ambiguities are fixed) and data obtained over a period of a few seconds or less is used to establish a position. Multipath error is less of an issue in static GPS surveying, where observations are made over periods of 15 minutes or more and any multipath is averaged out. Multipath has a considerably larger effect on the pseudorange observable than it does on the carrier phase observable (Iyiade, 2005). Multipath error is typically around 1 cm in the carrier phase observable and 1 m in the pseudorange (Misra and Enge, 2001).

2.1.1.2 Ionospheric Error

With GPS satellites orbiting at an altitude of approximately 20,200km, their electromagnetic signals must first travel through the ionosphere, located at an altitude of approximately 50 to 1000 km above the earth's surface. This region is defined by an abundance of free electrons, ions, and various molecules. These free electrons are formed by the sun's energy interacting with the neutral molecules of the earth's atmosphere. As the signals travel through the ionosphere, the pseudorange observable is delayed while the carrier phase observable is advanced by the same amount (Parkinson and Spilker, 1996), as modeled in Equations 2.1 and 2.2. Low elevation satellites experience larger errors as their signals must travel further through the ionosphere layer. The effect the ionosphere has on a signal depends on the total electron content (TEC), the number of free electrons located along the signal path within a 1 m column. The distribution of free electrons across the ionosphere is

not even. The TEC is higher in equatorial regions due to the sun's stronger influence. Under normal conditions, the TEC reaches a peak around 1400 local time and then falls to a minimum before sunrise as free electrons and ions recombine (Langley, 2000). Every eleven years or so, the ionosphere becomes very active as the sun reaches a solar maximum, resulting in an increased number of ionospheric storms (Kunches, 2007; Langley, 2000). While the previously discussed ionospheric effects are well mitigated through differencing and do not dramatically hinder the precise relative positioning performed by surveyors using short baselines, differential carrier phase positioning becomes very difficult during severe storms. Scintillations, or small irregularities within the ionosphere, cause rapid phase variations and shifts in signal amplitude. This makes the signal tracking very difficult, resulting in a large number of cycle slips (Datta-Barua et al., 2003). Horizontal gradients have major impacts on relative positioning as the ionospheric error decorrelates over short distances rendering differencing techniques ineffective (Skone and Shrestha, 2002).

For a satellite located at zenith, the ionospheric delay is typically between several metres (nighttime) to tens of metres (daytime) (Misra and Enge, 2001; Monteiro et al., 2005). This delay varies widely as the ionosphere goes through its daily, seasonal, and eleven year cycles. The ionosphere spatially decorrelates at a rate of approximately 2 cm per 10 km baseline (Misra and Enge, 2001). When horizontal gradients are present in the survey area, the rate is significantly larger. For the precise positioning that surveyors require, it is generally best to keep baselines as short as possible (~10 km) (Roberts, 2005) to keep the error to a minimum. Unless extremely active, the ionospheric error remains temporally correlated for about an hour(El-Rabbany, 1994; Raziq and Collier, 2006).

2.1.1.3 Tropospheric Error

The troposphere, the gaseous region below 50 km in altitude, is another significant source of error in GPS positioning. As GPS signals travel through the lower atmosphere, they are bent and delayed as different indices of refraction are encountered. Tropospheric delay, also known as tropospheric refraction, is a function of atmospheric pressure, temperature, water pressure, etc. It is a nondispersive medium which means that it cannot be eliminated through signal combinations. To mitigate tropospheric delay, a variety of models have been developed to estimate its magnitude based on these and other atmospheric parameters (Mekik, 1997). The error can be divided into two parts, hydrostatic delay and wet delay. The hydrostatic component contributes 90% of the total tropospheric error and can be accurately estimated using empirical models or surface measurements (Hofmann-Wellenhof et al., 2001). The wet component accounts for the other 10% of the error and is far more difficult to model due to the constantly shifting distribution of water vapour in the lower atmosphere. Tropospheric delay is a function of satellite elevation angle and gets substantially larger as the elevation angle decreases.

For a satellite located at zenith, the total tropospheric delay is typically around 2.5 m (Misra and Enge, 2001). Under normal conditions, the troposphere is correlated over short baselines, meaning that the error can often be successfully mitigated through observation differencing. Lawrence et al. (2006) shows an example of the troposphere decorrelating 3 cm over a baseline lengths of only a few kilometres, but this only occurs in periods of severe weather activity. On average, the tropospheric error decorrelates at a rate of 1 cm per 10 km baseline (Monteiro et al., 2005). With exception of the unpredictable water vapour in the lower troposphere, the atmospheric parameters in the upper troposphere change slowly, resulting in the tropospheric error being temporally correlated for several hours (Monteiro et al., 2005; Raziq and Collier, 2006).

2.1.1.4 Cycle Slips

Cycle slips are caused by the receiver losing lock on the satellite signals for a brief moment or more. This can happen for a variety of reasons including scintillations in the ionosphere, low elevation satellites with low signal-to-noise ratios, or obstructions in sky visibility such as a tree canopy. A cycle slip is simply a change in the number of complete cycles within the ambiguity. When a cycle slip occurs, the ambiguity is reset to a new value and ambiguity resolution must be repeated, making precise relative positioning very difficult when slips occur often. Cycle slips can be detected using Doppler measurements or by processing the data first using the triple differencing method (Leick, 2004).

2.1.1.5 Other Issues Specific to RTK Surveying

RTK GPS surveying, the technique used within this research, is performed as follows. Two receivers are used, a reference receiver and a roving receiver, both connected by radio link. The reference receiver remains stationary over a point, while the roving receiver observes any point in which the coordinates are desired. The observations made by the two different receivers are differenced (see Section 2.1.2) and the positional correction is broadcast over the radio link. In real time, the surveyor can determine the coordinates of the roving receiver, relative to the location of the reference receiver. For details, see Langley (1998).

In RTK GPS positioning, there is not one receiver collecting data, but two. The reference (base) receiver location is just as important, if not more important than the roving receiver position. If the base receiver is located in an area prone to multipath and cycle slips, then any position established by the roving receiver will be subject to those issues as well, for the duration of the survey. Another important consideration in RTK surveying is that shorter

baselines generally result in higher precision. Shorter baselines result in spatially correlated errors, errors common between receivers, being eliminated through differencing (see Section 2.1.2). When baselines are lengthened, surveyors also risk losing the radio connection linking the base and roving receivers which would halt the survey altogether. For more information regarding the importance of base receiver location, see Roberts (2005).

When GPS positions are first obtained, they are in an Earth-Centered, Earth-Fixed (ECEF) geodetic reference system, the World Geodetic System of 1984 (WGS 84). Surveyors often work within a local tangent plane coordinate system where the earth is assumed to be flat and the datum references a local point, assigned arbitrary coordinates. In order to utilize GPS positions, the WGS 84 positions must be transformed into the local coordinate system. The Helmert Transformation, a seven parameter transformation (3 translations, 3 rotations, 1 scale factor) is often used for this task, described in Section D.0.4. To perform a localization using the Helmert Transformation, GPS observations are first made on a minimum of 3 points (Trimble recommends 4 points for additional redundancy, see Trimble Navigation Limited (2001)) of which the coordinates in the local system are already known. With coordinates for the 3 (or 4) points being known in both the local and WGS 84 coordinate systems, the 7 transformation parameters can be estimated. With transformation parameters known, additional points can be surveyed using GPS and their WGS 84 coordinates rotated into the local system. The issue is that if any of the points used in the localization has bad local coordinates (often determined by traditional survey methods), or bad WGS 84 coordinates due to GPS errors, the estimated transformation parameters will be incorrect and any RTK surveying performed using the localization will be affected. To avoid problems during localization, the localization points should be in areas free of multipath and observed for as long as possible. For more on localizations and the seven parameter transformation, see Iliffe and Lott (2008) and Ghilani and Wolf (2006).

When using RTK GPS, it is important to consider that each position consists of only a single set of GPS observations (Featherstone and Stewart, 2001). In traditional surveying, side shots, points observed with only one distance and direction, are undesirable due to the inability to detect errors. It is only possible to detect errors when redundant observations are made. When only one location is used for the reference receiver during a project, RTK GPS also has very poor geometry, a radial pattern of individual rover observations originating from a single base receiver location. Using traditional survey methods, when high accuracies are required in a project, points will be observed from multiple baselines, enabling blunder detection and better geometry. When high accuracies are required using RTK, surveyors should follow the same cautionary methods used in traditional surveying. Points could be re-observed at different times using a different location for the base station. The British Columbia Guidelines for RTK Surveys (2008) suggests that unobserved baselines be observed with traditional methods to verify the validity of the RTK positions. A second base station could also collect raw data for processing of additional baselines post-mission (although there must be enough data to resolve the integer ambiguities). See also Wylde and Featherstone (1995).

2.1.2 Differencing Techniques

Differencing techniques were developed while selective availability (SA) was turned on (Georgiadou and Doucet, 1990). In an effort to increase national defence, the United States artificially degraded the civilian signal by artificially altering the satellite clocks. By operating two receivers, one over a known position, many of the errors found in the GPS observables, including SA, can be reduced or eliminated. A drawback with differencing is that the noise increases as the number of implemented differences increases (see Section 2.1.2.4). The reduction of error sources must justify the increase in additional noise.

2.1.2.1 Single Difference

The single difference is the differencing of observations between either two satellites, or two receivers. The between-receiver single difference is performed as follows for the carrier phase observable:

$$\triangle\Phi_{12}^{A} = \Phi_{1}^{A} - \Phi_{2}^{A} \tag{2.3}$$

$$\triangle\Phi_{12}^{A} = (p_{1}^{A} + cdT^{A} - cdt_{1} - I_{1}^{A} + T_{1}^{A} + \lambda N_{1} + e) - (p_{2}^{A} + cdT^{A} - cdt_{2} - I_{2}^{A} + T_{2}^{A} + \lambda N_{2}^{A} + e) \tag{2.4}$$

$$\triangle\Phi_{12}^{A} = \triangle p_{12}^{A} - c\triangle dt_{12} + \lambda\triangle N_{12}^{A} + e \tag{2.5}$$

In Equations 2.3, 2.4, and 2.5, $\triangle$ represents the between-receiver difference of the variable, *A* represents satellite A, and *1* and *2* indicate observations from separate receivers. When two receivers are collecting data at the same time, each receiver is observing the same satellite clock bias. When the measurements are differenced between the receivers, the satellite clock bias is eliminated. Another important aspect of between-receiver differencing to surveyors is the reduction of the atmospheric errors, the tropospheric error and the ionospheric error. Atmospheric errors are spatially dependent and in normal atmospheric conditions have a similar magnitude over short distances. If the distance between the two receivers stays relatively short, the errors will be effectively reduced through differencing and have little effect on the estimated positioning.

2.1.2.2 Double Difference

A double difference,the most common form of differencing used by surveyors, is performed by differencing observations made between-receivers as well as between-satellites. The phase observable double difference is performed as follows:

$$\nabla\triangle\Phi_{12}^{AB} = (\Phi_1^A - \Phi_2^A) - (\Phi_1^B - \Phi_2^B) \tag{2.6}$$

$$\triangle\Phi_{12}^{A} = \nabla\triangle p_{12}^{AB} - \lambda\triangle N_{12}^{AB} + e \tag{2.7}$$

In the Equations 2.6 and 2.7, ∇ represents the between-satellite difference of the observable, and B indicates the observation is from satellite B. When using double differencing, the receiver clock errors are canceled out, leaving the geometric ranges and the ambiguities as the only estimated parameters. Nominal errors, e, remain in the observable as these are errors that are independent to each satellite or receiver and cannot be effectively reduced through differencing.

2.1.2.3 Triple Difference

Triple differencing is when the double difference observable, $\nabla\triangle\Phi_{12}^{AB}$, is further differenced across two epochs. By triple differencing, the ambiguity is effectively canceled as it does not change as long as the satellite tracking is continuous. Over short distances, triple differencing is less desirable than double differencing as the measurement noise is increased (see Section 2.1.2.4). Generally, if the ambiguities in the double difference observable can be resolved, then double differencing is a better choice. Triple differencing is often used for cycle slip detection as a cycle slip will cause an outlier in the position solution Leick (2004).

2.1.2.4 Mathematical Correlation and Noise

Depending on the type of differencing performed, the observations become mathematically correlated as a result of the law of covariance propagation, shown in Equation 2.8 (Gao, 2008):

$$C_{D\Phi} = \left(\frac{\delta f}{\delta \Phi}\right) C_{\Phi} \left(\frac{\delta f}{\delta \Phi}\right)^{T} \tag{2.8}$$

where C_{Φ} is the initial VCV matrix containing the stochastic information for the carrier phase observations, $\left(\frac{\delta f}{\delta \Phi}\right)$ is the operator used for differencing satellites, and $C_{D\Phi}$ is the resulting VCV matrix, containing the stochastic information for the differenced carrier phase observations. Depending on which satellite is chosen to be differenced, the differencing operator can be formed in many ways. One example, where the first of 4 observed satellites is selected as the base satellite, is shown in Equation 2.9.

$$\left(\frac{\delta f}{\delta \Phi}\right) = \begin{bmatrix} -1 & 1 & 0 & 0 \\ -1 & 0 & 1 & 0 \\ -1 & 0 & 0 & 1 \end{bmatrix} \tag{2.9}$$

For simplicity purposes, the four satellites in this example are modeled using an indentical variance value, σ_{Φ}^2, as shown in Equation 2.10.

$$C_{\Phi} = \sigma_{\Phi}^2 \cdot \begin{bmatrix} 1 & 0 & 0 & 0 \\ 0 & 1 & 0 & 0 \\ 0 & 0 & 1 & 0 \\ 0 & 0 & 0 & 1 \end{bmatrix} \tag{2.10}$$

Applying the above example to the law of covariance propagation results in the new stochastic model, $C_{D\Phi}$, shown in Equation 2.11.

$$C_{D\Phi} = \sigma_{\Phi}^2 \cdot \begin{bmatrix} 2 & 1 & 1 \\ 1 & 2 & 1 \\ 1 & 1 & 2 \end{bmatrix} = \begin{bmatrix} -1 & 1 & 0 & 0 \\ -1 & 0 & 1 & 0 \\ -1 & 0 & 0 & 1 \end{bmatrix} \cdot \sigma_{\Phi}^2 \cdot \begin{bmatrix} 1 & 0 & 0 & 0 \\ 0 & 1 & 0 & 0 \\ 0 & 0 & 1 & 0 \\ 0 & 0 & 0 & 1 \end{bmatrix} \begin{bmatrix} -1 & 1 & 0 & 0 \\ -1 & 0 & 1 & 0 \\ -1 & 0 & 0 & 1 \end{bmatrix}^{T} \tag{2.11}$$

By performing double differencing, triple differencing, or single differencing between satellites, the observations become mathematically correlated, as seen by the off-diagonal

elements of $C_{D\Phi}$ containing non-zero values. The mathematical correlation does not model the temporal correlation found in the observations. Simply every differenced observation becomes related to one another by the commonality of using the same base satellite for differencing. Another byproduct of differencing is an increase in measurement noise, as modeled by the larger variances along the diagonal of $C_{D\Phi}$. Generally the noise increases with the number of times the observations are differenced. For more information regarding mathematical correlation, see Cao (2009).

2.2 Literature Review

2.2.1 RTK Repeatability

Some of the most thorough research performed on the subject of RTK repeatability was completed by Boey et al. (1996), El-Mowafy (2000), and Pirti et al. (2009). In Boey et al. (1996), RTK performance is evaluated to see whether or not it is accurate enough to meet the cadastral survey accuracy requirements in Victoria, Australia. After surveying a large parcel using both traditional total station and RTK positioning methods, they found that RTK was incapable of meeting the strict 10 mm + 60 ppm requirement over shorter baselines. The distribution of residuals for the RTK measurements appeared normal, indicating that the errors were random. With a 99 percent confidence level, the positions had a circular error of 26 mm, barely above the cadastral survey requirements of 25 mm. El-Mowafy (2000) surveyed a very accurate network of 18 points, completed using an electronic distance measurement (EDM) device with redundant observations. The network was surveyed twice using RTK, and the positions were compared between each session. Both RTK sessions were repeatable horizontally with an average difference around 1.2 cm. Vertically,

the RTK sessions were less repeatable with an average difference close to 5 cm. The Fishers statistical test was completed and found the RTK measurements to be compatible to the EDM measurements. Pirti et al. (2009) completed a similar test to that of El-Mowafy (2000), but with a larger network of 120 points and using 3 different reference receiver positions. They found that as long as there were enough satellites with good geometry, a good position could be obtained in any location. In good conditions, the horizontal accuracy was 10 mm + 1-2 ppm and the vertical accuracy was 15-20 mm + 2 ppm.

Due to a correlation between the vertical component and the clock state, GPS has never been as accurate at measuring the vertical position component as it is at measuring the horizontal position (see Zhang (1997)). With an interest in determining whether or not RTK is accurate enough to meet the specified requirements of various applications, multiple papers have been written on the subject. Featherstone and Stewart (2001) had three different contractors survey multiple points over a 10 km baseline, each using their individual methods and equipment to generate the vertical positions. Using solutions established using a single epoch of data, they found that the accuracy of the height component is approximately 5 cm at the 95 percent confidence level, but when the baseline length surpasses 5 km, the vertical error increases. These statistics exclude positions obtained when the PDOP exceeded 10. In Saghravani et al. (2009), an automatic level was used to investigate the accuracy of RTK heights over an 11 point network. Depending on the sky visibility, they found the difference between the two methods to vary between 0 and 11 cm. This is verified in Pirti (2007) which seeks to verify whether or not RTK positioning is adequate for construction surveying. Surveying the same network of points from two different reference stations, found some points had an estimated height difference of 11 cm. It is well known that GPS derived height estimates are not as accurate as the horizontal direction.

An important aspect of surveying with RTK GPS, is knowing when it is possible to achieve

the required accuracies. Planning software is available to aid a surveyor in determining when the highest number of satellites is available, along with the best geometry. Lemmon and Gerdan (1999) tested how the number of visible satellites affects the accuracy of the position solution. They found that more satellites did not necessarily result in better accuracy, but did lead to a faster and more reliable ambiguity resolution. They also found that surveying while the satellite geometry was ideal did not necessarily result in a better positional accuracy. This finding is also shown in Lee and Ge (2006) and Featherstone and Stewart (2001). To obtain a low Position DOP (PDOP) value, the satellite geometry must be optimal, meaning that multipath prone low elevation satellites are included in the solution as well. For calculation of PDOP, see Section 6.2.2. Once a position is obtained, it is necessary to know whether or not the estimated (internal) accuracy reflects the absolute (external) accuracy. In this case, internal accuracy refers to the estimated accuracy that is produced within the RTK software. RTK software relies on stochastic models to describe the noise in the observations. These models cannot detect systematic errors which, along with noise, effects the external accuracy. The external accuracy is the absolute (true) positional accuracy within the survey network. Jarroush et al. (2005) shows that the internal accuracy displayed by RTK software isn't always correct. Using static GPS techniques, a 35 point network was created which was then repeatedly surveyed using RTK. Within the data, various unstable conditions were found, reportedly caused by multipath or cycle slips, in which the internal accuracy was significantly different from the external accuracy within the network. For more research performed on internal and external accuracy, see Mekik and Arslanoglu (2009).

Surveyors cannot always choose only the best, most capable environments to survey in. Sometimes, a base receiver must be located over a less than optimal reference point, or a position must be obtained underneath a thick tree canopy or in an urban canyon. It is important to understand whether or not RTK is capable of achieving accurate and repeatable

positions in these environments or if it would be better to resort to traditional survey methods. Bakula et al. (2009) observed a network of points, within a thick deciduous forest, 24 times over a period of 2 days. Out of the 24 groups of observations, only 5 of them had internal precisions that coincided with the external accuracy. High accuracy positioning was possible within this environment, but only after lengthy ambiguity resolutions of up to 80 minutes. Another good example of GPS positioning within a tough environment, although focused on differential GPS (DGPS) which does not utilize carrier phase observations, is presented in Yoshimura and Hasegawa (2003). Four different points were established, 3 of them within a thick forest, each with various amounts of sky obstruction. The points located within the forest had horizontal and vertical errors 4 to 10 times greater than the point out in the open. Serious signal degradation and multipath occurred with decreased the precision of the observations significantly. For more research on positioning in difficult areas, see El-Mowafy (2000); Lee and Ge (2006); Iyiade (2005).

2.2.2 Considering Temporal Correlation in GPS Observations

Several studies have been performed which study the temporal characteristics of the GPS errors. Using a static GPS dataset, a kinematic GPS dataset (marine), and a dataset collected in an airplane, Olynik (2002) analyzed the temporal correlation of individual errors in L1 and L2 code and phase observables. The satellite clock, orbital errors, and ionospheric errors are each analyzed independently, while the tropospheric error, multipath error, and receiver noise are all analyzed together. Using the autocorrelation function, the orbital error is found to be highly correlated (>97%) for periods of up to 50 seconds, and shows signs of correlation (>20%) for up to 30 minutes. The satellite clock error is also temporally correlated, especially the Block II and II A satellites which produce a correlation coefficient greater than 0.97 after 50 seconds. Block II R satellites show a slight

improvement. When ionospheric conditions are normal, the ionospheric error remains 50% correlated after a period of 30 minutes. More active conditions reduce the length of temporal correlation in half. Results are similar for both kinematic and static applications, all of which reveal these GPS errors to be temporally correlated.

Using a zero-baseline, where essentially measurements observed at the exact same location are differenced, Borre and Tiberius (2000) analyzed the temporal correlation of receiver noise. The authors performed a time-series analysis of the L1 and L2 GPS signals and determined that with a 1 Hz data rate, the L2 signal was only correlated for approximately 10 seconds and the L1 signal was not correlated at all. Temporal correlations were only found within the L1 signal when the data rate exceeded about 5 Hz. According to the authors, any temporal correlation is likely the result of the receiver tracking loops or internal software, meaning the results would vary depending on the receiver used.

One of the first papers to recognize the importance of considering the temporal correlations in GPS errors was written by Craymer et al. (1990). Written as GPS was just becoming an option for land surveyors to use in their work, the paper introduces the idea that the VCV matrix should be scaled in order to ensure that the results are not over-optimistic. The scale factor is chosen at the discretion of the surveyor and is based only on their experience and knowledge of GPS. The scale factor chosen by the surveyor must be applied evenly across the entire VCV matrix and must be greater than one indicating the matrices output from the software are always optimistic. For land surveying applications, the importance of properly scaled VCV matrices is seen when forming control networks. If measurements obtained using conventional equipment, with realistic accuracy estimates, are combined with GPS measurements, with overly-optimistic accuracy estimates, the GPS measurements will be weighted more heavily then they should. This would result in a survey network with erroneous coordinates. There are advantages and disadvantages to dealing with temporal

correlations by simply scaling them. The advantage is that the positioning accuracy, if a large enough scale factor is used, will no longer be over-optimistic, a very important aspect for critical-to-life applications. Another advantage is that it is computationally very simple. By scaling the VCV matrix, very little processing power is used and energy is saved. The disadvantage is that the estimated accuracy may still be unrealistic by becoming over-pessimistic. Over-pessimistic results are not used to their full advantage.

One of the most thorough studies to date on GPS temporal correlation was performed by El-Rabbany (1994), see also (El-Rabbany and Kleusberg, 2003, 2004). El-Rabbany used observations from 47 different baselines, up to 100 km in length, to determine how long each of the signals used in GPS positioning were correlated. An exponential function, shown in Equation D.15 was fit to the satellite residuals autocorrelation. For baselines of less than 10km, the best estimate of the temporal correlation time, T, used in the exponential function and described in greater detail in Section 4.2, was 256 seconds. For longer baselines, or for a more generic use of the L1 carrier phase signal across all baselines lengths, 263 seconds was the best estimate.

In addition to determining the correlation time of the GPS signals, El-Rabbany (1994) presents a modified least squares estimation method that estimates the position using fully populated VCV matrices, see D.0.6. On the first epoch of observations, the VCV matrix of the observations is the conventional matrix used in double differencing, containing only the mathematical correlation found in double differences (Equations D.13 and D.14). In additional epochs, the correlation coefficient, calculated using the exponential function in Equation D.15, is used as a scale factor to de-weight the influence of the correlated observations and fill the matrix. With each consecutive epoch, the VCV matrix grows increasingly larger. To simplify the inverse of the growing matrix, a constant is computed, P (Equation D.17), which is used to form the inverted VCV matrix used in least squares estimation. In

order to accommodate the large VCV matrix, the least squares estimation process had to be modified, as shown within Section D.0.6. Over longer observation periods, the VCV matrix would grow to huge proportions, especially in RTK systems which typically uses a 1 Hz data rate. The author showed an interest in static surveying (slow data rates, post-processing) and the proposed method appears to be designed to accommodate the needs of that specific positioning application.

A simpler method of obtaining results similar to those developed by El-Rabbany (1994) is presented by Han and Rizos (1995). A scale factor, shown in Equation 2.12, is computed for the VCV matrix of the estimated parameters.

$$\alpha = \frac{n(1+f)}{n(1-f)+2f} \tag{2.12}$$

The scale factor, α, is a function of the number of epochs within the observation, n, and the correlation coefficient, f, which is calculated with the exponential function found in Equation D.15 as well as Equation 2.14. The difference between the methods presented by Craymer et al. (1990) and Han and Rizos (1995) is that the scale factor within the latter is based on actual data and is not just a choice made by the operator. Computing the scale factor, α, assumes that the method presented by El-Rabbany (1994) is entirely correct, as the function was created by comparison between results computed using El-Rabbany's approach, to results where the temporal correlations were entirely ignored. The benefit of this method is in its computation simplicity. There are no large matrices to manipulate and the least squares estimation process remains unchanged. It is also beneficial if commercial software that does not account for temporal correlations is used. The accuracy output from the software can simply be scaled to a more realistic level. One of the downfalls to this approach is revealed within the paper itself; the calculated scale factor is only applicable for data sets a half an hour or less.

Radovanovic (2002) implemented the methods presented within El-Rabbany (1994) in an effort to determine whether or not GPS was a tool capable of being used in deformation monitoring applications. Interested in whether or not the deformation capabilities could be improved through increasing the data rate, a test was performed on 5 points located on the University of Calgary campus. Accounting for the temporal correlation found within the observations, Radovanovic (2002) found no increase in accuracy by increasing the sampling rate as the temporally correlated observables contained limited useful information at such a high rate. The author found that temporal correlations and multipath error limited the highest acheivable height accuracy of GPS to be 5 mm at the 1-sigma level, acheived after a minumum of 1 hour of static surveying.

Focused on the physical correlations found between observations of the same epoch, Schon and Brunner (2008b) presents an alternative method of developing a realistic VCV matrix. As stated earlier, in Section 2.1.0.1, most if not all commercial RTK software uses an oversimplified stochastic model which ignores any cross correlation in the measurements. This results in a diagonal VCV matrix (zeros on the off-diagonal) used to describe the observations. Understanding that wind speed and direction in the lower atmosphere results in cross-correlation in the observations, Schon and Brunner (2008b) use turbulence theory to derive a new method of producing a fully populated (non-zero elements off the diagonal) VCV matrix to describe the observations. Although physical, not temporal, correlations are the focus of the paper, the sole purpose is to obtain a more realistic estimated accuracy which this method reportedly does. The drawback is that this would require RTK users to carry around sophisticated meteorological equipment and would most suitable for fixed receivers located near meteorological stations. See also Schon and Brunner (2006, 2008a).

Correct stochastic modeling plays an important part on the reliability of GPS. It is important to remember that the PCF depends on the VCV matrix (of the float ambiguity values) being

correctly scaled or estimated. Using simulated data, O'Keefe et al. (2006) shows that taking the temporal correlations into consideration is critical for reliably resolving the ambiguities to integer values. If the ambiguities are incorrectly fixed, the estimated position will be very poor, without any knowledge of its quality. An over-optimistic VCV matrix results in over-optimistic PCF, possibly resulting in the incorrect integer values being selected and reducing the system reliability. When the temporal correlation was by increased by a factor of 3, from 40 seconds to 120 seconds, the number of epochs required to achieve a certain PCF was also increased by a factor of 3. If GPS observations are assumed to only contain white noise, the PCF is likely to be optimistic, important to know while using GPS applications that utilize carrier phase.

An altogether different approach to dealing with the for time correlated errors is through time differencing in a Kalman filter. Unlike the previously described approaches which deal with correlated measurements by enlarging or populating the VCV matrix, the time-differencing approach strives to whiten (make more random) the measurements through cancellation of the time correlated errors. This method was originally presented by Bryson and Henrikson (1968), but has since been modified by Petovello et al. (2009). Application of the latter is one of the focuses of this research and is described in Chapter 3. This method differs only slightly from triple differencing where consecutive observations are differenced entirely, effectively eliminating the ambiguity terms from the positioning equations.

In the time differencing Kalman filter, henceforth called the modified Kalman filter, only the correlated portion of the previous measurement is differenced, as determined by the correlation coefficient. The transition matrix of the time correlated errors, Equation 2.13 (Petovello et al., 2009; O'Keefe et al., 2006), maps out the correlated portion of the errors between consecutive epochs.

$$S_k = diag(f) \tag{2.13}$$

where

$$f = e^{-\frac{1}{T}(dt)} \tag{2.14}$$

The diagonal matrix S, shown in Equation 2.13, contains the correlation coefficient as determined by the exponential function, f, calculated using Equation 2.14, where T is correlation time (seconds), and dt is the elapsed time (seconds) between measurement epochs. The selection of T is performed by best fitting the exponential function to autocorrelation results of satellite residuals. Through this best fit, the temporal correlation is modeled, see Chapter 4. The time differencing is performed by subtracting the correlated portion of the previous observation from the current observation as shown in Equation 2.15,

$$z_k = l_k - S_k l_{k-1} \tag{2.15}$$

where z is the measurement vector at epoch k, and is a function of the current and previous observation vectors, l_k and l_{k-1}. The correlated errors from the previous observation are mapped into the current observation using S, where they are then eliminated through differencing. To show how the correlated errors are eliminated, the error within an observation is theoretically separated into correlated and uncorrelated parts, as shown in Equation 2.16:

$$l_k = A_k x_k + u_k + n_k \tag{2.16}$$

Where l is the observation vector, A is the design matrix which relates the states to the observations, u represents the time correlated error present in the measurement, and n represents the errors that are random with time. The time correlated error is predicted ahead as shown in Equation 2.17.

$$u_k = S_k u_{k-1} + \varepsilon_{k-1} \tag{2.17}$$

In Equation 2.17, ε is a vector of white noise that is uncorrelated with either the white process noise, w or the white measurement noise, n. S is the transition matrix for the time

correlated errors shown in Equation 2.13. By applying Equations 3.2 (shown in Chapter 3), 2.16, and 2.17 to the time differencing equation, Equation 2.15, the time correlated errors are eliminated. This is shown in the following simplification:

$$z_k = l_k - S_k l_{k-1} = (A_k(\Phi_{k-1}x_{k-1} + w_{k-1}) + (Su_{k-1} + \varepsilon_{k-1}) + n_k) \\ -S_k(A_{k-1}x_{k-1} + u_{k-1} + n_{k-1}) \tag{2.18}$$

$$= A_k\Phi_{k-1}x_{k-1} + A_k w_{k-1} + Su_{k-1} + \varepsilon_{k-1} + n_k - S_k A_{k-1}x_{k-1} - S_k u_{k-1} - S_k n_{k-1} \tag{2.19}$$

$$= A_k\Phi_{k-1}x_{k-1} + A_k w_{k-1} + \varepsilon_{k-1} + n_k - S_k A_{k-1}x_{k-1} - S_k n_{k-1} \tag{2.20}$$

$$z_k = (A_k\Phi_{k-1} - S_k A_{k-1})x_{k-1} + A_k w_{k-1} + \varepsilon_{k-1} + n_k - S_k n_{k-1} \tag{2.21}$$

As shown in Equation 2.21, the resulting measurement vector is free of temporally correlated error. The issue with this approach, and one of the reasons that it has not been implemented in RTK positioning software, is that there is a 1-epoch time delay. During measurement epoch *k*, the states from epoch *k-1* are being estimated. Although GPS surveying is very possible with this 1-epoch time delay, productivity can be increased and surveyor frustrustion minimized through it's elimination. To alleviate the time latency problem, Petovello et al. (2009) has modified the method presented by Bryson and Henrikson (1968), described in detail within Chapter 3.

One of the newest, and still unpublished, studies on the eliminated of time correlated errors in a Kalman filter is presented in Wang et al. (2010). The performance of the Kalman filters presented by Bryson and Henrikson (1968) and Petovello et al. (2009) is reviewed using simulated data. Two new approaches are developed: the Tikhonav algorithm, a modification of the the state-augmented approach which was originally developed by Bryson and Henrikson (1968), and the Perturbed-P algorithm, where the diagonal of the VCV matrix is perturbed by a certain amount to eliminate singularity issues. Using simulated data, Wang

et al. (2010) found that the modified filter presented by Petovello et al. (2009) takes a large amount of computing power and is not robust due to the inverse of an ill-conditioned transition matrix. The Perturbed-P algorithm outperformed the others in terms of speed and computational burden.

Chapter 3

The Modified Kalman Filter

To understand the modified Kalman filter, the time differencing, latency-free Kalman filter presented by Petovello et al. (2009), it is best to first understand the typical discrete Kalman filter, explained in detail within Brown and Hwang (1997). The discrete-time Kalman filter strives to model a random process at a discrete moment in time, k. The measurement is modeled as shown in Equation 3.1:

$$z_k = H_k x_k + v_k \tag{3.1}$$

where z is the measurement vector of size $(m \times 1)$. H is the design matrix $(m \times n)$ which describes the relationship of the measurement to the states, where x is the state vector $(n \times 1)$. Measurement noise is contained within the vector, v $(m \times 1)$. The discrete-time Kalman filter is comprised of a prediction step, using information from the past to predict how the process will behave in the future, and an update step, when actual data is combined with the prediction to make the best estimate. In the prediction steps, both the states (the desired information), and their VCV information are estimated, an estimate based solely

on past information and assumptions on how the process should behave. The prediction step is performed as shown in Equations 3.2 and 3.3:

$$x_{k+1}^{-} = \Phi_k x_k + w_k \tag{3.2}$$

$$P_{k+1}^{-} = \Phi_k P_k \Phi_k^T + Q_k \tag{3.3}$$

The measurement noise, v, is assumed to be completely uncorrelated with the process noise, w ($n \times 1$). Both v and w are assumed to be white and have known covariance information contained within matrices R and Q. The transition matrix, Φ, describes the relationship of the states from one epoch to another. The covariance information containing the estimated accuracy of the states is contained within P ($n \times n$), where x^- and P^- denote the predicted states and their covariance information. When new data becomes available, the update step is performed following Equations 3.4 through 3.6:

$$K_k = (P_k^- H_k^T)(H_k P_k^- H_k^T + R_k)^{-1} \tag{3.4}$$

$$x_k^+ = x_k^- + K_k(z_k - H_k x_k^-) \tag{3.5}$$

$$P_k^+ = P_k^- - P_k^- K_k H_k \tag{3.6}$$

where K ($n \times m$) is the gain matrix, and $x^+$and P^+ are the updated states and their covariance information. Returning focus to the modified Kalman filter presented by Petovello et al. (2009), the one epoch delay found within the method described by Bryson and Henrikson (1968) can be eliminated by manipulating the discrete filter state prediction step found in Equation 3.2 and solving for x_{k-1}, as shown in Equation 3.7.

$$x_{k-1} = \Phi_{k-1}^{-1}(x_k - w_{k-1}) \tag{3.7}$$

Applying Equation 3.7 to the measurement vector, as determined by Bryson and Henrikson (1968) in Equation 2.20, results in the following simplification:

$$\begin{aligned} z_k &= A_k\Phi_{k-1}[\Phi_{k-1}^{-1}(x_k - w_{k-1})] + A_k w_{k-1} + \varepsilon_{k-1} + n_k \\ &\quad -S_k A_{k-1}[\Phi_{k-1}^{-1}(x_k - w_{k-1})] - S_k n_{k-1} \end{aligned} \tag{3.8}$$

$$\begin{aligned} z_k &= A_k\Phi_{k-1}[\Phi_{k-1}^{-1}x_k - \Phi_{k-1}^{-1}w_{k-1}] - S_k A_{k-1}[\Phi_{k-1}^{-1}x_k - \Phi_{k-1}^{-1}w_{k-1}] \\ &\quad -S_k n_{k-1} + A_k w_{k-1} + \varepsilon_{k-1} + n_k \end{aligned} \tag{3.9}$$

$$z_k = A_k x_k - S_k A_{k-1}\Phi_{k-1}^{-1}x_k + S_k A_{k-1}\Phi_{k-1}^{-1}w_{k-1} - S_k n_{k-1} + A_k w_{k-1} - A_k w_{k-1} + \varepsilon_{k-1} + n_k \tag{3.10}$$

Further simplification of the measurement vector can be made by substituting Equation 3.11.

$$\chi_k = S_k A_{k-1}\Phi_{k-1,k}^{-1} \tag{3.11}$$

Explained simply, χ is the correlated portion of the design matrix, mapped from the current epoch to the previous epoch. χ is introduced in order to simplify the mathematical formulas and facilitate any changes in the visible satellite constellation, see Section 3.1. The resulting measurement vector, which is now free of any time latency and time-correlated errors, is shown in Equation 3.12,

$$z_k = (A_k - \chi_k)x_k + \chi_k w_{k-1} - S_k n_{k-1} + \varepsilon_{k-1} + n_k \tag{3.12}$$

To further simplify the modified filter, Petovello et al. (2009) shows that the measurement model for the modified filter, Equation 3.12, can be related to the measurement model from the typical discrete Kalman filter, shown in Equation 3.1, by making the following substitutions for the design matrix, H, and the measurement noise vector, v.

$$H_k = A_k - \chi_k \tag{3.13}$$

$$v_k = \chi_k w_{k-1} + \varepsilon_{k-1} + n_k - S_k n_{k-1} \tag{3.14}$$

Equation 3.13 shows the design matrix, H, of the time-differenced observations. Subtracting the correlated portion of the previous epoch design matrix, χ, from the design matrix from the current epoch, A_k, the time-correlated errors are eliminated. The measurement noise vector of the modified Kalman filter, Equation 3.14, is assumed to white because of the elements inside it are assumed to be white. As explained earlier, one of the main assumptions in a discrete time Kalman filter is that the process noise and the measurement noise are uncorrelated. Note that the measurement noise is now a function of the process noise, w, breaking this assumption. As a result, a new variable, C, is computed to deal with this correlation as shown in Equation 3.15.

$$C_k = Q_{k-1}\chi_k^T \tag{3.15}$$

The update step is performed using the following equations:

$$K_k = (P_k^{(-)}H_k^T + C_k)(H_k P_k^{(-)} H_k^T + R_k + H_k C_k + C_k^T H_k^T)^{-1} \tag{3.16}$$

$$x_k^{(+)} = x_k^{(-)} + K_k z_k \tag{3.17}$$

$$P_k^{(+)} = P_k^{(-)} - K_k(H_k P_k^{(-)} H_k^T + R_k + H_k C_k + C_k^T H_k^T)K_k^T \tag{3.18}$$

where

$$R_k = M_{k-1} + N_k + S_k N_{k-1} S_k^T + \chi_k Q_{k-1} \chi_k^T \tag{3.19}$$

The covariance of the measurements, R, is calculated based on estimates of the measurement white noise covariance, N, and correlated noise covariance, M, based upon user estimates regarding the signal errors within the specific survey environment. Going back to

the original issue of over-optimistic VCV matrices when temporal correlation is ignored, as the length of temporal correlation increases, R becomes larger, resulting in a more realistic accuracy estimate of the states.

In the described filter, if the length of temporal correlation is zero, S reduces to zero, resulting in χ and C also becoming zero. Equations 3.13 through 3.19 then simplify into the normal discrete Kalman filter equations shown in Equations 3.2 through 3.6. The measurement noise, R, also reduces to what it normally should be, the correlated measurement noise variance plus the white measurement noise variance.

To further clarify recommended usage of the modified Kalman filter, Figure 3.1 shows the flow of events that occur during usage of the modified Kalman filter.

3.1 Implementation

Previous to this research, the above equations had yet to be implemented using real data. The challenge of using real data to simulated data, is that data collected in the field is prone to constant changes in the visible satellite constellation. This can be due to cycle slips, satellites rising above or descending below the elevation mask, or from measurements being discounted through blunder detection methods. When performing time differencing, the design matrices from consecutive epochs must be differenced, a problem when the matrices have different dimensions which happens when the satellite constellation changes. To simplify the issue, χ_k was created using Equation 3.11 so that all of the difficulties of aligning matrices of different dimensions are contained within one variable. As long as χ_k is the same dimension as the current design matrix, A_k, there are no problems with incompatible matrices throughout the entire estimation process.

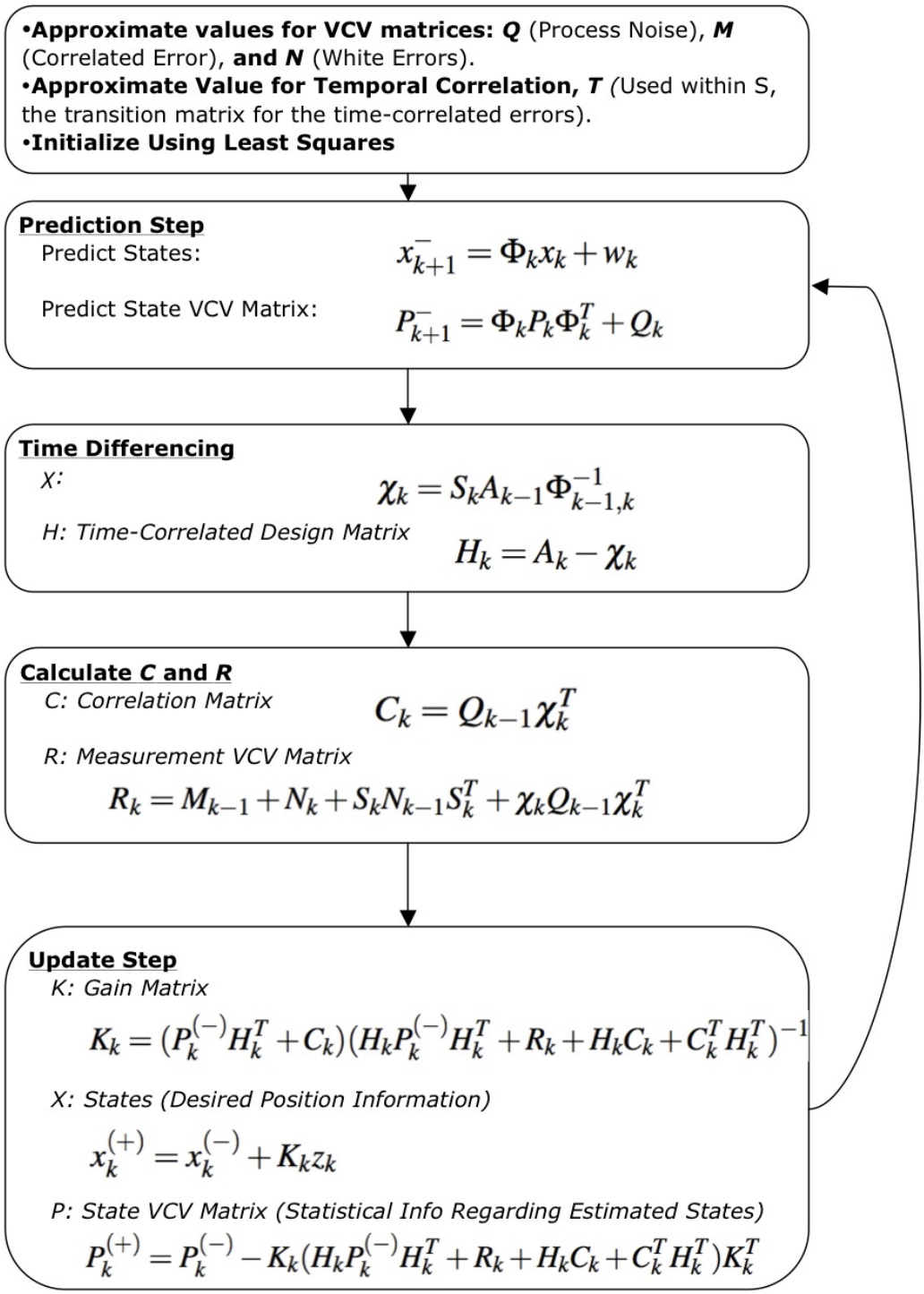

Figure 3.1: Flow chart of the time-differencing, modified Kalman filter.

When a new satellite is observed during epoch k, but not during epoch *k-1*, a new row must be added to χ_k to make its dimensions compatible to that of A_k. Equation 3.20 demonstrates the calculation of H_k when a new satellite observation, X^3, is allowed into the solution. This single-state example assumes a random walk process where the transition matrix, Φ, is an identity matrix.

$$H_k = A_k - \chi_k = A_k - S_k A_{k-1} \Phi^{-1}_{k-1,k}$$

$$H_k = \begin{bmatrix} X^1_k \\ X^2_k \\ X^3_k \end{bmatrix} - \begin{bmatrix} f & 0 & 0 \\ 0 & f & 0 \\ 0 & 0 & 0 \end{bmatrix} \begin{bmatrix} X^1_{k-1} \\ X^2_{k-1} \\ X^3_{k-1} \end{bmatrix} \begin{bmatrix} 1 \end{bmatrix} = \begin{bmatrix} X^1_k - f(X^1_{k-1}) \\ X^2_k - f(X^2_{k-1}) \\ X^3_k \end{bmatrix} \tag{3.20}$$

X^1 and X^2 are observations made at both epochs k and *k-1*, and X^3 is observed only at epoch k. Regardless of X^3 only being observed during epoch k, it is still included within χ_k, but with a correlation coefficient of zero. Since X^3 is a new observation, all of the information contained within it is independent because it was not previously observed. This results in the entire X^3 observation being used to estimate the state, while the time-correlated portions of X^1 and X^2 are differenced from the current observation.

When a satellite observation used during epoch *k-1* is not used during epoch k, it must be removed from χ_k to ensure compatible matrix dimensions. Since the satellite is no longer observed, there is no longer any correlated measurement and the previous epoch information, found in χ_k, can simply be removed for that satellite.

In real GPS data, the following scenario will occasionally occur. A satellite will temporarily be dropped from a solution before the signal is once again picked up. This scenario will frequently occur with low elevation satellites with low signal-to-noise ratios. If the satellite reenters the solution before enough time has elapsed to be considered an independent observation, it must be differenced from the last observation made before the tracking was

lost. Even though the satellite was not continuously tracked, for a certain period of time, the observations are still temporally correlated and need to be differenced.

Figure 3.2 shows what can happen to the position estimate, the estimated height in this case, when a satellite comes into or leaves the solution using the process shown in Equation 3.20. This dataset was observed using a ~100 m baseline. In this case, both L1 and L2 signals were used, resulting in 12 fixed ambiguities at one point. To simplify the Figure and save space, only the centimetre level component of the estimated height is shown. As long as the visible satellite constellation remains constant, the estimated position changes very slowly, reflecting both the small process noise (see Section 3.2) and little observability the measurements have on the states. Each time a satellite enters or leaves the solution, the estimated position is often drastically altered. In this case, when a new satellite signal was accepted into the solution, the height estimated immediately changed 1 cm.

Allowing new satellites into the time differencing filter can be risky. Using a correlation

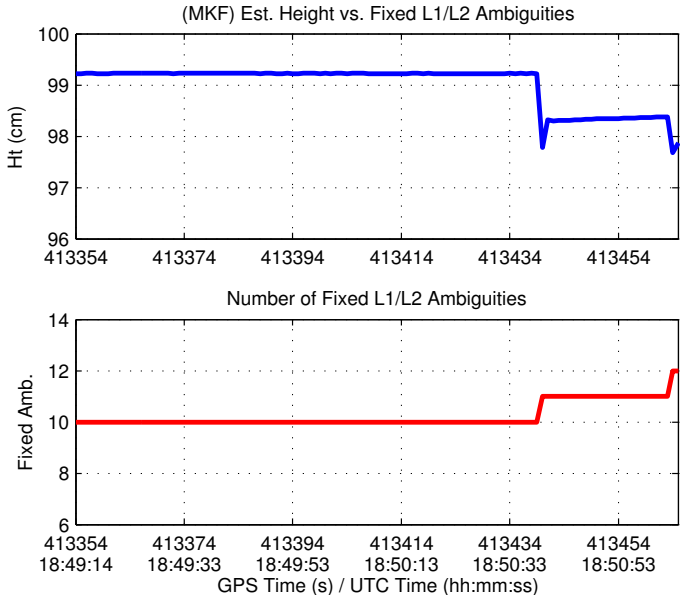

Figure 3.2: The estimated height component (Using the modified Kalman filter (MKF)) vs. the number of fixed L1/L2 ambiguities.

time of 5 seconds, the initial epoch a satellite comes into the solution, it has 20 times the weight of the other observations (see Section 4.2.2.2). If the new observation contains large errors, the errors will propagate into the estimated position with much greater consequences than if the errors were in the time-differenced observations. For this reason, any observations from newly acquired satellites should strictly be analyzed using blunder detection methods.

An interesting observation was made during filter tuning (see Section 3.2) regarding process noise. If the process noise was so large that the filter would fail to converge (i.e. the estimated variance of the state gets better with time), any new satellites that would come into the solution would cause any previously fixed ambiguities to be lost. This would result in a float solution that would rarely regain fixed ambiguities for the remainer of the dataset. For new satellites to reliably be accepted into the solution, the filter should be converging.

3.2 Filter Tuning

A critical part in the successful use of this time differencing Kalman filter is filter tuning, or selecting values to describe the errors found within the system. Typically, when tuning a discrete, random walk Kalman filter, values are chosen for the VCV matrices of the process and measurement noise, Q and R. The chosen values need to realistically describe the true noise within the system, while allowing the filter to run in an optimal and robust manner. In the time differencing Kalman filter, the measurement noise is divided into two separate parts, the white measurement noise, n, and the correlated measurement noise, u, with their respective VCV matrices, M and N. The length of temporal correlation must also be considered during filter tuning. All of these variables must be selected with appropriate values that reflect the true error characteristics within the system, yet still produce an efficient, optimal

filter. To understand the impact that each parameter has on the filter, each is changed one at a time, while the rest are held constant at initially selected values. The initially selected values for each parameter are shown in Table 3.1. The position components were modeled as random walks, meaning that the direction of change is unknown between moments. The ambiguity states are modeled as random constants. The impact each parameter has on the estimated accuracy of the estimated latitude, simply referred to as the estimated accuracy within this section for simplicity purposes, is shown in Figures 3.4 through 3.8.

Essential to this research is determining an appropriate value to describe the temporal correlation that exists in GPS observations. Like the other stochastic parameters that must be estimated, the amount of temporal correlation varies with time and location. Chapter 4 is dedicated to the determination of a realistic value of T for the L1 carrier phase observable, and analyzes how the temporal correlation of the signal errors vary changes with location, satellite elevation angle, and baseline length. Within this Section, the effect that the chosen temporal correlation value has on the estimated accuracy is analyzed. Using Equation 2.14, the correlation coefficient, f, is calculated using different values for temporal correlation, as shown in Figure 3.3.

As seen in Figure 3.3, a signal that uses a temporal correlation value of 10 epochs, seconds in this case, has a correlation coefficient of approximately 0.90 between consecutive epochs. This is to equivalent to saying that 90% of the consecutive signal is redundant to the original signal. As long as the signals are assumed to be independent, this redundant

Table 3.1: Initially selected values used for tuning the modified Kalman filter.

	Pseudorange	Carrier Phase
Process Noise	0.0075 cm/$\sqrt{Hz}$	
Measurement Noise (White) 1-σ	15 cm	0.50 cm
Measurement Noise (Correlated) 1-σ	85 cm	1.50 cm
Temporal Correlation, T	60 seconds	

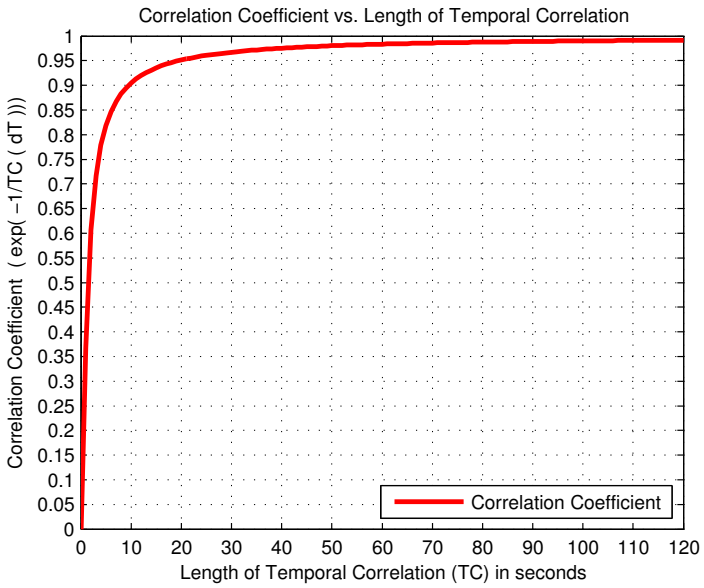

Figure 3.3: Correlation coefficient, f, vs. temporal correlation, T, $(f = e^{-\frac{1}{T}})$

information should not be used to update the filter. As the length of temporal correlation increases, the correlation coefficient edges closer and closer to 1, meaning that the consecutive signals are nearly 100% correlated. The correlation coefficient is used in time differencing, Equations 3.11 and 3.13, in an attempt to eliminate the redundant information from the consecutive epochs.

As seen in Figure 3.4, as the temporal correlation increases in length, the states become less observable as there is less new information contained within consecutive epochs. All filter parameters remain the same as shown in Table 3.1, with exception of the length of temporal correlation.

In Figure 3.4 it is obvious that when temporal correlation is not accounted for, or is minimal, the filter continues to converge. Filter convergence is detectable when the estimated accuracy continues to improve with time. This often occurs in static surveys where very little process noise is added to the filter. Regardless of the minimal process noise (see Table 3.1), as the length of temporal correlation increases, the filter begins to lose observability

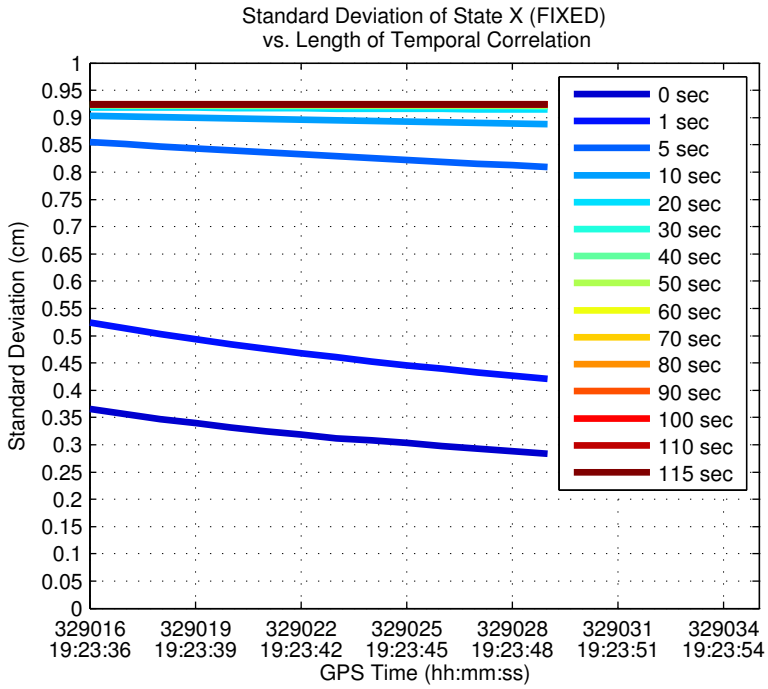

Figure 3.4: Estimated $1-\sigma$ accuracy (State X) vs. length of temporal correlation, T.

and the estimated accuracy stops improving with time. Observability is lost as there is not enough new information to update the estimated states. Although the dataset in Figure 3.4 is very short, the same result was found when the dataset was increased to 30 minutes. Note that once the length of temporal correlation reaches 40 or 50 seconds, there is little change in the resulting accuracy estimate. When using a correlation time of 50 seconds, the consecutive epochs are already nearly 100% correlated, and a larger temporal correlation time will not make a significant difference in the observability of the states.

The measurement noise, R, should realistically describe all of the errors within each measurement. This includes multipath and atmospheric errors. In this research, additional noise was given to low elevation satellites in an effort to compensate for the larger errors that signals from these satellites typically have. It was assumed that there was no cross-correlation between the observations (Off-diagonal elements of R equal zero). As in all filter tuning, there is no specific value for the measurement noise that best describes every scenario. The

errors contained within the measurements, such as multipath, constantly change with location and time and ideally should be approximated on a per-case basis. As shown in Table 3.1, measurement noise is approximated for both the carrier phase and pseudorange noise individually.

Figure 3.5 shows the impact of changing the standard deviation of the correlated measurement noise on the estimated accuracy. As expected, the as the approximated standard deviation gets smaller, the estimated accuracy improves. The carrier phase observable has a larger impact on the estimated accuracy than the pseudorange. When the correlated noise of the carrier phase observable has a standard deviation of zero, the estimated accuracy is 0.30 cm. When the same variable is given a standard deviation of 0.3 cm, the estimated accuracy is approximately 0.95 cm. Regardless of the selected pseudorange standard deviation, the estimated accuracy is approximately 0.92 cm.

Figure 3.6 shows the effect the estimated white measurement noise has on the 1-sigma estimated accuracy. Although any difference is minimal, the smaller the white measurement noise, the better the estimated accuracy.

Although each RTK manufacturer chooses different values for the stochastic parameters which are not generally available to the public, it is understood that process noise is added to account for kinematic movement. This process noise also prevents the estimated positional accuracy from falling below 2 cm. In static positioning, the process noise is either significantly reduced or eliminated, allowing the estimated accuracy of the position to get increasingly better.

The VCV matrix of the process noise, Q, in this research where a random walk model is used, can be estimated by the amount the receiver is expected to move between epochs. A diagonal Q matrix, used in this research, assumes any horizontal or vertical movement is

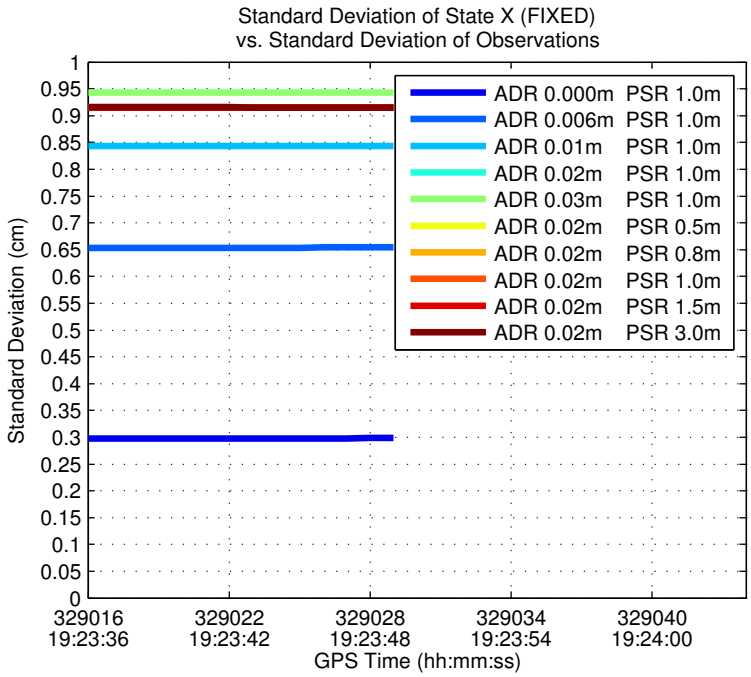

Figure 3.5: Estimated $1-\sigma$ accuracy (State X) vs. standard deviation of correlated measurement noise. PSR signifies the pseudorange standard deviation while ADR (accumulated doppler range) signifies that of carrier phase.

independent from one another. Process noise is not added to the ambiguity states as their values remain constant as long as the satellite signals remain locked. Figure 3.7 shows the estimated accuracy when the process noise uses values appropriate for kinematic surveying and Figure 3.8 shows the same information with process noise more appropriate of static surveying.

When using process noise values appropriate for RTK kinematic movement in the modified Kalman filter, the filter fails to converge. For convergence to occur, process noise must be virtually eliminated, see Figure 3.8. Although the data shown in 3.8 covers a short time span, a similar result was seen in data up to 30 minutes in length. Process noise allows for filter divergence. Regardless of the value chosen to approximate the temporal correlation, a filter cannot diverge until process noise is added. For the time differencing filter to function reliably, the process noise must be carefully chosen to allow for filter convergence while

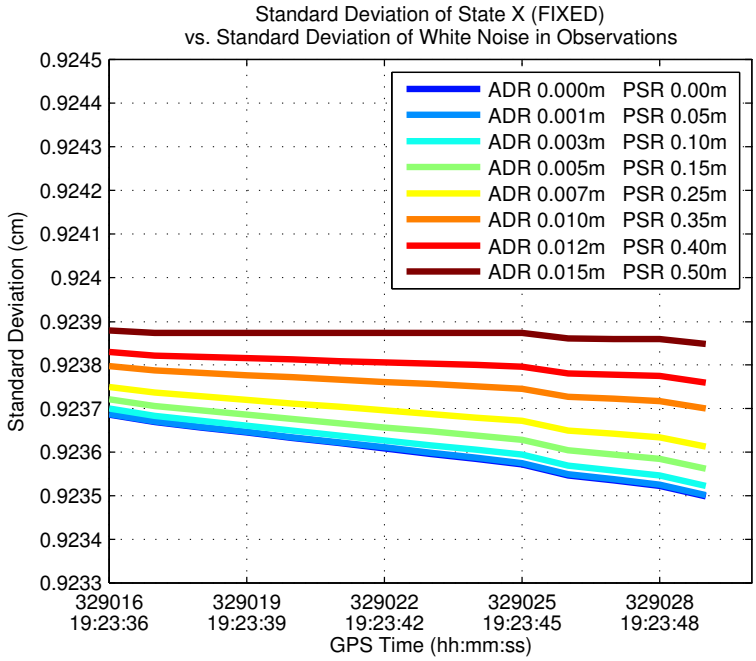

Figure 3.6: Estimated $1-\sigma$ accuracy (State X) vs. standard deviation of white measurement noise. PSR signifies the pseudorange standard deviation while ADR (accumulated doppler range) signifies that of carrier phase.

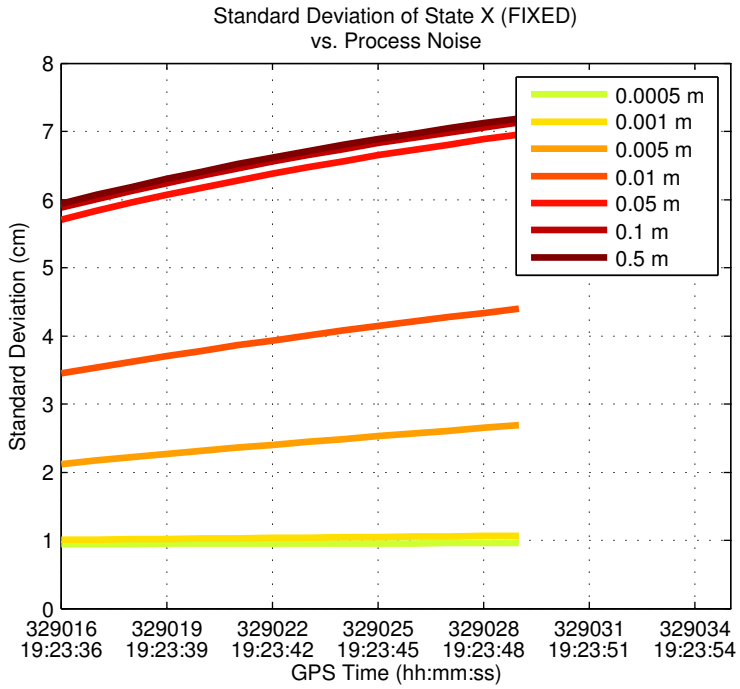

Figure 3.7: Estimated $1-\sigma$ accuracy (State X) vs. standard deviation of process noise (Zoomed out).

still allowing for movement.

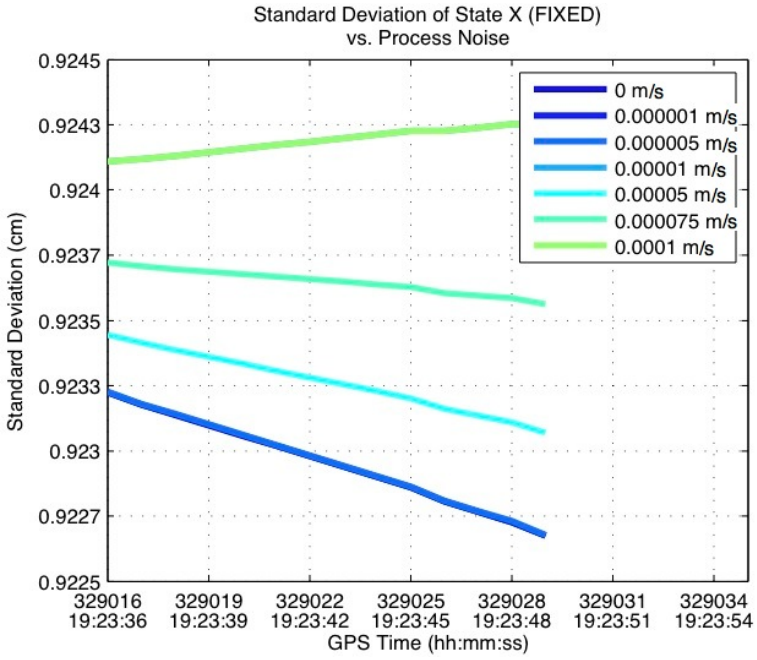

Figure 3.8: Estimated $1-\sigma$ accuracy (State X) vs. standard deviation of process noise (Zoomed in).

The challenge is in finding a set of values that realistically describes the kinematic movement, the length of temporal correlation within the observations, and the measurement noise, both coloured and white, while still allowing the filter to converge. Accounting for temporal correlation takes away so much observability that it is difficult to allow the filter to converge. As seen in Figure 3.7, when using the values found in Table 3.1, the filter is not adequate for the kinematic movement that is found in RTK surveying.

After analyzing the impact each parameter has on the filter, the values shown previously in Table 3.1 were selected to describe the system. These values are used to process GPS data using the modified Kalman filter, the results of which are shown in Chapter 6. The selection of the correlation length parameter is described in Chapter 4.

Chapter 4

L1 Carrier Phase Signal Time-Correlation

One of the key assumptions in this research is that GPS signals are time-correlated. This Chapter describes the process taken to determine if the L1 carrier phase observable is temporally correlated, and if it is, for how long. Influencing factors such as satellite elevation angle and baseline length are considered.

4.1 Data Collection

In order to obtain an independent assessment of the correlation time of the L1 carrier phase signal, static carrier phase data was collected. Over 3 different days, various baselines of different lengths (up to 10-km) were observed using Novatel® and Trimble® receivers. The observed baselines are shown within Table 4.1. Baselines collected on the same day were collected simultaneously. Points S4 and S5 are located 3-metres apart on the roof of the

Table 4.1: Baseline locations and statistics.

Date	Equipment	Baseline Length	Base Location	Rover Location
June 29^{th} 2009	Novatel® OEM3	3 m	S4	S5
July 6^{th} 2009	Trimble® R8	3 m	S4	S5
July 6^{th} 2009	Trimble® R8	2 km	S4	Edworthy Park
July 6^{th} 2009	Trimble® R8	2 km	S5	Edworthy Park
July 6^{th} 2009	Trimble® R8	5 km	S4	Nose Hill Park
July 6^{th} 2009	Trimble® R8	5 km	S5	Nose Hill Park
July 6^{th} 2009	Trimble® R8	7 km	Edworthy Park	Nose Hill Park
July 7^{th} 2009	Trimble® R8	3 m	S4	S5
July 7^{th} 2009	Trimble® R8	10 km	S4	Rocky Ridge
July 7^{th} 2009	Trimble® R8	10 km	S5	Rocky Ridge

engineering building at the University of Calgary. These two receivers were expected to experience the most multipath due to reflective metal surfaces in the vicinity. The receiver located in Edworthy Park had some nearby deciduous trees that could have possibly caused some multipath while the receivers in Nose Hill Park and Rocky Ridge were located in open fields. All points were located within locations that would be considered adequate for GPS surveying purposes. All points were observed for a minimum of 3 hours using a stationary receiver and a data rate of 1-Hz. The baselines were processed using GrafNAV® 7.0 and the double difference residual for each satellite pair was obtained. A 10-degree elevation mask was applied for all post-processing.

4.2 Data Processing

When processing static data, any changes in the error magnitude is seen in the double difference residuals. The combined influence of the atmospheric errors, multipath error, and a number of other nominal systematic errors are all contained within the residuals. In order to analyze the temporal correlation found within the baseline residuals, the same satellite pair must be used throughout the entire residual data set, requiring that the same

base satellite be used in the differencing. If the base satellite was changed, a shift would have been seen in the residuals, altering the results in the correlation analysis. An additional requirement was that only residuals from fixed ambiguity solutions would be used in the analysis. All residual analysis was performed using Matlab™.

4.2.1 Spectral Analysis

A spectral analysis was performed on the residuals from each double differenced satellite pair. The spectral analysis reveals any frequencies or repeating patterns within the signal. Since this research is focused on time-correlation in RTK GPS positioning which typically uses a 1-Hz data rate, it was of greatest interest to analyze the low frequencies of less than 1 Hz. All of the residuals show at least a 15 db shift in the spectrum magnitude within a frequency of approximately 0.02-Hz, or within approximately 50 seconds of the original signal. An example, using PRN pair 7-13 from the 2 km baseline, is shown in Figure 4.1. A shift of 15 db signifies that the 97% of the power of the signal is within the following 50 seconds. After approximately 50 seconds has elapsed, the signal has very little remaining influence. For more on performing a spectral analysis, see Semmlow (2005).

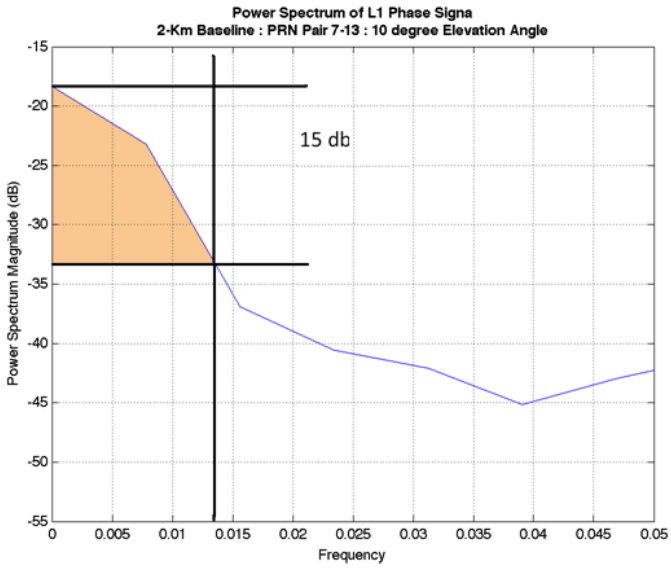

Figure 4.1: Power spectrum magnitude, using satellite pair at low elevation angle from the 2 km baseline. Much of the power is located at low frequencies.

4.2.2 Estimating Correlation Time, *T*

The residuals from each satellite pair were analyzed using the autocorrelation function to determine the temporal correlation within the signal. The autocorrelation function is shown in Equation 4.1,

$$R_{XX}(\tau) = \lim_{N\to\infty} \frac{1}{N} \sum_{k-1}^{N} x(k)x(k+\tau) \tag{4.1}$$

where *Rxx* is the desired correlation coefficient between the signal at time *k*, and the signal after a time lag, τ (Semmlow, 2005). *N* represents the total number of observations in the data set. The results were normalized so that when the lag equalled zero, the correlation of a signal with itself was equal to one. Every satellite pair that contained an acceptable amount of fixed observations (greater than 30 minutes) was processed from the observed baselines. Using iterative least squares, the exponential function shown in Equation 2.14

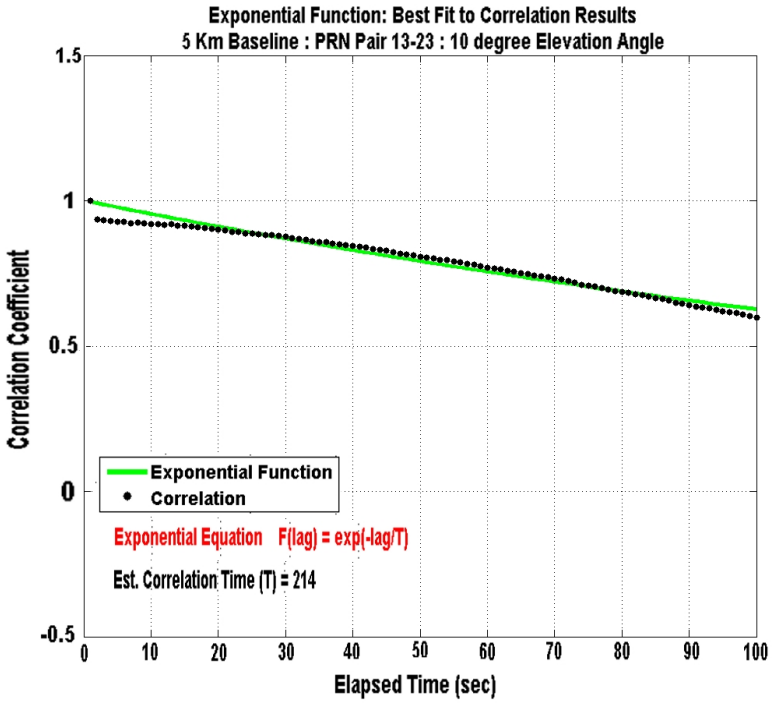

Figure 4.2: Exponential function fit to residuals from PRN pair 13-23.

was fit to R_{xx} for each satellite pair to determine the best fitting estimate of the correlation time, T.

Based on the spectral analysis, the exponential function was only fit to the first 100 seconds of autocorrelation data. Figure 4.2 shows an example of the exponential fit from one of the double differenced pairs, PRN 13-23. After 100 seconds had elapsed from the original epoch, a correlation coefficient of 0.6 was still observed. The field data did not follow the characteristics of white noise. Figure 4.2 can be compared to Figure 4.3 which shows an exponential fit to the autocorrelation results of uncorrelated (white) errors. In Figure 4.3, R_{xx} falls to zero after only one epoch, showing no correlation with the previous epoch. The best fitting exponential function used a correlation time, T, of only 2-seconds.

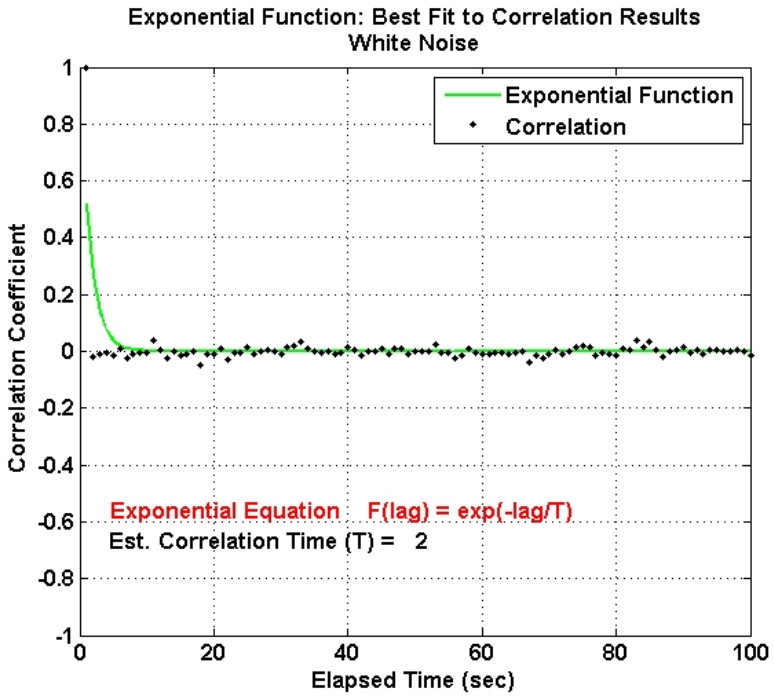

Figure 4.3: Exponential function fit to white noise.

4.2.2.1 Correlation Time vs. Length of Dataset

After compiling the correlation time for all satellite pairs collected over the five baselines, a small trend was found in the correlation time as a function of observation length. The amount of available data to be analyzed ranged from approximately 0.5 to 3 hours. Figure 4.4, which shows a line fit to the samples using least squares, shows this trend.

As seen in Equation 4.1, the correlation coefficient R_{XX} is a function of the total number of observations, N. In an ergodic process, where the mean value and statistical variance depend on the dataset selected, the length of the dataset plays an important part in the estimated correlation coefficient, see Brown and Hwang (1997). As the dataset grew in length for a specific satellite pair, the probability increased that the estimated temporal correlation would be large. This is the result of longer data sets having a higher probability of experiencing fluctuations in the residuals from multipath and other errors. If a data

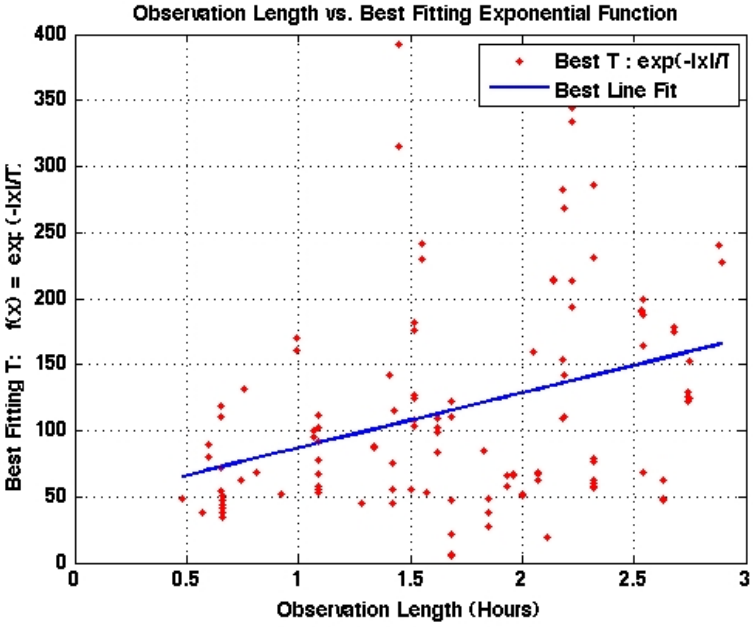

Figure 4.4: Length of dataset vs. best fitting temporal correlation value, *T*.

set is only a minute long, even if multipath is experienced during that time, the residuals will likely appear white since the data would be too limited to reveal any fluctuations with time. In order to remove any influence of *N* in the autocorrelation results, all data sets were fixed to a length of 1.5 hours. Data sets shorter than 1.5 hours were omitted from the analysis and longer datasets were shortened. By fixing the data length, any differences in correlation time would be due to other variables such as baseline length, elevation angle, or the environment surrounding the receiver.

4.2.2.2 Correlation Time vs. Time Between Independent Observations

There is a key difference between the length of time between fully independent observations, and the temporal correlation time, *T*. In this research, *T* is the variable used in the exponential function to model Rxx as a function of time, calculated using the autocorrelation results. Figure 4.5 shows an exponential function (using $T = 5$ seconds) vs. the time

lag, where the time lag refers to the amount of elapsed time from the observation being analyzed. Using this model, after 5 seconds have elapsed, there is still an estimated correlation coefficient of approximately 0.4. This is the equivalent to saying that 40 percent of the information contained in an observation after only 5 seconds is redundant to that of the original observation. The correlation coefficient does not approach zero, indicating a fully independent measurement, until approximately 20 seconds have elapsed from the original epoch. The chosen value for T is not equivalent to the length of time between fully independent observations.

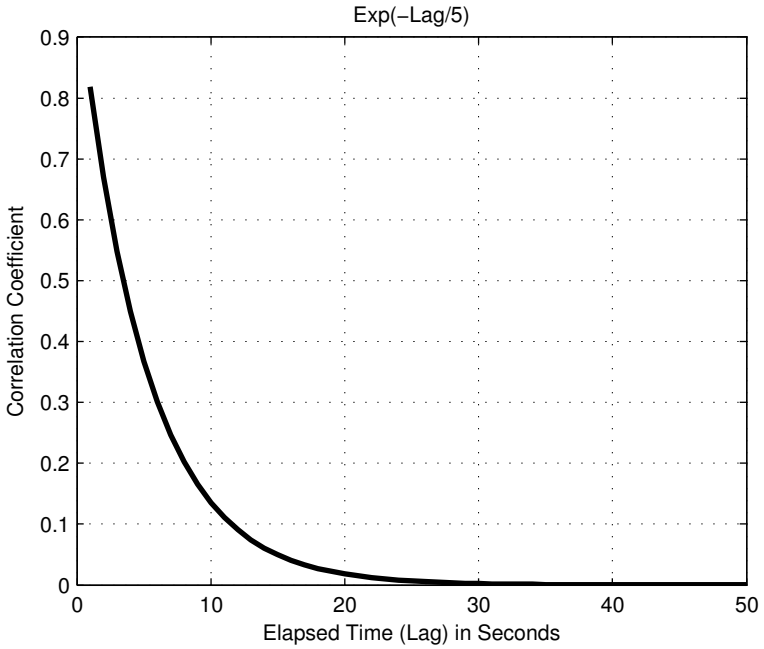

Figure 4.5: Exponential Function ($e^{-\frac{\tau}{T}}$) vs. Time Lag, τ, calculated using a temporal correlation time, T = 5 seconds

4.3 Data Analysis

Suprisingly, the resulting correlation times, *T*, did not have a normal distribution, as shown in Figure 4.6. Since the correlation time cannot be a negative, the distribution was unbalanced. With only five different baselines, the data quantity was also limited.

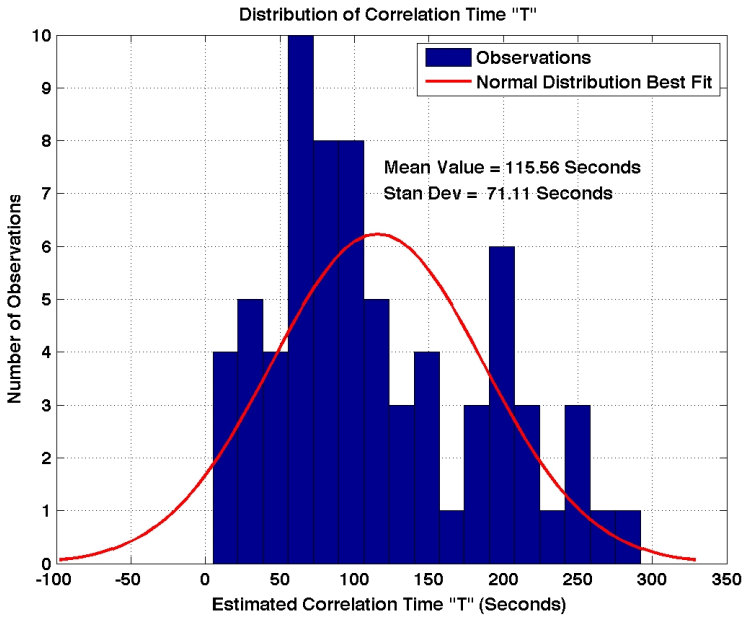

Figure 4.6: Distribution of estimated temporal correlation time, *T*.

4.3.1 Estimated Correlation Time vs. Receiver Location

By sorting the correlation times according to the location of the base receiver used for the double differencing, an analysis can be made of the different roving receiver environments. Figures 4.7, 4.8, and 4.9 compare estimated correlation times of similar satellite pairs formed over different baselines using the same base station. All the data shown within each individual figure was collected simultaneously.

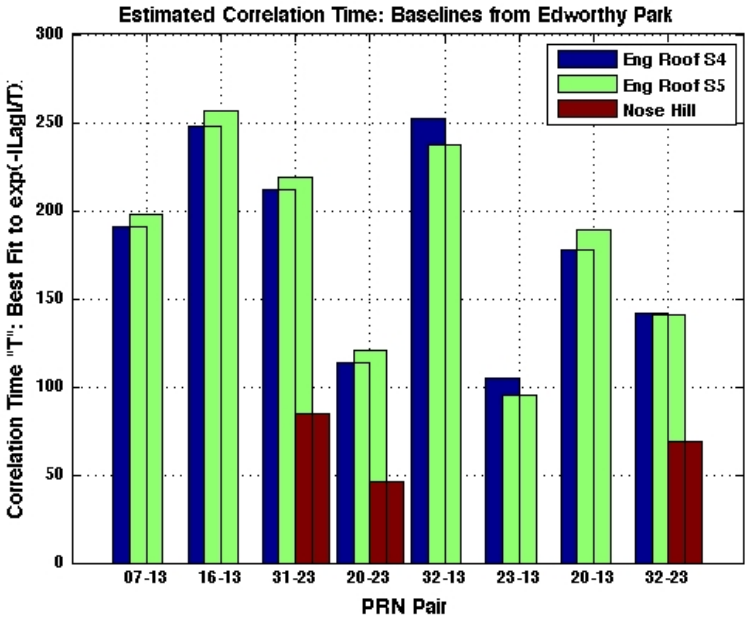

Figure 4.7: Estimated temporal correlation, *T*, for PRN pairs with baselines originating from Edworthy Park.

Figure 4.7 compares the correlation times of all observations collected using Edworthy Park as the base station. It clearly shows that two receivers on the roof of the engineering building had longer correlation times than the receiver located in Nose Hill Park. The receiver located on Nose Hill was located in an open field where little multipath was expected. The two receivers on the roof, only 3 metres apart, were nearly surrounded by flat, metallic surfaces, located both above and below the antennas. Both receivers on the roof, when similar satellite pairs are compared, showed correlation times of the same magnitude. The baseline Edworthy-Nose Hill, for a portion of the solution, used a different satellite for the double differencing than the roof receivers, resulting in only three satellite combinations that could be legitimately compared.

Figure 4.8 compares the correlation times estimated using Nose Hill as the base station. The analysis is similar to that of Figure 4.7. The estimated correlation times of the baselines to Edworthy Park were smaller in every instance when compared to the baselines to

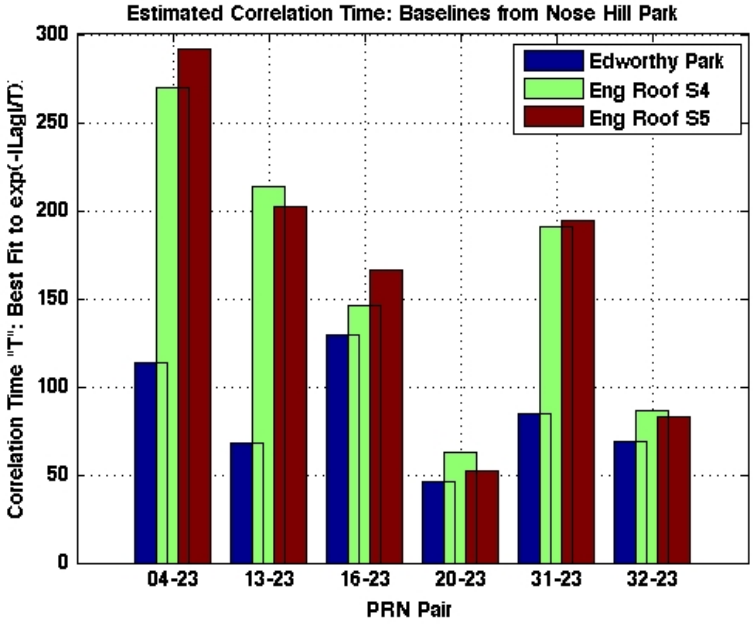

Figure 4.8: Estimated temporal correlation, *T*, for PRN pairs with baselines originating from Nose Hill Park.

the roof receivers. Both Figures 4.7 and 4.8 include comparisons of baselines of different lengths. In Figure 4.7, a 7 km baseline is compared to 5 km baselines and in Figure 4.8, a 7 km baseline is compared to 2 km baselines. Although striving to only compare effects of different receiver environments on the correlation time, atmospheric effects can influence the observations when the comparison includes different baseline distances. The ionosphere was not very active (this dataset, collected between June and July 2009, was during solar minimum) during the observation period, and the Hopfield model was used to reduce any tropospheric errors.

Figure 4.9 compares the estimated correlation times using Rocky Ridge as the base station. No comparisons could be made to Nose Hill or Edworthy Park as those baselines were observed on a different day. Both baselines to the roof points once again show correlation times of similar magnitude. By analyzing Figures 4.7, 4.8, and 4.9, it is apparent that the estimated correlation times are a result, in part, of the environment surrounding the

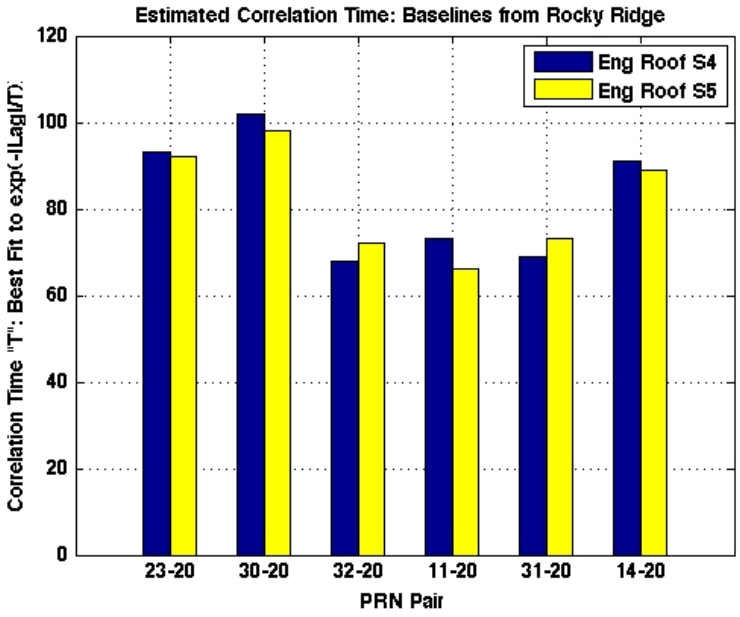

Figure 4.9: Estimated temporal correlation, *T*, for PRN pairs with baselines originating from Rocky Ridge.

receivers. Multipath prone environments are expected to experience higher correlation times than receivers located in an open field.

The 3 metre baseline was observed on 3 different occasions. On June 29th 2009, it was occupied by Novatel® OEM3 receivers and on July 6th and July 7th 2009, it was occupied by Trimble® R8 receivers. The correlation times were estimated from each observation and compared in Figure 4.10. Since the observations were made on different days, similar satellite pairs cannot be compared, as the visible satellites were different during each period. As a result, only the magnitude of the temporal correlation is compared. The estimated correlation times of data collected by Trimble® R8 receivers showed similar magnitudes. The data was collected on back-to-back days, but at different times each day. The data collected by the Novatel® receivers had estimated correlation times that were significantly longer. One potential explanation for the different magnitudes of temporal correlations found between receiver types can be attributed to receiver noise. If receiver noise is increased, assumed to

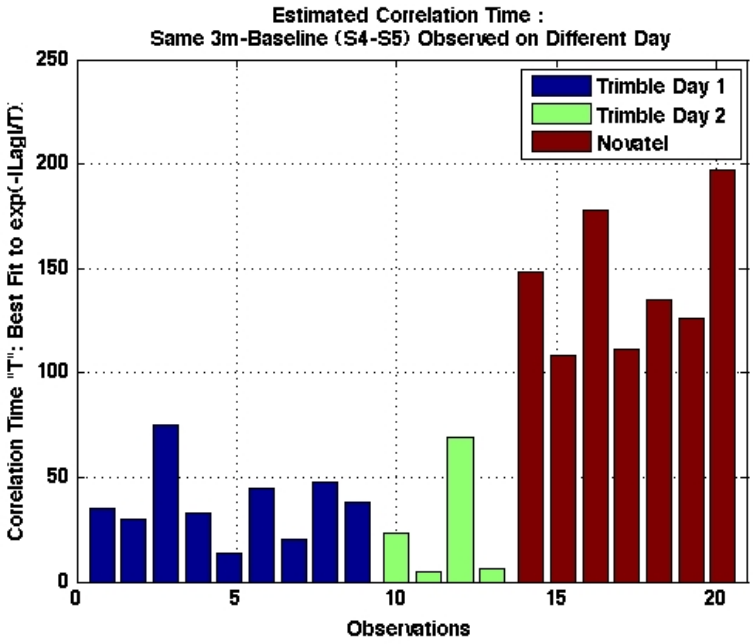

Figure 4.10: Estimated temporal correlation, *T*, for PRN pairs using the 3 m baseline between points S4 and S5. Collected on three different days using 2 types of receivers.

be white in this case, any temporally correlated errors will be masked by the white noise, resulting in the temporal correlations appearing shorter. This is likely the case here, the two receivers contained different levels of receiver noise.

When comparing the estimated correlation times of the 3-metre baselines, collected using Trimble® equipment, to longer baselines which include roof points S4 and S5, shown in Figures 4.7, 4.8, and 4.9, the short baseline has correlation times which on average are significantly less. Baseline S4-S5 has correlation times of approximately 10-50 seconds while S4-Edworthy has correlation times of 150-200 seconds. Although still not white in nature, the satellite residuals from the 3 m baseline were less effected by temporally correlated errors. Only several scenarios can explain this phenomenon. Explanation 1: The multipath effect is so similar at each receiver that it is essentially cancelled out in double differencing, resulting in an observable that contains less temporal correlation. This is unlikely as the frequency of multipath error is directly proportional to the distance between

the receiver and the reflector, see Ray (2000). Reflectors located far away from the receiver antenna cause rapidly changing multipath effects while those caused by reflectors close to the antenna change very slowly. Given that each antenna is located a different distance from the reflectors, it is very unlikely that multipath error can be mitigated through differencing. Explanation 2: The correlation times of the longer baselines are larger as a result of introduced atmospheric errors. This explanation would make sense except for the fact that the longer baseline (7 km) between Edworthy Park and Nose Hill consistently had lower correlation times than the shorter baselines (2 km, 5 km). In order to investigate more fully, other comparisons of the estimated correlation time have be made.

4.3.2 Estimated Correlation Time vs. Baseline Length

Using least squares, a plane was fit to the data in order to search for a relationship between the length of temporal correlation and the baseline length or elevation angle. By fitting a plane to the data, the two variables could be analyzed independently without influencing one another. According to the data collected and the fitted plane, correlation time is not a function of baseline length. This agrees with the research performed by El-Rabbany (1994). He estimated the temporal correlation using 47 baselines up to 100 km in length and didn't see any relationship with the length of the baseline. In this research, all the baselines were limited to the typical distances used in land surveying. In baselines of 10 km or less, atmospheric errors are marginal in all but the most active ionospheric and tropospheric conditions. That said, the temporal correlations analyzed in this research are most likely the result of multipath.

Understanding that temporal correlation is not a function of baseline length shows that Explanation 2, regarding the observed temporal correlation of the 3 metre baseline, is not valid. The exact reason the correlation times seen in S4-Nose Hill (5 km) and S4-Edworthy

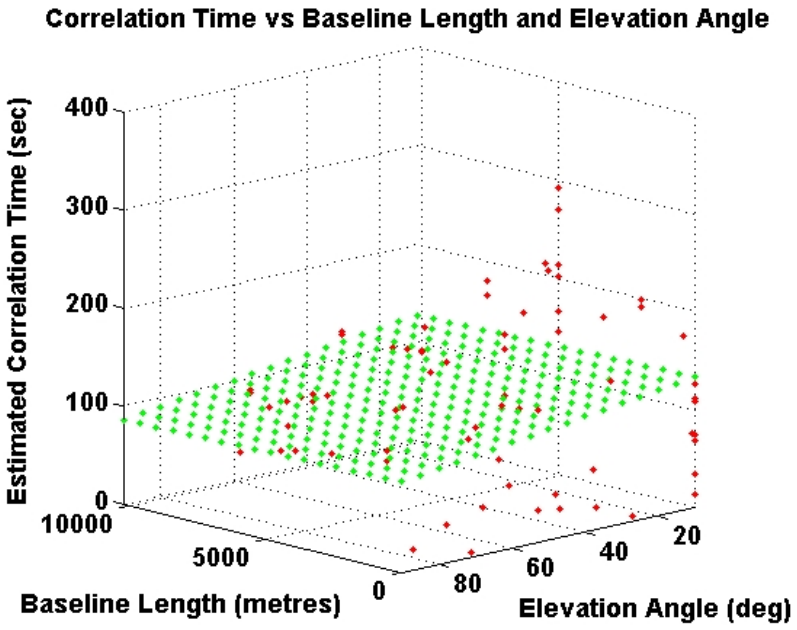

Figure 4.11: Estimated correlation time, *T*, vs. baseline length and satellite elevation angle.

(2 km) are likely longer than the correlation times seen in the 3 metre baseline is unclear at this time.

4.3.3 Estimated Correlation Time vs. Satellite Elevation Angle

Figure 4.11 shows only a small decrease in correlation time as the elevation angle increases. It is expected that the higher the elevation angle, the less time the signal would remain correlated, as incoming signals from higher elevation angles see fewer atmospheric and multipath effects. Sorting according to elevation angle is always going to be imperfect when double differencing is taking place. The double difference measurement is a combination of two satellite signals, located at different elevation angles. The base satellite used in the double differencing is the highest elevation satellite at the time it is chosen. Since double differencing is the method used in RTK positioning, this is the appropriate method in use

in the analysis. Nonetheless, the elevation angle used in the analysis is from the unique satellite, not the base satellite.

Analyzing the temporal correlation of the data collected for this research, the environment in surrounding the receiver is the most important factor in determining the temporal correlation that can be expected. Each baseline, depending on the receiver environment, resulted in temporal correlations of varying magnitudes. In order to look for trends according to elevation angle, each baseline must be analyzed independently. Figures 4.12, 4.13, and 4.14 show the correlation times for individual baselines according to elevation angle. In every example, a trend was detected by fitting a line to the data using least squares. Although the magnitude of the correlation time is still receiver environment dependent, as the elevation angle increases, the correlation time decreases. Depending on where the receivers are located, the correlation time decreases at a rate between 0.4 to 1.5 seconds per degree. When compared to another satellite in the same dataset, a low elevation satellite is likely to be correlated longer than a high elevation satellite.

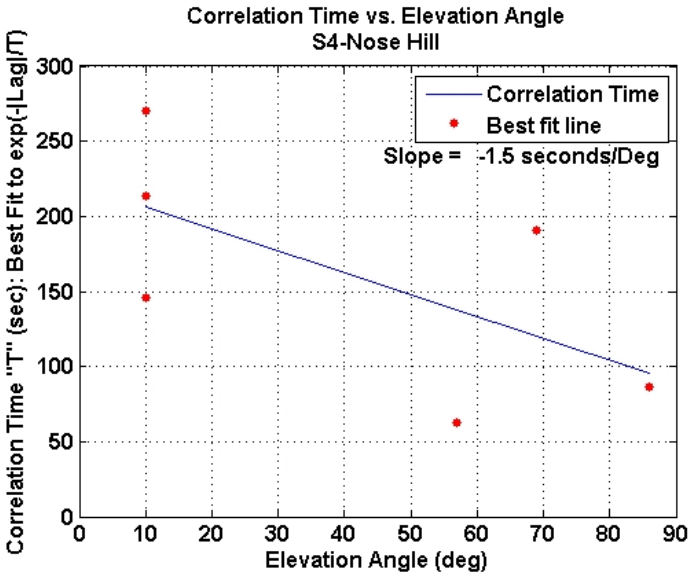

Figure 4.12: Estimated temporal correlation, *T,* vs. satellite elevation angle for the 5 km baseline, S4-Nose Hill.

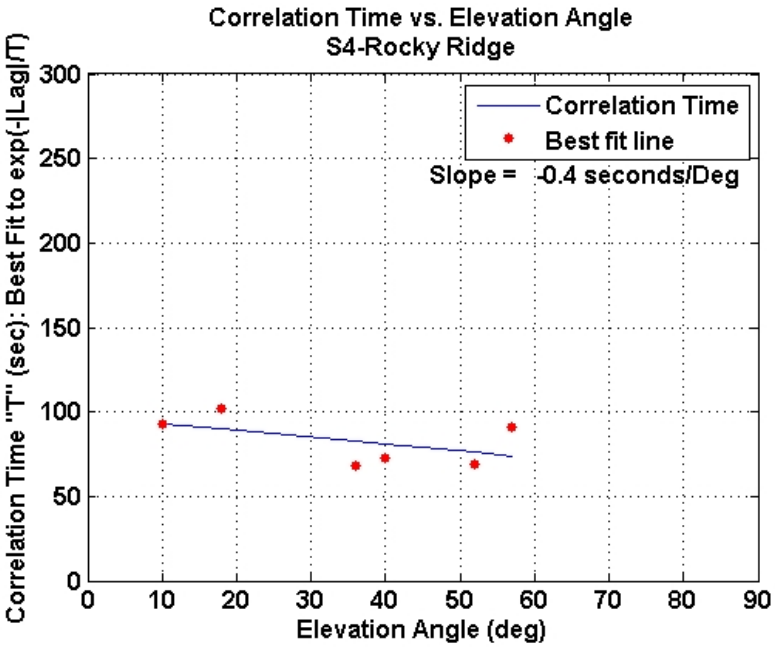

Figure 4.13: Estimated temporal correlation, *T,* vs. satellite elevation angle for the 10 km baseline, S4-Rocky Ridge.

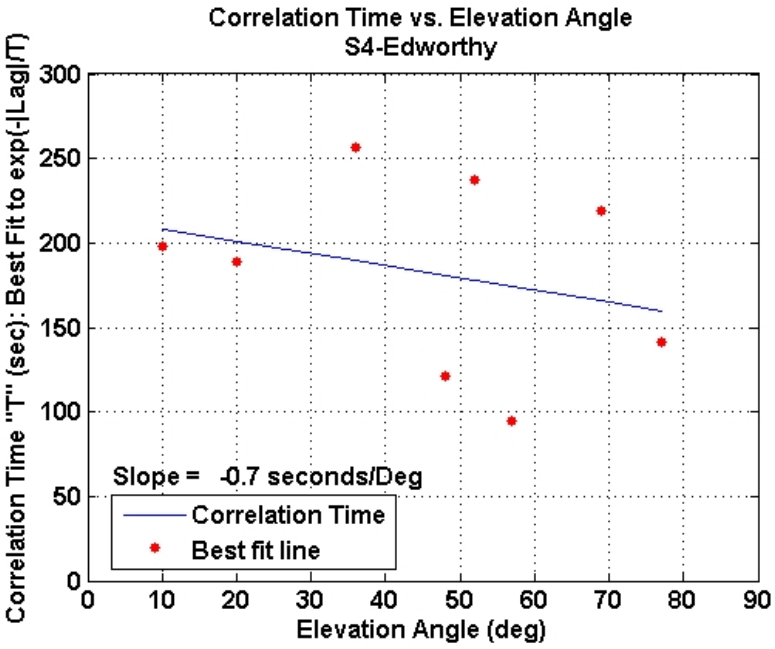

Figure 4.14: Estimated temporal correlation, *T,* vs. satellite elevation angle for the 2 km baseline, S4-Edworthy Park.

4.4 Conclusions and Future Work

GPS measurements are not white. In surveying, it is important to account for the temporal correlations, especially when GPS measurements and terrestrial measurements are combined into a network. If one of the more advanced methods of implementation referred to within the references of this research is not feasible, the VCV matrix should at least be scaled to obtain a more realistic accuracy estimate. In this test, baseline distance did not have any impact on the temporal correlation of the signal. The length of the temporal correlation was a function of elevation angle, as satellites located at lower elevation angles are more susceptible to the effects of multipath. When the baselines are relatively short (<10 km) and most of the atmospheric errors are small, most of the temporal correlation is the result of the dominant error source, multipath. Since multipath error is unique to receiver environment, the length of temporal correlation depends largely on the receiver environment. Proper site selection for both the base and roving receivers can mitigate multipath error, potentially reducing the effects of temporal correlation over short baselines. Surveying over baselines of less than 10km, the L1 carrier phase signal was correlated for an average of 115 seconds. This differs from the result of El-Rabbany (1994) who found the signal to remain temporally correlated for 263 seconds. This difference is likely the result of different receiver environments used within each of the analyses.

In future research, the baselines should be observed during a solar maximum when atmospheric errors can potentially have an influence over the shorter baselines. The work can also be completed on the pseudorange observable and on the L2 and L3 (Ionosphere Free) signals.

Currently under review, as manuscript number SUENG-94, for admission into the Journal of Surveying Engineering.

Chapter 5

RTK Field Testing

In order to test the performance of both commercial RTK and the modified Kalman filter, a network of points was established. The test network consisted of 11 points, each point carefully selected based on the characteristics of the environment surrounding it. Four of the points, to be used in the localization process, the process of rotating the points from the GPS coordinate system to the local coordinate system, were chosen in locations along the exterior of the survey site with few sky obstructions. The other 7 points, points to be used to test the accuracy of RTK GPS, were placed in a variety of locations which represent environments that surveyors would consider reasonable to survey using GPS. As shown in Table 5.1, the environments chosen for these points include parking lots, trees, fences, fields, and buildings. Surveyors use RTK in these types of environments everyday and it is important to understand how RTK performs in them. Depending on its location, each point was established using a very large spike or magnetic nail marked with survey flagging. Each point was assigned a Pt. ID, used throughout the remainder of this research. Photos of each point are found in the Appendix Section A, with the Figure number for each point shown in Table 5.1.

Table 5.1: Description of each point in the test network, along with a photo of the point, found in the Appendix, and its usage (L = Localization, T = Test Point).

Pt ID.	*Usage*	*Description*	*Photo*
1	L	Located within soccer field	Fig. A.1
2	L	Located on island in parking lot	Fig. A.2
3	L	Located on a grassy knoll	Fig. A.3
4	L	Located in center of soccer field	Fig. A.4
5	T	Within soccer field, minimal obstructions	Fig. A.5
6	T	Along sidewalk, on the edge of a large open field	Fig. A.6
7	T	Asphalt parking lot, trees to the west and south	Fig. A.7
8	T	Adjacent to large building with shiny, angular surfaces	Fig. A.8
9	T	Grass, tall coniferous trees to north.	Fig. A.9
10	T	Underneath a deciduous tree canopy (Late fall conditions)	Fig. A.10
11	T	Just north of tall chain link fence surrounding a tennis court	Fig. A.11

5.0.1 Establishment of Truth Coordinates

To establish the truth coordinates of each point, necessary to determine the absolute error of the positions generated using RTK GPS, traditional surveying techniques were performed using a Leica® TCR803 total station. The specifications of this instrument are shown in Table 5.2, with a photo in Figure 5.1. The survey procedure is as follows. Using a tripod, the total station is leveled over a point in the network. Two other points, a backsight and a foresight, have reflectors (prisms) centered over them using tripods. The angle between the backsight and the foresight is measured using a built-in electronic transit. The distance is also measured from the point occupied by the total station to the foresight using a built-in Electronic Distance Measurement (EDM) device. Using trigonometry, the XYZ coordinates for the foresight can be determined relative to the coordinates of the other two points.

Various techniques were used in order to minimize errors. To reduce angular instrumen-

tal errors, the angular observation was obtained from the average of the direct and reverse measurements. Blunders in the distance measurements were minimized by taking the average distance from for separate observations. In surveying, it is very desirable to have redundant observations, which allow for the detection of erroneous measurements and allows for adjustments using least squares. As seen in Figure 5.2, where the yellow lines indicate EDM measurements between points, which are marked by triangles, every point was established using multiple observations. Observations made with a total station require intervisible points, and the baselines for every set of intervisible points in the network were observed. When determining coordinates through triangulation and trilateration, as is the case when using conventional survey techniques, geometry is an important consideration. Redundant observations should ideally be made perpendicular to one another to increase the probability of achieving high accuracies. As seen in Figure 5.2, 9 out of the 11 points in the network were established using multiple observations that were perpendicular to one another.

The survey was performed on October 14-16th, 2009, in temperatures of 0 to 10 degrees Celsius. To establish the local coordinate system, Pt. 5, centralized in the project area, was assigned the 3 dimensional coordinates, E = 10,000.00 m, N=10,000.00 m, U=1,100.00 m. Pt. 1 was used to define the rotation of the local coordinate system, with coordinates calculated using a distance measurement and an assigned azimuth of 330 degrees. Holding the coordinates for these two points fixed, Microsurvey® software was used to perform a least squares adjustment, estimating the accuracy and best possible 3-dimensional coordinates for each point. The adjustment results, including observation residuals, are presented in the Appendix, in Section B.0.2. Given the small physical size of the network, the results are desirable, with an average vertical and horizontal angular residual of 5 seconds and an average distance residual of only 2 mm.

Figure 5.1: Leica TCR803 total station, used during the in the initial creation of the survey network and establishment of the *truth* coordinates.

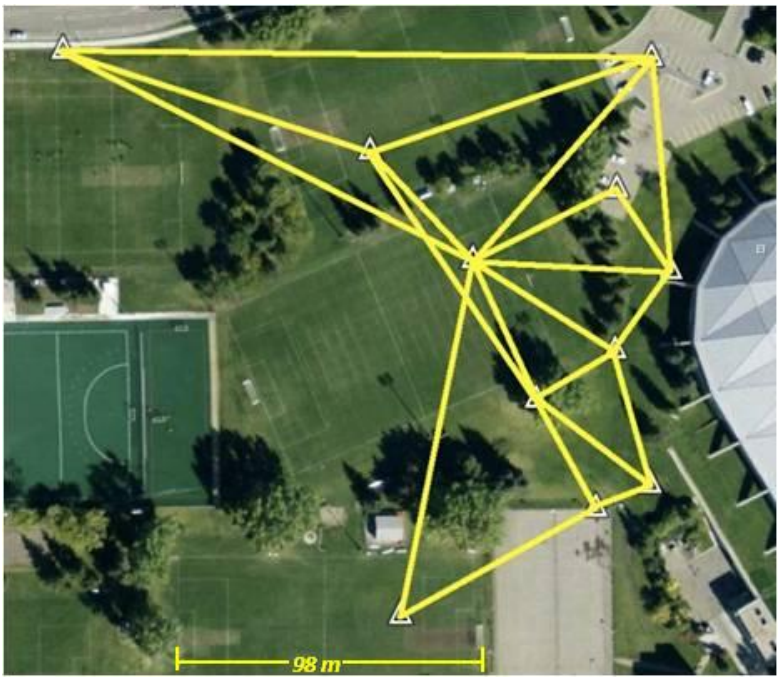

Figure 5.2: Aerial view of the survey network, and the distance measurements (in yellow) made with the total station. Triangles represent network points.

Table 5.2: Specifications for TCR803 Leica total station, see Leica Geosystems (2010).

Leica TCR803 Specifications	
Year of Make	2004-2007
Angular Accuracy	3 seconds
EDM Accuracy	2mm + 2ppm
Wavelength	780 nm
Frequency	100 mHz

5.0.2 GPS Data Collection

After truth coordinates were established for each of the points using traditional survey techniques, the survey was repeated an additional 10 times using RTK GPS. The same Trimble® R8 GNSS receivers, shown in Figure 5.3, were used during all of the GPS data collection. The proclaimed accuracy of these receivers is shown in Table 5.3. While capable of utilizing signals of multiple Global Navigation Satellite Systems (GNSS), only GPS signals were used. Both L1 and L2 GPS signals were utilized. Using Trimble's Survey Controller® software, version 12.45, data was collected using RTK mode, providing results on-the-fly, while also logging raw GPS data to the receivers for post-processing using the modified Kalman filter.

The roving receiver, the receiver used to occupy the points within the survey network of which the coordinates are desired, was leveled over the points using a 2.0 m carbon fiber rod with level bubble. A bi-pod attached to the carbon fiber rod was firmly placed into the ground to keep the receiver level over each point. To the best of the author's knowledge, the level bubble had been calibrated prior to use. The base receiver was carefully leveled over each point using a tripod. These leveling techniques were chosen in an effort to emulate the procedures typically found in the surveying industry.

Table 5.3: Accuracy of Trimble® R8 GNSS Receivers (Trimble Navigation Limited, 2009)

Trimble® R8 GNSS Proclaimed Accuracy	
Horizontal Accuracy	10 mm + 1 ppm RMS
Vertical Accuracy	20 mm + 1 ppm RMS

Figure 5.3: Trimble® R8 GNSS receiver.

In RTK surveying, there is an initialization period during where data is accumulated which is then used to resolve the ambiguity values. Once the ambiguities are resolved, the surveyor levels the roving receiver over each point that the coordinates are desired. The surveyor then stores the positional and accuracy information generated for each point during a short occupation period, as short as a single epoch. Although temporal correlation is not expected over a single epoch, the stored position and accuracy is the result of the initialization

period and other epochs of data collected previously, during which temporal correlations are likely present.

5.0.2.1 Jobs

Each of the 10 GPS surveys are referred to as a Job. As seen in Table 5.4, the Jobs were completed over a two week period. Each Job consisted of each point in the survey network being occupied once by the roving receiver, with occupation times varying between 8 and 12 minutes. Pt's. 1, 2, 3, 4, 5, 6, 9, and 11 were occupied for 8 minutes. Those with more sky obstructions, Pt's. 7, 8, and 10, were each occupied for 12 minutes to ensure the dataset was long enough to resolve ambiguities during post-processing.

Once the receiver was carefully leveled over a point, data was collected for as brief a moment as possible. In most cases, positions were established using only 1 epoch of stored data. The roving receiver would remain in place for the remaining 8 to 12 minutes, with an observation made every minute. Following Trimble's recommendations (Trimble Navigation Limited, 2001), Pt's. 1 through 4, used in the localization, were observed using a 15 second data rate. The static observations were then averaged to produce the best estimate for the coordinates of each point.

In order to evaluate how baseline length, the distance between the base and the roving receiver, affects the accuracy of RTK, three different baseline lengths were tested. The short baseline, surveyed during Jobs 1 through 5, was limited to approximately 400 metres in length. The medium baseline, surveyed during Jobs 6 through 8, was approximately 5 km in length. The longest baseline, approximately 10 km in length, was surveyed during Jobs 9 and 10.

Table 5.4: Base station locations and statistics, according to Job number.

Job	Date	Start Time	Baseline Length	Base Pt. ID
1	10/28/2009	12:30 PM	Short (~10 - 150 m)	20
2	10/28/2009	3:00 PM	Short (~400 m)	21
3	10/29/2009	5:30 AM	Short (~10 - 150 m)	20
4	10/29/2009	11:30 AM	Short (~10 - 150 m)	20
5	10/29/2009	12:30 PM	Short (~10 - 150 m)	20
6	11/5/2009	12:00 PM	Medium (~5 km)	22
7	11/5/2009	3:30 PM	Medium (~5 km)	23
8	11/6/2009	5:00 AM	Medium (~5 km)	22
9	11/13/2009	2:30 PM	Long (~10 km)	24
10	11/14/2009	5:00 AM	Long (~10 km)	24

To evaluate the effects of ionospheric error on RTK GPS accuracy, each baseline was surveyed at least once in the afternoon, when the ionosphere is typically most active, and again in the early morning hours, when the ionosphere is typically most quiet (Langley, 2000). Jobs 3, 7, and 10 were all performed during the pre-dawn hours, while the remaining Jobs were all performed during the day.

5.0.2.2 Reference Receiver

RTK GPS surveying requires the use of a secondary receiver for differencing spatially correlated errors. For each Job, the reference (base) receiver was leveled over a point, as shown in Table 5.4, located a certain distance from the project area. Similarly to the points in the survey network, each point was established using long spikes or magnetic nails marked with survey flagging. After several minutes of satellite acquisition, the coordinates of the base receiver were determined using a single-point autonomous position. Considering a single-point autonomous position is typically only accurate to a metre, the four point localization was performed at the beginning of each Job to acheive centimetre level accuracy of the roving receiver relative to the local coordinate system. To evaluate the importance of base receiver location, 2 locations were chosen, one good location and one less than opti-

Table 5.5: Description of each point occupied by reference (base) receiver, along with a photo of the point, found in the Appendix.

Pt ID.	***Baseline***	***Description***	***Photo***
20	Short	Within project area on soccer field	None Taken
21	Short	~400 m from project on rooftop	Fig. A.12
22	Medium	~5 km from project, minimal obstructions	Fig. A.13
23	Medium	~5 km from project, large trees to south	Fig. A.14
24	Long	~10 km from project, excellent visibility	Fig. A.15

mal location, for both the short and medium baselines. A description of the points occupied by the base receiver, along with a reference to a photo located in the Appendix is shown in Table 5.5.

5.0.2.3 Performing the Localization

The first four points to be surveyed during each Job were the four points to be used in the localization. As seen in Figure 5.4, these four points, Pt's. 1 through 4, were placed in locations that surrounded the remaining points. Pt. 6 was the exception, being located approximately 100 m outside of the localization area. This point was included purely to show the importance of choosing localization points on the exterior of the project area. Being only 100 m project area, which is represented in red within Figure 5.4, would not be a concern during larger projects, but given the small size of the project area (~100 m east-west x ~200 north-south), any errors in the observation of the localization points could lead to a significant error in the estimated rotation or scale parameters, which would then manifest itself in the estimated position of Pt. 6. The localization residuals produced using the commercial software, along with the 7 estimated parameters defining the coordinate transformation, are shown in Appendix Section B.0.1.

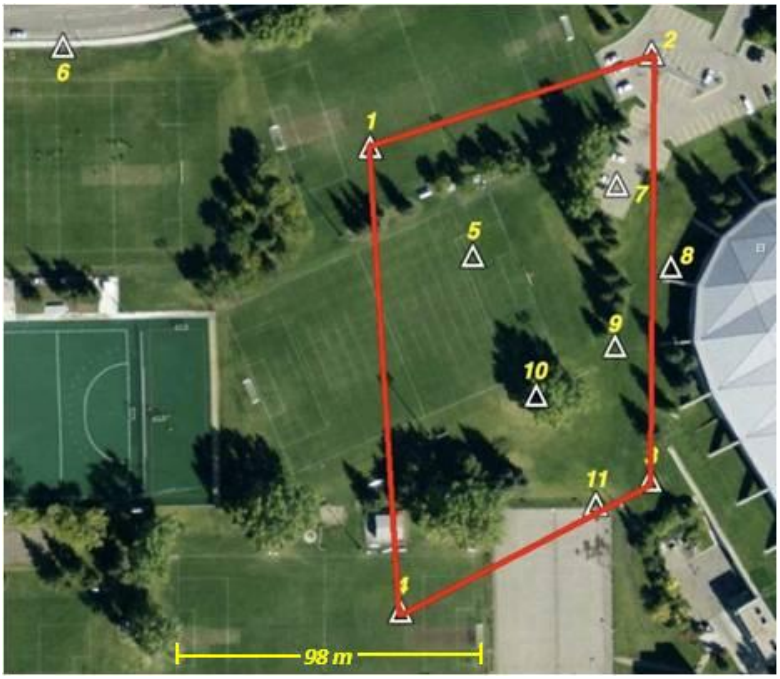

Figure 5.4: The various points (marked by triangles) that make up the survey network, and the localization area (marked in red).

5.0.2.4 Generating Results using the Modified Kalman Filter

The commercial RTK generated results were obtained straight from the data collector at the end of the survey while the results generated using the modified Kalman filter required additional work. The raw GPS data that was collected during the survey by both the base and roving receivers was converted to Receiver INdependent EXchange format (RINEX) version 2.11. These files were then read in a C++ program which implemented the modified Kalman filter to produce the estimated positions and accuracy. The stochastic model used in the modified Kalman filter is that shown in Table 3.1. Similar to the commercial RTK software, both L1 and L2 signals were utilized for both ambiguity fixing and positioning.

Using the 8-12 minute datasets for each point, the ambiguities were reinitialized every 15

seconds, with the position obtained on the final epoch before reinitialization being used within the analysis. Since professional surveyors only place confidence in fixed positions, float ambiguity solutions were filtered from the results. The fixed results for each Job were rotated from the ECEF WGS84 coordinate system to the local coordinate system, using the localization equations shown in Section D.0.4. The fixed WGS84 positions for the localization points, Pt's. 1 through 4, were rotated to the Easting, Northing, and Up (ENU) coordinate system and averaged according to Pt. ID. With the coordinates for each point being known in both coordinate systems, the 7 transformation parameters could then be determined for the transformation of the 7 remaining test points.

Comparing the truth coordinates, established using the total station and reflectors, to the GPS coordinates, established using the commercial RTK software and modified Kalman filter, the absolute errors were computed. These errors are analyzed in Chapter 6.

Chapter 6

Results

The results shown within this Chapter were obtained from using both commercially available RTK software, and software written specifically for this research, the implemented time-differencing Kalman filter. To repeat, the first motivation of this research is to determine the repeatability and accuracy of modern RTK GPS software and see if it produces realistic accuracy estimates regardless of ignoring the temporal correlations found in the observations. The second motivation is to determine whether or not the time-differencing Kalman filter is feasible for use in RTK surveying, analyze its performance, and see if more realistic accuracy estimates can be obtained.

To accomplish these tasks, an 11-point survey network was established on the University of Calgary campus, as described in Chapter 5. One of the key assumptions in this work is that the survey network coordinates, established using traditional terrestrial survey methods, are correct. The survey network was resurveyed 10 times using RTK GPS, over a period of 2 weeks. Within this Chapter, each of these resurveys is referred to as a Job. Each of the ten Jobs were performed using the same methods and procedures, and were observed using

baseline lengths ranging from 400 m to 10 km. The network was surveyed using equipment and procedures common to the surveying industry. To evaluate how the accuracy of RTK GPS in different scenarios, the observations are filtered according to Pt. ID, baseline lengths, and satellite constellation.

6.1 A Description of Statistical Measures

To clarify, there is a difference between repeatability and accuracy. Repeatability refers to the ability of RTK GPS to produce the same coordinate values, at the same location, regardless of the coordinates being correct. This can be refered to as internal consistency. To describe the repeatability of RTK GPS, the standard deviation of the mean is calculated, as shown in Equation 6.1:

$$\sigma_x = \sqrt{\frac{(x_1 - \bar{x})^2 + (x_2 - \bar{x})^2 + (x_3 - \bar{x})^2 + (x_N - \bar{x})^2}{N}} \tag{6.1}$$

where $\bar{x}$ indicates the mean value of variable x, N is the total number of samples, and σ_x is the 1-sigma standard deviation of the sample. When the distribution is normal, 68% of the samples should be contained within 1-sigma of the mean value. A small standard deviation indicates a precise (repeatable) solution, where all of the values are close to one another. A larger standard deviation indicates that the values are more spread out and that the observables likely contain large, fluctuating errors, such as multipath.

Accuracy refers to the proximity of the position estimate to the known true position. In this case, the true position is considered to be the adjusted network coordinates, obtained using the total station. When analyzing accuracy, it isn't the deviation from the mean value that is important, but instead the deviation from the true position. The root mean square is used

to describe the accuracy of the sample, as calculated in Equation 6.2. (Root Mean Square, 2010)

$$x_{RMS} = \sqrt{\frac{x_1^2 + x_2^2 + x_3^2 + x_N^2}{N}} \tag{6.2}$$

The close relationship between the root mean square (RMS) and the standard deviation (σ) is shown in Equation 6.3 Root Mean Square (2010),

$$(x_{RMS})^2 = \bar{x}^2 + \sigma_x^2 \tag{6.3}$$

which shows that the RMS will always be of larger magnitude than the standard deviation. RMS was chosen for its ability to describe the magnitude of the positional errors regardless of being positive or negative. In addition to analyzing the precision and accuracy of RTK GPS using the standard deviation and RMS values, the minimum, maximum, and mean values are used as well. The mean value simply shows the average signed (negative values considered) error and does not reveal the magnitude of the errors being averaged. Minimum and maximum describes the minimum and maximum absolute (unsigned) deviation from the *truth* network coordinate value.

6.2 RTK Commercial Software Performance

With surveyors relying on commercial RTK equipment and software everyday for engineering projects with strict specifications, it is important to know whether or not the positions are accurate, and whether or not the estimated accuracies are realistic. This section focuses solely on the accuracy and repeatability of RTK GPS, using commercially produced software. These results were not post-processed, but generated in the field. Again, all of the

procedures used to generate the results within this section are similar to those used everyday by surveyors in North America. The points occupied by the roving receiver, although each has different signal obstructions and challenges, are not meant to represent extreme examples of each environment, but meant to represent a variety of locations that surveyors would commonly consider adequate enough to occupy using GPS, without resorting to other methods.

6.2.1 Error Distributions

Figures 6.1 through 6.3 show the error distribution in the easting, northing, and vertical directions for the commercial RTK obtained positions. Each of the distributions, composed of 797 samples, appear to be normal, resembling a bell curve with a large concentration of samples at and around the mean value. By determining that the error distribution is indeed normal, this validates the use of the standard deviation and mean values to describe the precision and accuracy of the estimated positions.

Table 6.1 shows the accuracy and repeatability statistics for the combined total of all the fixed positions obtained using commercial RTK GPS. Although uncommon, errors up to approximately 10 cm and 13 cm were observed horizontally and vertically. This is a far cry from the 2 cm accuracy expected from surveyors. Regardless of the few occasions where large errors were experienced, the positions were very repeatable with standard deviations close to 1 cm horizontally and just over 2 cm vertically. The RMS errors were only slightly

Table 6.1: Commercial software RTK repeatability and absolute error statistics, using every collected observation in the 10 Jobs.

	Samples	Min (cm)	Max (cm)	Mean (cm)	σ (cm)	RMS (cm)
E	797	0	7.4	0.0	0.9	0.9
N	797	0	9.9	-0.6	1.3	1.4
U	797	0	12.9	-0.2	2.3	2.3

larger showing that, as a whole, the positions obtained using commercial RTK fit well with the traditionally obtained positions.

Note that the maximum and RMS error is significantly higher in the northing than the easting error statistics. One explanation for this is based on the latitude of the survey area. The field work was performed on the University of Calgary campus at a latitude of approximately 51.07^o *N*. Understanding that the inclination angle of the GPS orbital planes is 55^o, means that the majority of visible satellites will be located in the southern sky, poor geometry for achieving great north-south accuracy. Another explanation could be poor geometry within the truth survey network for the North-South direction.

Figures 6.4 and 6.5 compare the absolute horizontal and vertical errors generated using commercial software, to the expected accuracy as advertised by the RTK manufacturer. The blue line represents the advertised accuracy which is a function of baseline distance.

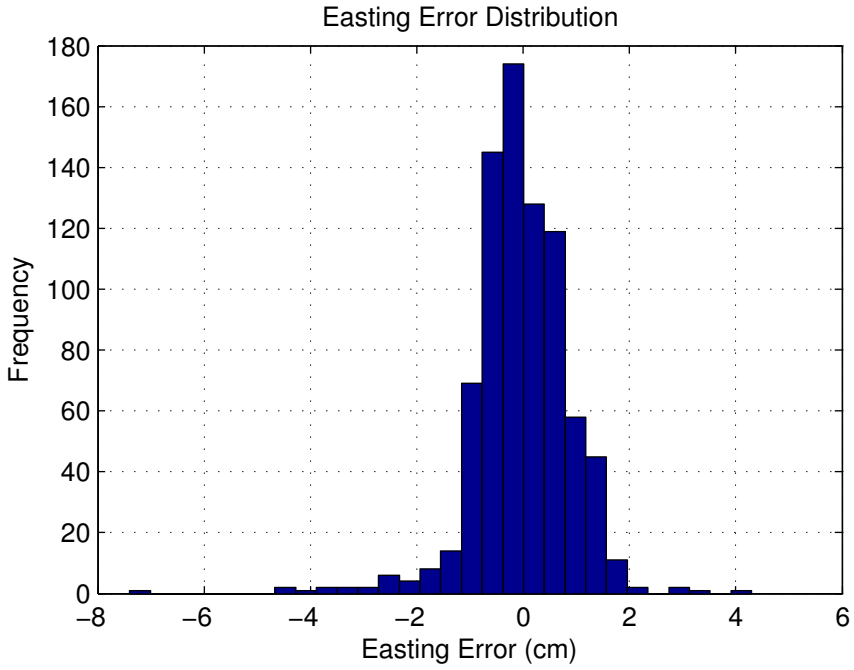

Figure 6.1: Commercial RTK easting error distribution, relative to established survey network coordinates.

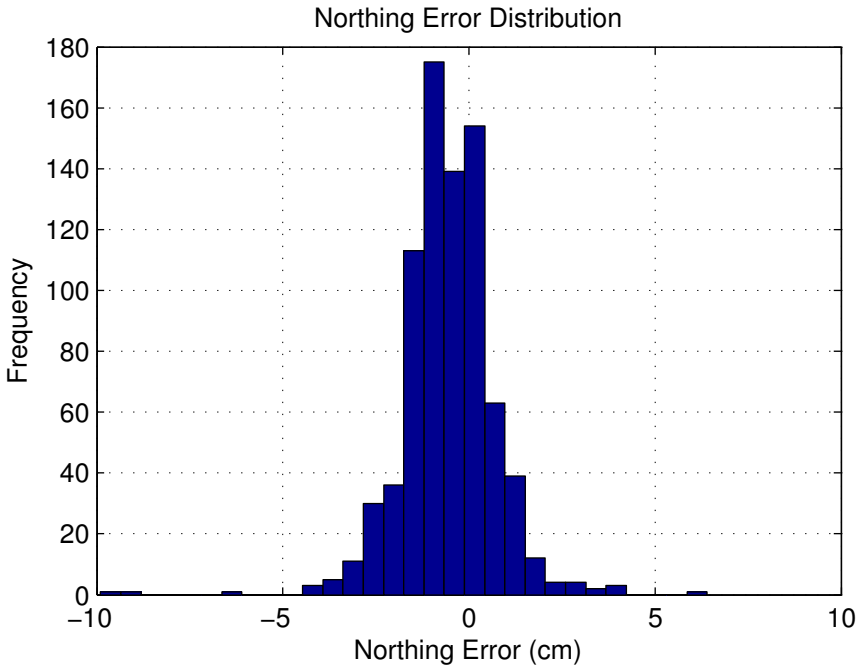

Figure 6.2: Commercial RTK northing error distribution, relative to established survey network coordinates.

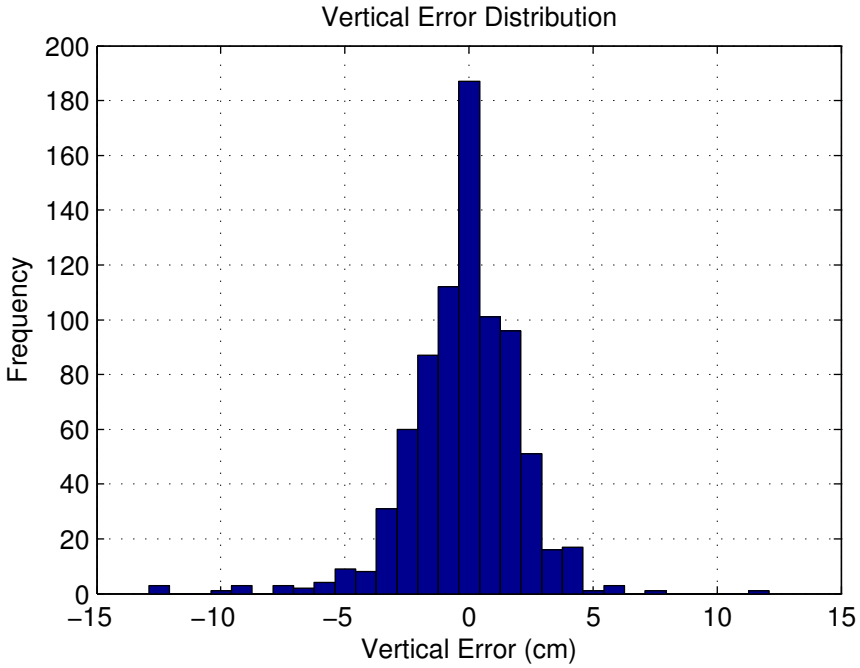

Figure 6.3: Commercial RTK vertical error distribution, relative to established survey network coordinates.

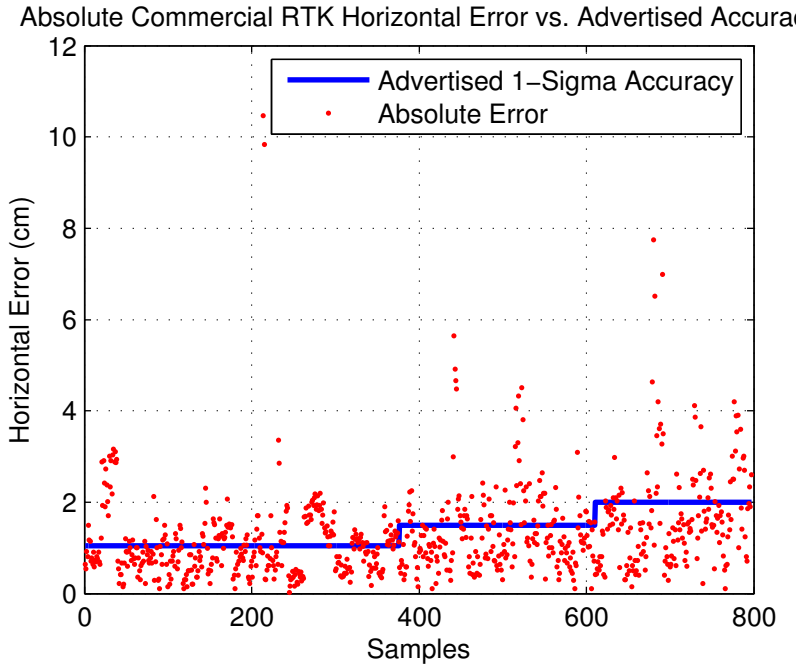

Figure 6.4: Absolute commercial RTK horizontal accuracy vs. the horizontal accuracy as advertised by the manufacturer (1 cm + 1 ppm).

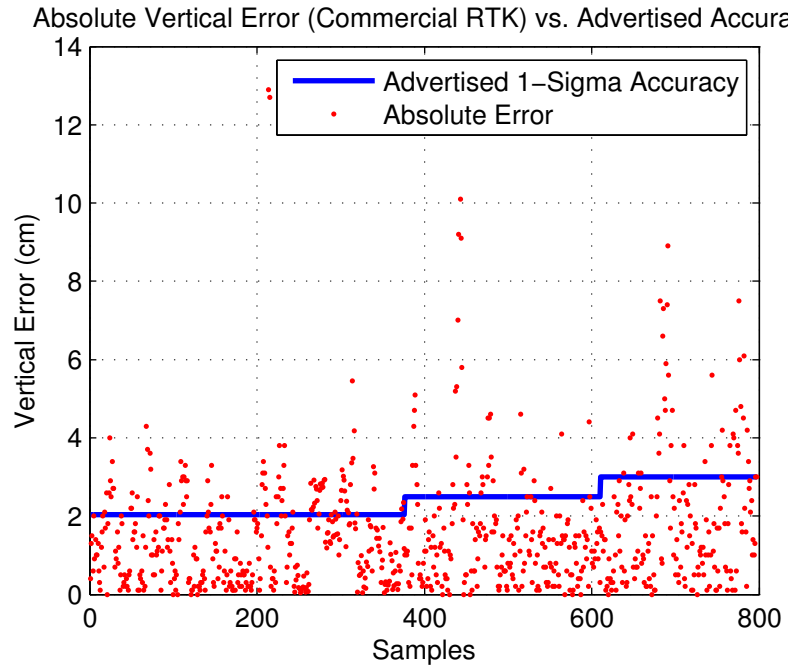

Figure 6.5: Absolute commercial RTK vertical accuracy vs. the vertical accuracy as advertised by the manufacturer (2 cm + 1 ppm).

The advertised accuracy is 10 mm + 1 ppm RMS horizontally, and 20 mm + 1 ppm RMS vertically (Trimble Navigation Limited, 2009). The variation of the blue line is due to the 3 different baseline lengths being observed. The advertised horizontal accuracy is at the 1-sigma level (39% CI) meaning that only 39% of the samples should be within this value.

Vertically the advertised accuracy at 1-sigma represents a 68% CI, different due to a comparison between a 1-dimensional value to a 2-dimensional value. As seen in Figures 6.4 and 6.5, aside from a few large outliers, the majority of the points lie within the advertised accuracies. In fact, 63% and 78% of the horizontal and vertical errors were within the advertised value, better than expected.

6.2.2 Commercial RTK: DOP vs. Accuracy

There are a number of statistical measures that surveyors can monitor in real-time to get a general understanding of the expected accuracy. One of these measures is known as the Dilution of Precision, more commonly known as the DOP value. The DOP value describes the geometry of the satellite constellation. The preferable small DOP values are achieved when satellites are evenly distributed around and above the receiver. Less desirable high DOP values occur when there are few satellites above the horizon, or when many of the satellites are concentrated within a small part of the sky. Theoretically, the achievable positioning accuracy is a linear function of the DOP value as shown in Equation 6.4 (Misra and Enge, 2001):

$$EPE_{RMS} = \sigma_{URE} \cdot DOP \tag{6.4}$$

where *EPE* is the Estimated Position Error, and *URE* is the User Range Error. URE describes the magnitude of the errors found in the satellite signals such as atmospheric errors

and multipath. Achieving high accuracy is more probable when both the satellite geometry and URE are small. According to the British Columbia Guidelines for GPS RTK Surveys(2008), an ideal DOP value for surveying is anything less than 3, with acceptable DOP values being between 3 and 6, and values larger than 6 considered not suitable for surveying. DOP is a generic term that describes one of many different calculated terms such as Position DOP (PDOP), Geometric DOP (GDOP), Horizontal DOP (HDOP), Vertical DOP (VDOP) and others. To estimate the position error in a particular coordinate direction, the DOP variable in Equation 6.4 would be replaced with the DOP parameter that describes the satellite geometry for that specific direction. For example, to determine the estimated vertical position error, the DOP variable would be replaced with VDOP. The DOP is calculated using the elements found within the design matrix, A, as seen in Equations 6.5 through 6.9 (Hofmann-Wellenhof et al., 2001; Lachapelle, 2008). In this research, only PDOP, HDOP, and VDOP are considered.

$$Qx = (A^T A)^{-1} = \begin{bmatrix} q_{xx} & q_{xy} & q_{xz} & q_{xt} \\ q_{xy} & q_{yy} & q_{yz} & q_{yt} \\ q_{xz} & q_{yz} & q_{zz} & q_{zt} \\ q_{xt} & q_{yt} & q_{zt} & q_{tt} \end{bmatrix} \tag{6.5}$$

$$PDOP = \sqrt{q_{xx} + q_{yy} + q_{zz}} \tag{6.6}$$

The calculation of PDOP is performed simply using the elements of the cofactor matrix, Qx. PDOP describes the satellite geometry for 3-dimensional positioning in the ECEF coordinate system.

$$QxL = RQ_xR^T = \begin{bmatrix} q_{xLxL} & q_{xLyL} & q_{xLzL} & q_{xLtL} \\ q_{xLyL} & q_{yLyL} & q_{yLzL} & q_{yLtL} \\ q_{xLzL} & q_{yLzL} & q_{zLzL} & q_{zLtL} \\ q_{xLtL} & q_{yLtL} & q_{zLtL} & q_{tLtL} \end{bmatrix} \tag{6.7}$$

$$HDOP = \sqrt{q_{xLxL} + q_{yLyL}} \tag{6.8}$$

$$VDOP = \sqrt{q_{zLzL}} \tag{6.9}$$

In order to calculate the HDOP and VDOP, the cofactor matrix must first be rotated to the local tangent plane coordinate system as shown in Equation 6.7, where R the same rotation matrix used to rotate the VCV matrix for the formation of the error ellipses, as shown in Section D.0.5. For additional details regarding the calculation of DOP values, see Misra and Enge (2001), Hofmann-Wellenhof et al. (2001), Lachapelle (2008), and Leick (2004).

Another source of invaluable information for the surveyor is the number of visible satellites used in the positioning solution. As in all Kalman filter and least square solutions, additional observations, satellites in this application, results in higher redundancy which enables the system to better detect measurements blunders. The removal of true blunders will result in a better, more robust, solution. The number of satellites does not have a linear relationship with the DOP. As stated earlier, very few satellites well distributed across the sky can provide good satellite geometry, while 10 or more satellites can result in a high DOP values if they are in close proximity to one another. Ideally, a user would have a high number of satellites well distributed above and around the receiver. For more information, see Lemmon and Gerdan (1999).

The error statistics for the commercial RTK obtained positions, filtered according to the number of satellites used in the solution, are shown in Table 6.2. When considering the value of the revealed statistics, it is important to consider the total number of samples collected within each dataset. More than half of the observed positions were obtained when 7 or 8 satellites were included in the solution. Observations obtained using only 5 satellites or 10 satellites were relatively rare and there may not contain enough samples to make any conclusions or comparisons to other datasets.

Table 6.2: RTK repeatability and true error statistics according to the number of satellites available during the time of observation.

	Satellites	Samples	Min (cm)	Max (cm)	Mean (cm)	σ (cm)	RMS (cm)
E	5	10	0.1	0.8	-0.4	0.5	0.6
	6	82	0.0	3.2	-0.1	0.9	0.9
	7	278	0.0	7.4	0.0	0.9	0.9
	8	223	0.0	4.5	0.0	0.9	0.9
	9	183	0.0	3.0	0.0	0.9	0.9
	10	21	0.0	1.7	-0.3	0.9	0.9
N	5	10	0.2	1.4	-0.4	0.9	0.9
	6	82	0.0	9.3	-0.5	2.1	2.1
	7	278	0.0	9.9	-0.5	1.1	1.2
	8	223	0.0	4.1	-0.8	1.0	1.3
	9	183	0.0	4.1	-0.5	1.3	1.3
	10	21	0.3	1.5	-0.1	0.8	0.8
U	5	10	0.1	2.0	-0.5	0.9	1.0
	6	82	0.0	12.7	-1.1	3.2	3.4
	7	278	0.0	12.9	0.0	2.1	2.1
	8	223	0.0	12.8	-0.6	2.2	2.3
	9	183	0.0	7.5	0.3	2.0	2.0
	10	21	0.1	2.7	0.4	1.1	1.1

Figure 6.6 shows the RMS error for the easting, northing, and vertical directions as a function of the number of satellites. Analyzing this figure, it appears that good accuracy results are more likely as the number or satellites used in a solution increases. With exception of the easting direction which remains fairly flat, the RMS error is the largest when only six satellites are available and decreases as more satellites come into the solution. The precision of the observations, revealed by the standard deviation of the mean in Table 6.2 follows this same trend. Although the probability of high accuracy increases with the number of satellites, it is not guaranteed as very low minimum errors were achieved regardless of the number of satellites.

Figure 6.7 shows the 3-dimensional position error, calculated using the square root of the sum of the squares (RSS) of the 3 error components, as a function of the calculated PDOP at the time of observation. A line was fit to the data using the least squares method. This

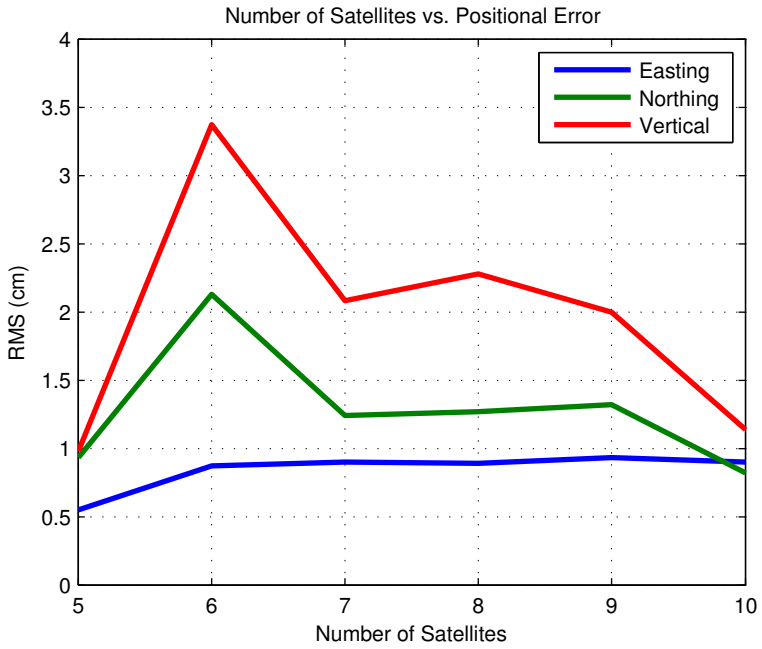

Figure 6.6: Number of visible satellites during time of observation vs. RMS error in the east, north, and vertical directions.

best fit line shows that as the PDOP decreases, there is a higher probability of achieving good positional accuracy. It is apparent that surveying during moments that the PDOP is low is not a guarantee of obtaining excellent accuracy. The worst positional accuracy was obtained while the PDOP was less than 2.0, while very desirable positional accuracies were obtained while the PDOP was greater than 4.0. This is also seen in Figures 6.8 and 6.9, where the HDOP and VDOP values are compared to the horizontal and vertical errors. In all three figures, the best fitting line reveals an upward trend as the DOP values get larger.

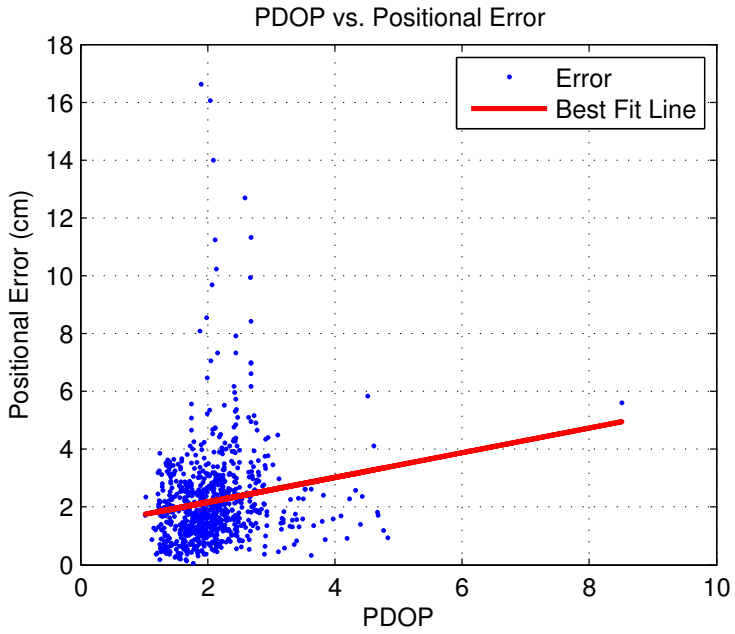

Figure 6.7: PDOP vs. 3-D positional error, with a best line fit to the data using least squares.

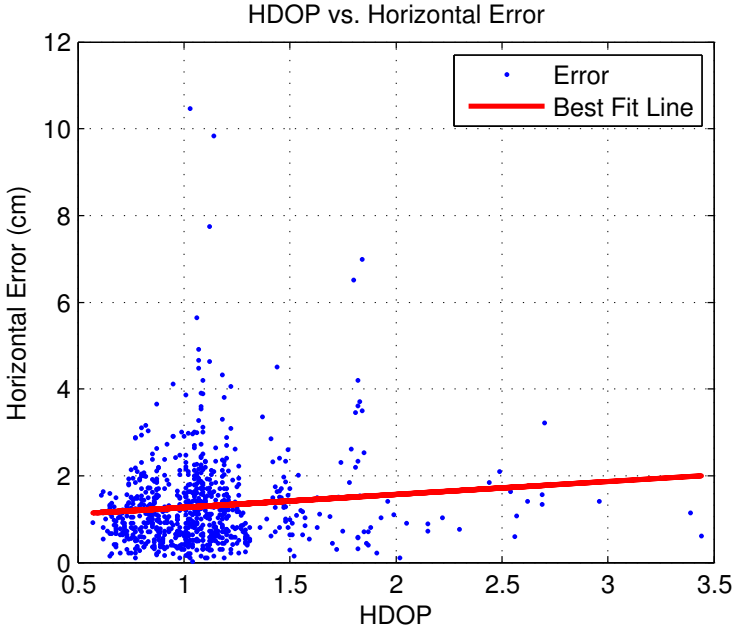

Figure 6.8: HDOP versus 2-D horizontal error, with a best line fit to the data using least squares.

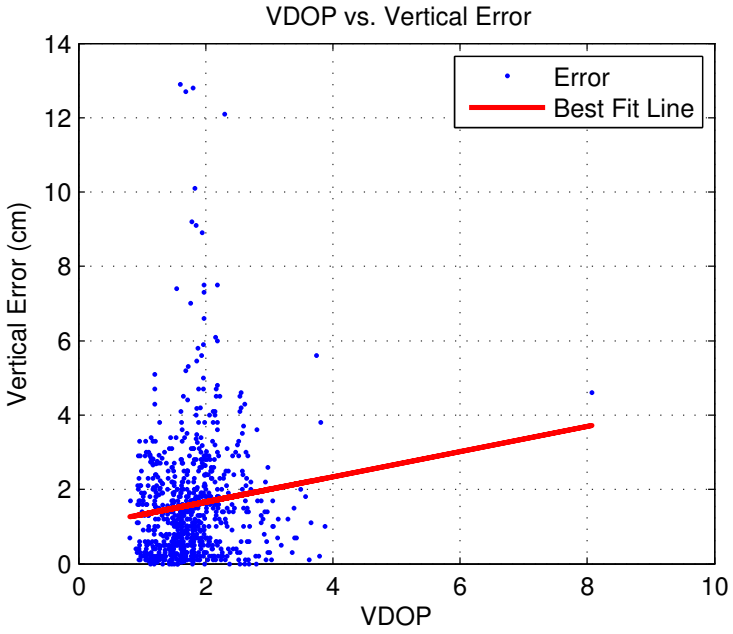

Figure 6.9: VDOP versus 1-D vertical error, with a best line fit to the data using least squares.

6.2.3 Commercial RTK: Baseline Length vs. Accuracy

Baseline length, the distance between the base and roving receivers, is an important consideration when striving to obtain sub-centimetre accuracy. As baseline length increases, spatially correlated errors, that would be mitigated over short baselines, decorrelate, gradually having a larger influence on the estimated positions.

In this research, three different baseline lengths were observed: Short, between 10 - 400 m, Medium, approximately 5 km, and Long, approximately 10 km. Table 6.3 shows the error statistics filtered according to baseline length. As seen in Table 6.3, both the standard deviation and the RMS values increase as the baseline length increases. This trend is even more apparent in Figure 6.10. It is interesting to note that the largest maximum errors

in both the north and vertical directions were observed over the shortest baseline, even though the shortest baseline had the smallest standard deviation. This shows that while the precision of the positions decreases as the baseline becomes longer, large gross errors may be experienced regardless of baseline length.

Table 6.3: RTK repeatability and true error statistics vs. the length of the baseline used during the observation: Short (<400 m), Med (~5 km), and Long (~10 km).

	Baseline	Samples	Min (cm)	Max (cm)	Mean (cm)	σ (cm)	RMS (cm)
E	**Short**	376	0.0	3.4	-0.1	0.6	0.6
	Med	234	0.0	4.5	0.1	1.1	1.1
	Long	187	0.0	7.4	0.0	1.1	1.1
N	**Short**	376	0.0	9.9	-0.6	1.1	1.3
	Med	234	0.0	4.4	-0.5	1.1	1.2
	Long	187	0.0	6.4	-0.5	1.7	1.8
U	**Short**	376	0.0	12.9	-0.2	1.9	1.9
	Med	234	0.0	12.8	-0.2	2.4	2.4
	Long	187	0.0	8.9	-0.2	2.6	2.6

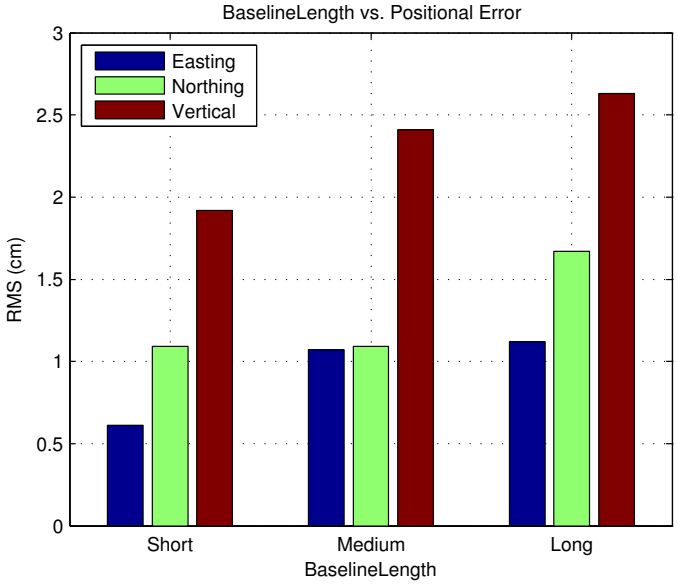

Figure 6.10: RMS errors in the east, north, and vertical directions vs. baseline length (Short = 400 m, Medium = 5 km, Long = 10 km.

6.2.4 Commercial RTK: Receiver Location

According to Hofmann-Wellenhof et al. (2001), there are three different elements that should be considered when selecting a location for performing a GPS survey. First, the location should be free of any obstructions above 20 degrees to keep satellite signal blockage to a minimum, and allow the best possible satellite geometry. Second, the location should be clear of any reflective surfaces to minimize the influence of multipath. Lastly, the location should not be within the vicinity of electrical installations to avoid difficulties in tracking the signal.

Often, the locations that RTK surveys are performed in fail to satisfy one or more of these considerations. The survey must be performed whether the environment surrounding the points is ideal or not. RTK might be chosen as an alternative to traditional survey techniques when the majority, not all, of the points to be surveyed are ideal for RTK GPS. In an effort to save time and money, the points within the project that are less ideal for GPS observations may surveyed using the same techniques. How does the environment surrounding the receiver effect the accuracy of the position?

It is important to reiterate that, within this research, none of the locations selected for RTK GPS observations have such hostile environments that GPS would not be considered. The surveyed locations represent conditions that surveyors face on an everyday basis. Table 6.4 shows the commercial RTK error statistics filtered according to Pt. ID.

Point 5 was located within an open field, within the localization area. This point represents an ideal location with good satellite geometry facilitated by an open sky, and minimized signal multipath and interference. As seen in Table 6.4, this location obtained some of the best positioning results with a horizontal RMS of less than 0.70 cm and a vertical RMS of 1.04 cm.

Table 6.4: RTK repeatability and true error statistics vs. Pt. ID.

	Pt ID	Samples	Min (cm)	Max (cm)	Mean (cm)	σ (cm)	RMS (cm)
E	5	99	0.0	2.1	0.3	0.6	0.7
	6	95	0.0	1.6	0.6	0.7	0.9
	7	124	0.0	1.9	0.0	0.6	0.6
	8	136	0.0	2.0	-0.3	0.5	0.6
	9	106	0.0	3.4	-0.1	0.8	0.8
	10	130	0.0	7.4	-0.4	1.5	1.5
	11	107	0.0	2.0	0.0	0.7	0.7
N	5	99	0.0	1.9	-0.1	0.6	0.6
	6	95	0.0	2.3	-1.1	0.6	1.2
	7	124	0.0	4.1	-1.0	0.8	1.3
	8	136	0.0	2.6	-0.1	1.0	1.0
	9	106	0.0	9.9	-0.4	1.6	1.6
	10	130	0.0	6.4	-0.3	1.9	1.9
	11	107	0.0	3.8	-1.1	1.1	1.6
U	5	99	0.0	3.8	-0.2	1.0	1.0
	6	95	0.1	5.1	-1.3	1.7	2.2
	7	124	0.0	4.6	1.0	1.4	1.7
	8	136	0.0	5.6	0.4	2.0	2.0
	9	106	0.0	12.9	0.2	2.1	2.1
	10	130	0.0	12.8	-1.1	3.4	3.6
	11	107	0.0	12.1	-0.5	2.1	2.1

Point 8 was located adjacent to a large building. This building had an interesting architecture featuring many flat, metallic, surfaces at a variety of angles. These surfaces were expected to generate large amounts of multipath. As seen in Table 6.4, the positioning results of this point were on par with the results obtained at the other positions. This reveals the unpredictability of multipath error. Multipath error is a function of many variables including surface material, surface angle, and the position of the satellite in the sky. If the receiver were located in a different location adjacent to the building, the errors at this point may have been worse. In this test, the building did not seem to affect these signals as much as expected.

Point 10, located underneath a tree canopy was expected to perform poorly. Occasionally when pressed for time, a surveyor will obtain fixed ambiguities away from trees and then try to walk the receiver to the point, located underneath the tree canopy, without losing signal lock. This practice needs to be reconsidered as the tree canopy affected the positioning

results more than any other environmental scenario. At the 1 sigma level (68% CI), the horizontal accuracy was between 1.5 and 2 cm. At the 95% CI, this accuracy nears 4 cm. Vertically the results were even worse, with a 1 sigma accuracy of more than 3.5 cm. If sub-centimetre level positioning is required where serious signal blockage is unavoidable, other survey methods should be considered more appropriate.

Points 9 and 11 performed surprisingly poor. Point 9 was located in a field with adjacent trees to the north and Point 11 was located to the north of a tall chain link fence which enclosed a tennis court. Point 9 experienced the largest maximum horizontal and vertical errors of all the points, nearly 10 cm in the northing and 13 cm in the vertical, likely due to an incorrect fix. Vertically, Point 11 performed poorly with a high standard deviation and maximum error. Although positioning next to a chain link fence provides plenty of open sky, the metallic pieces of the fence, attached at multiple angles, seem to have an impact on the receiver, likely due to short periods of signal blockage and multipath.

Point 6 was surveyed in ideal conditions, similar to Pt. 5, with the one exception being that it was outside of the localization area by approximately 100 m. When choosing a localization area, it is important to entirely surround all of the points to be surveyed. Any errors in the seven parameter transformation, performed during the localization, magnify the further one goes from the localization area.These can be errors in the GPS observations of the localization points, or errors in the establishment of the local coordinate system. The process of localizing is explained in Section D.0.4. As seen in Table 6.4, the RMS error of Point 6 was twice that of Point 5 both vertically and in the north direction.

Figures 6.11 and 6.12 show the easting error distributions, established using commercial RTK software, for Pt's. 6 and 10. The error distribution for Pt. 6 is definitely not normal. There are multiple clusters of observations, revealing that the errors observed at this location were not random. This is compared to the error distribution to Pt. 10, which experienced errors of larger magnitude, but of random nature. There are two possible explanations for this, the first explanation being the localization error. As seen in the Appendix Section B.0.1, although the same four points were consistently used in the localization process, the estimated scale factor ranged from -0.99989908 to -1.000042801. At a distance of 100 m from the survey area, the coordinates generated using these scale factors would differ by approximately 1.5 cm. Another explanation that cannot be ruled out is leveling error. A receiver is only capable of high accuracy if the surveyor can place the receiver precisely over the point. All of the GPS observations collected during this research used the identical leveling techniques. No one point should be more susceptible to leveling error than the rest. If the systematic error found in Pt. 6 was due to leveling, then it should have been experienced by other points as well.

Selection of an adequate location, as seen in these results, is a critical consideration when using RTK GPS. This is not only true for the location of the roving receiver, but of the base receiver as well, see Section 2.1.1.5. Accuracy and repeatability statistics according to the Job number and Pt. ID of the base station are shown within the Appendix, in FigureB.1. Although it is not reasonable to only use RTK GPS in perfect site conditions, surveyors need to understand that when surveying in less than ideal locations, less than ideal results can be expected.

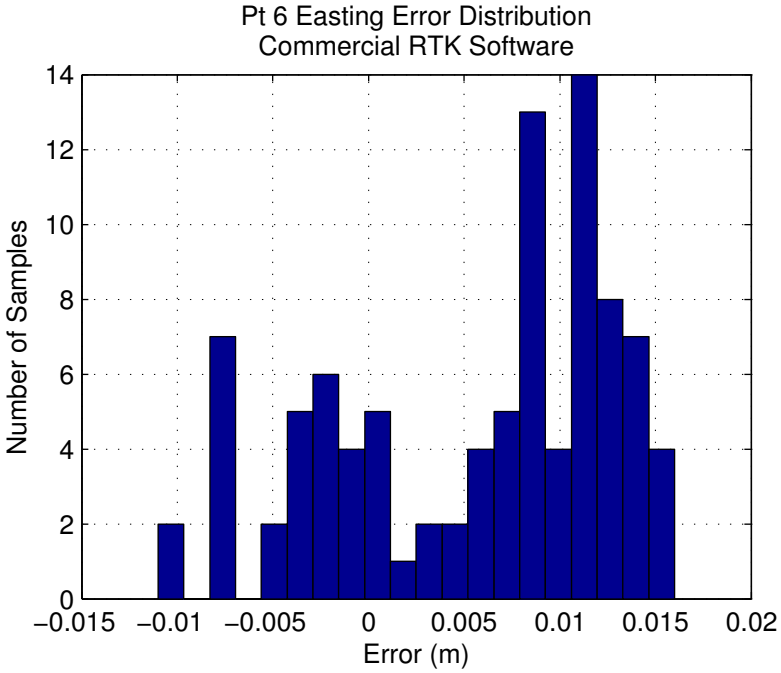

Figure 6.11: Commercial RTK easting error distribution of Pt. 6.

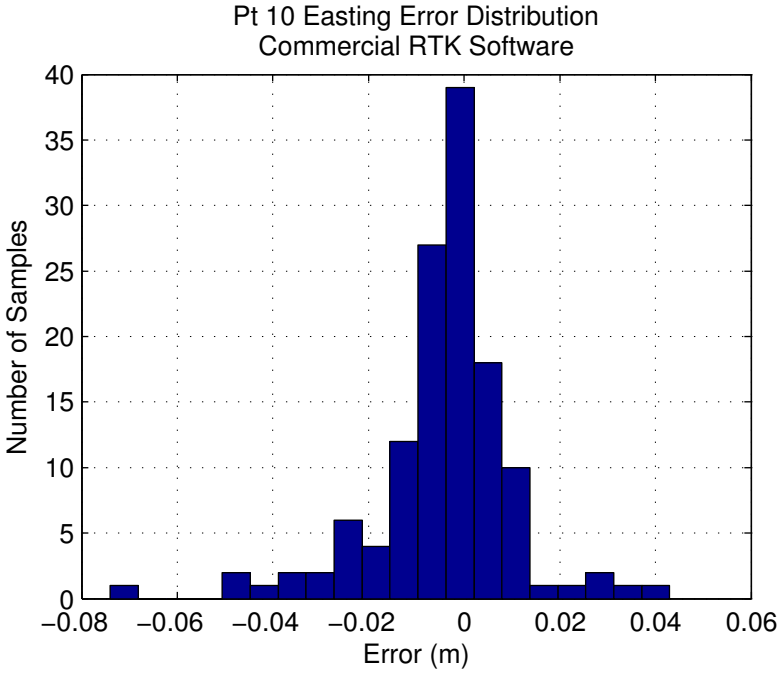

Figure 6.12: Commercial RTK easting error distribution of Pt. 10.

6.2.5 Commercial RTK: Estimated Accuracy vs. Absolute Accuracy

A key motivation of this research is to determine whether or not the estimated accuracy of a position, provided by the modern commercial RTK GPS software is realistic. A key assumption when processing GPS data with a Kalman filter is that the errors are random. Random errors are a stationary process where the mean value and variance do not depend on the chosen dataset. Random errors, void of any systematic errors, will result in a mean error of zero. Using Equation 6.3, a mean error of zero means that the estimated standard deviation equals the RMS error. Temporally correlated errors not stationary because their mean value and variance vary with the dataset. This is not to say that temporally correlated errors cannot have a mean value of zero, but depending on the dataset, a bias may be introduced. In this case, when the mean true error is not zero, the estimated standard deviation is smaller than the RMS positional error, resulting in an over-optimistic accuracy estimate.

To evaluate whether or not the estimated accuracy of a solution is realistic, 95% confidence interval (95% CI) error ellipses are used. The specifics regarding the calculation of these error ellipses is described in Section D.0.5. To summarize, a horizontal error ellipse is a function of the horizontal parameters within the VCV matrix, P. Since P is originally obtained in the ECEF WGS84 coordinate system, it first must be rotated to the local tangent plane coordinate system.

In a normal distribution, an unscaled two-dimensional error ellipse should contain the truth position within its borders ~35-39% of the time. To scale the error ellipse to the 95% CI, the semi-major and semi-minor axes are scaled by a factor of 2.45 (Ghilani and Wolf, 2006). For simplicity purposes, and to avoid the use of error ellipsoids, error ellipses are only computed for the horizontal components. To analyze whether or not the estimated vertical accuracy is realistic, the estimated vertical standard deviation is obtained from the

rotated VCV matrix. The vertical standard deviation is scaled by 1.96 to obtain a 95% CI accuracy estimate. If the 95% CI horizontal error ellipses or 95% CI vertical sigma do not contain the true horizontal or vertical positions at least 95% of the time, then P is over-optimistic, resulting in too much confidence being placed in the results. Likewise, if they contain the truth positions more than 95% of the time, then P is over-pessimistic and not enough confidence will be placed in the results. Figures 6.13 through 6.15 compare the absolute positional error to the estimated positional accuracy at the 95% CI (1.96 σ) for the easting, northing, and vertical directions.

Table 6.5 shows the percentage of horizontal positions where the truth position, the established survey network coordinates, are within the bounds of the estimated 95% CI error ellipse. For the vertical direction, Table 6.5 shows the percentage of positions where the

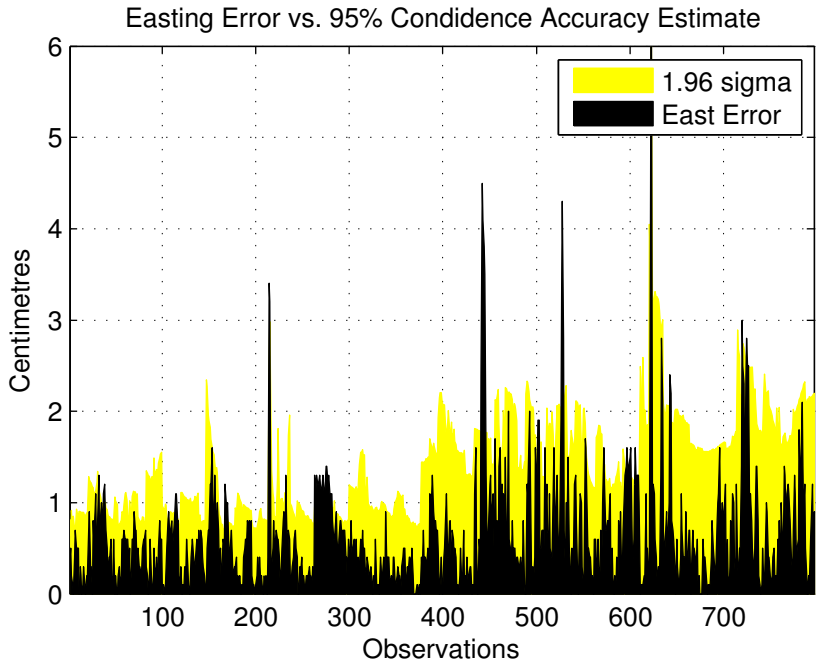

Figure 6.13: East error vs. east estimated accuracy, calculated at 95% CI (1.96-σ).

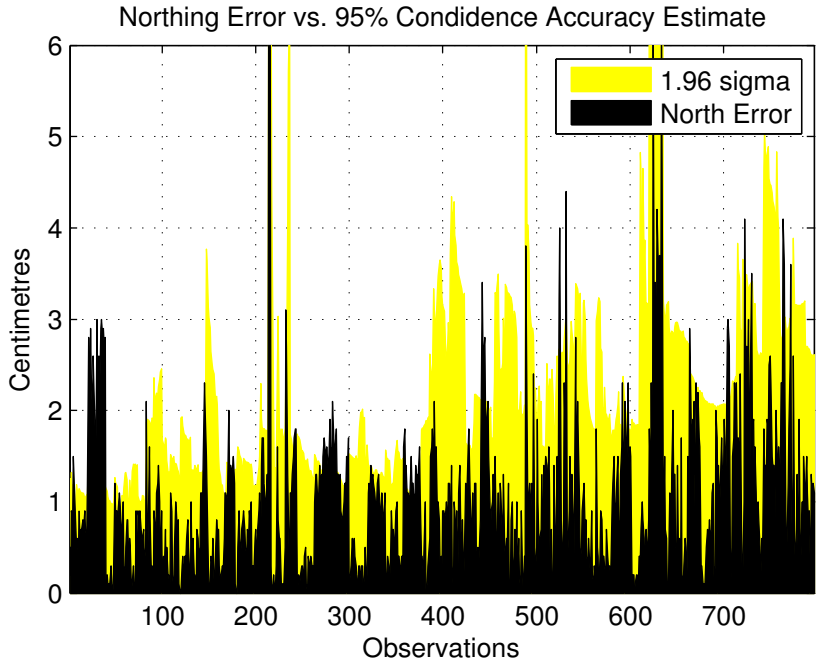

Figure 6.14: North error vs. north estimated accuracy, calculated at 95% CI (1.96-σ)

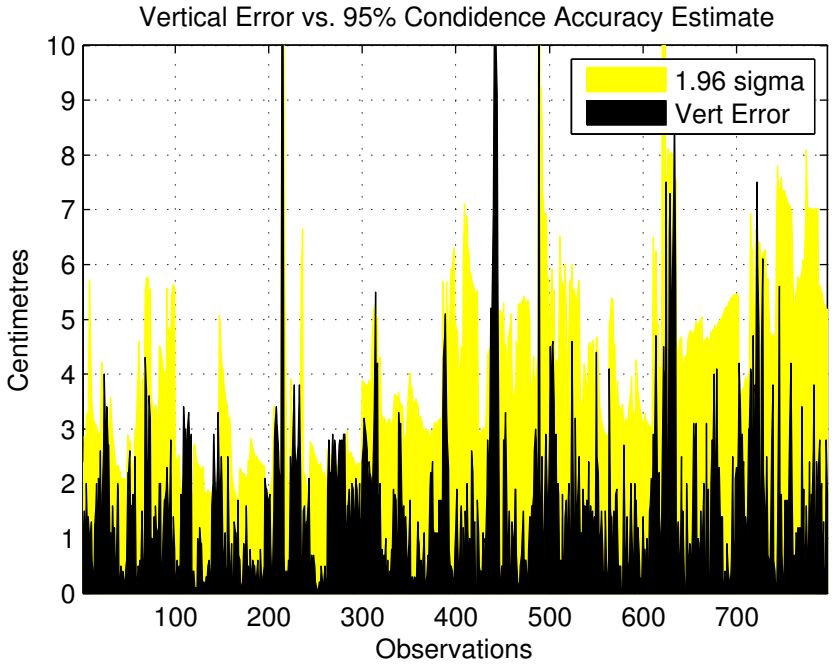

Figure 6.15: Vertical error vs. vertical estimated accuracy, calculated at 95% CI (1.96-σ)

Table 6.5: Percentage of the 95% CI Error Ellipses and 95% CI vertical accuracy estimates that contain the absolute position, as established by the truth survey network.

Data Filter		Samples	95% CI Horz. Error Ellipses Containing True Position	95% CI Vertical Sigmas Containing True Position
Pt ID	5	99	99.0%	99.0%
	6	95	64.2%	75.8%
	7	124	70.2%	97.6%
	8	136	88.2%	92.7%
	9	106	87.7%	99.1%
	10	130	75.4%	84.6%
	11	107	51.4%	96.3%
Satellites	5	10	90.0%	100.0%
	6	82	79.3%	87.8%
	7	278	87.8%	95.7%
	8	223	69.1%	91.5%
	9	183	66.7%	89.1%
	10	21	85.7%	95.2%
Baseline	Short	376	67.8%	87.8%
	Med	234	86.3%	95.3%
	Long	187	82.9%	97.3%
Total		797	76.8%	92.2%

the vertical error is smaller than the estimated vertical standard deviation, scaled to the 95% CI. The total sample of positions are once again filtered according to the Pt. ID, the number of satellites used in the solution, and the baseline length.

Figure 6.16 shows an example of this process. In this example using Pt. 8, observed during Job 4, only half of the horizontal error ellipses contain the true horizontal coordinates. Ellipses marked in red do not contain the true coordinates within their boundaries while the ellipses marked in green ellipses do. The position of each ellipse is determined by the absolute error (estimated horizontal coordinates - true network coordinates).

When analyzing the results, remember that the best case scenario is for the software to realistically estimate the error of the position. This means at 95% CI, only 95% of the

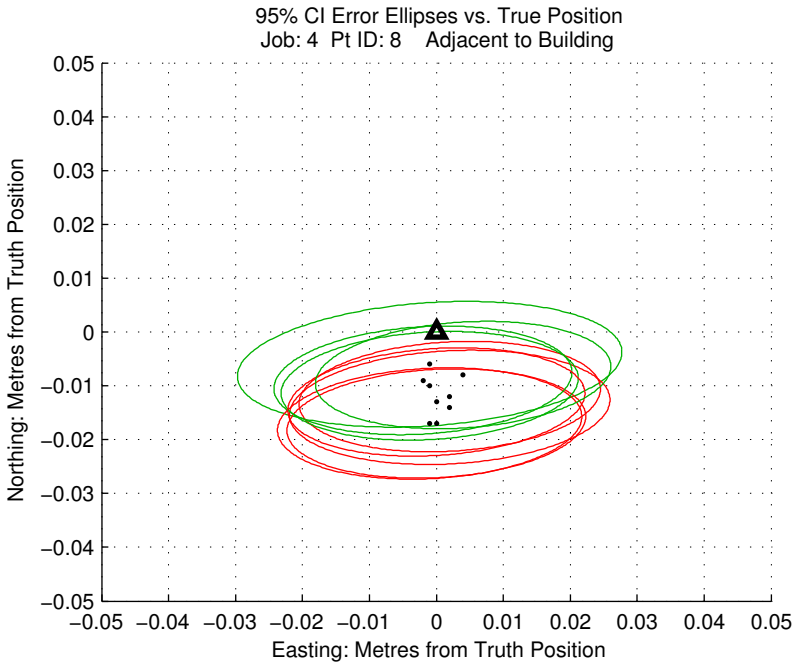

Figure 6.16: Horizontal 95% CI error ellipses generated using commercial RTK software for Pt. 8, observed during Job 4 (~100 m baseline). Green error ellipses contain the true coordinates (Marked as a triangle) within their bounds while red error ellipses do not.

horizontal error ellipses and vertical sigmas should include the true position within their bounds. Given the nature of random errors, this percentage will never be exact, but should be close. If the percentage exceeds 95%, then the accuracy estimate is over-pessimistic and the surveyor will not weight the position as much as they should. This is seen when the roving receiver observed Pt. 5, located within an open field. The stochastic model used within the commercial RTK software did not correctly reflect the characteristics of the incoming signal, resulting in an over-pessimistic estimated accuracy. In this case, there was probably too much process noise applied to overcome the effects of multipath which were likely minimal at this location.

The estimated vertical accuracy provided by this manufacturer, for the most part, are more

realistic than the estimated horizontal accuracy. Still open for debate, this may be because process noise value well selected by the manufacturer for the vertical direction.

Even though Pt. 10, being located underneath a tree canopy, experienced the worst positioning errors, the horizontal error ellipses generated for this point were more realistic than those of Pt. 6, 7, and 11. The error ellipses and vertical sigma generated were not adequately large for Pt. 6. As explained earlier, systematic errors were observed at Pt. 6, either due to leveling or localization, neither of which can be stochastically modeled. Surprisingly, only 51% of the horizontal error ellipses generated for Pt. 11 contained the true horizontal position. This point, located north of a large chain link fence, unexpectedly received far greater errors that the software was able to account for.

As seen in Table 6.5, the horizontal accuracy estimates is consistently over-optimistic. As a whole, only 77% of the horizontal error ellipses, contained the true position within their bounds. This shows that there is a problem and that surveyors should not place all of their confidence in current commercial software to provide realistic accuracy estimates. The VCV matrices must be properly scaled, or the stochastic models used within the Kalman filters must account for the temporal correlation found within the observations.

6.3 Performance of the Modified Kalman Filter

To determine whether or not more realistic accuracy estimates could be obtained by accounting for temporal correlation, the time-differencing modified Kalman filter was implemented using the C++ programming language. For information regarding this filter, see Chapter 3. The raw data used in this comparison is identical to the data used to generate the commercial RTK results (see Section 6.2), the only difference being that the commercial RTK results were generated on-the-fly with the commercial software, while these results

were post-processed using the specially written C++ software. The ambiguities were reset every fifteen seconds to provide an independent sample. Without reinitializing, the solutions from the static and modified Kalman filter processing modes would not have moved due to the minimal process noise added to the filter. The position and accuracy estimates used within the analysis were obtained using the final values before the reinitialization.

For reasons to be explained later (Section 6.3.4), solutions which were obtained using incorrectly fixed ambiguities were removed from the results. These were detected by positional errors greater than 15 cm in at least one direction. In almost all cases, these cases were easily identified by large errors (>0.5 m) in all three directions. The results for Pt. 6 were also removed from the analysis. This judgement was made because Pt. 6 contained systematic errors due to leveling or localization issues, not errors related to GPS signals.

6.3.1 Processing Styles

An important aspect in determining whether or not the modified Kalman filter is a valid option for use in RTK surveying is comparing its accuracy to other processing methods. Not knowing the exact details regarding the stochastic models used within the commercial software, the results generated using the modified Kalman filter are compared against results using the same software, but without temporal correlation accounted for in the observation modeling. As seen within Table 6.6, three different processing styles were chosen for this comparison, each of which uses different parameters to model the observations.

The modified Kalman filter (MKF), the filter upon which this research is most interested, separates the measurement noise (MN) into both white and correlated components. The magnitude of these noise components is open for debate, but for this research, values were selected based upon Misra and Enge (2001) and the filter tuning shown in Section 3.2. To

Table 6.6: Selected stochastic parameters for the three different processing styles. (PN = Process Noise, MN = Measurement Noise, T = Temporal Correlation)

Filter Tuning						
Type	Observable	PN (cm/sec)	MN (cm)			T (sec)
			Total	White	Correlated	
MKF	Pseudorange	0.0075	-	15	85	60
	Carrier Phase		-	0.2	0.8	
RTK	Pseudorange	5	100	-	-	0
	Carrier Phase		1	-	-	
Static	Pseudorange	0.0075	100	-	-	0
	Carrier Phase		1	-	-	

describe the amount of temporal correlation found within the observations, a correlation time, *T*, was also selected based upon tests shown within Chapter 4. To allow for kinematic movement, the process noise parameter was set at the highest value possible before the filter would stop converging. Due to very little observability within the modified Kalman filter, the selected process noise value is very small, and therefore more appropriate for static surveying. For more on the establishment of the stochastic model used within the modified Kalman filter, see Section 3.2.

The RTK processing style strives to emulate those results found within commercial RTK GPS software. To allow for the kinematic movement seen in RTK, the process noise was increased to 5 cm. To make a valid comparison to the modified Kalman filter, the measurement noise parameters used in the RTK processing style equal the sum of the white and correlated measurement noise components used within the modified Kalman filter. The correlation time, T, not accounted for in the RTK processing style, was set to zero.

A static GPS processing style is also used in this comparison. Static, in this sense, does not refer to long occupation times using a slow data rate, but refers to the process noise being set to a very small value not conducive to kinematic movement. The static processing style uses the same parameters as the RTK style but will less process noise, in this case, the

same amount of process noise used in the MKF processing style. The static processing style, similar to the other two processing styles, uses a data rate of 1 Hz.

6.3.2 MKF: Accuracy and Repeatability

6.3.2.1 Error Distribution

Figures 6.17 through 6.19 show the distribution of the easting error, as determined by the MKF, RTK, and Static processing styles. The northing and vertical error distributions are included in the Appendix in Section C. As seen in Figures 6.17 and 6.18, the easting error distribution for the MKF and RTK processing styles appear to be normal. The mean value is close to zero with relatively few samples significantly above or below the mean. This is not the case with the Static easting error distribution, shown in Figure 6.19. The mean

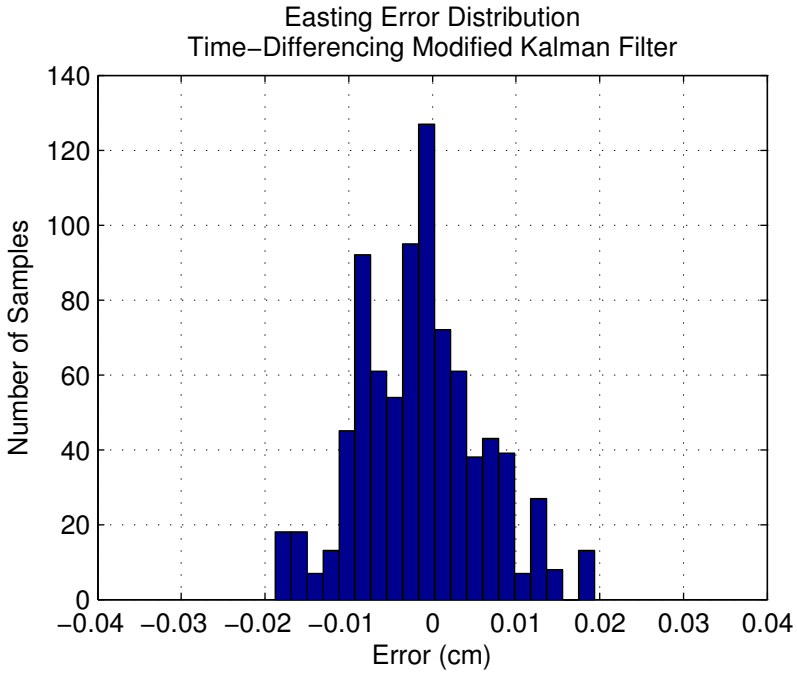

Figure 6.17: East error distribution using the time-differencing modified Kalman filter.

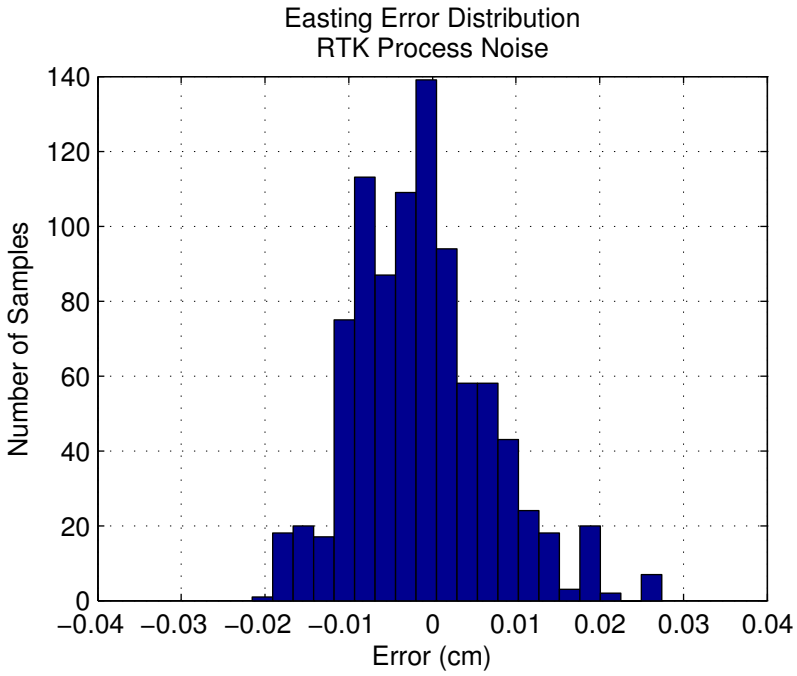

Figure 6.18: Easting error distribution using the RTK processing style (Additional process noise).

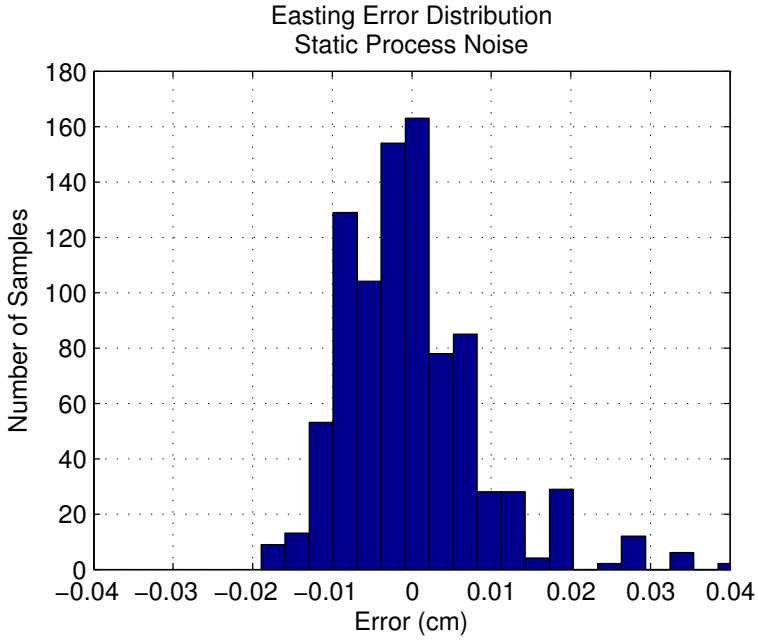

Figure 6.19: Easting error distribution using the Static processing style (Minimal process noise).

value is still close to zero with the majority of samples clustered around the mean, but there is significant number of outliers clustered around between 3 and 4 cm.

Table 6.7 shows the accuracy and repeatability statistics generated with the three processing styles using all of the samples. Bold and italicized values represent the best between the three styles. The modified Kalman filter was very accurate, achieving the smallest mean errors for the north and vertical directions, and the smallest standard deviations in the easting and northing directions.

Table 6.7: Accuracy and repeatability statistics for each of the three processing styles. **Bold** and *italicized* values represent the best result between the three processing styles.

Style	Samples		Min (cm)	Max (cm)	Mean (cm)	σ (cm)	RMS (cm)
MKF	838	E	0.0	***1.9***	-0.1	***0.7***	***0.7***
		N	0.0	***3.5***	***-0.5***	1.0	***1.1***
		U	0.0	7.1	***0.0***	1.8	1.8
RTK	906	E	0.0	2.7	-0.1	0.8	0.8
		N	0.0	***3.5***	***-0.5***	1.0	1.1
		U	0.0	6.1	-0.1	1.7	1.7
Static	899	E	0.0	4.1	***0.0***	0.9	0.9
		N	0.0	4.2	-0.7	1.1	1.3
		U	0.0	***5.9***	-0.1	***1.7***	***0.7***

6.3.2.2 Accuracy vs. Pt. ID

Table 6.8 shows the accuracy and repeatability statistics for the three different processing styles, filtered according to Pt. ID. There is no clear conclusion in terms of which processing style performed the best on a specific point. For all observations made on Pt. 11, located adjacent to a chain link fence, one could argue that the MKF style was most accurate horizontally, while the static processing style performed the best vertically. In general, the MKF and Static processing styles were the most accurate, followed by the RTK style.

Table 6.8: Repeatability and true error statistics vs. Pt. ID for the MKF, RTK, and Static processing styles. **Bold** and *italicized* values represent the best result between the three processing styles.

		MKF					RTK					Static				
	Pt ID	Min (cm)	Max (cm)	Mean (cm)	σ (cm)	RMS (cm)	Min (cm)	Max (cm)	Mean (cm)	σ (cm)	RMS (cm)	Min (cm)	Max (cm)	Mean (cm)	σ (cm)	RMS (cm)
E	**5**	0.0	***1.9***	***0.3***	***0.8***	***0.8***	0.0	2.7	0.4	1.0	1.1	0.0	4.1	0.6	1.2	1.3
	7	0.0	***1.2***	-0.2	***0.5***	***0.5***	0.1	1.4	-0.2	0.6	0.6	0.0	2.9	***-0.1***	0.8	0.8
	8	0.1	1.8	-0.5	0.7	0.9	0.0	1.9	-0.5	0.7	0.8	0.0	***1.5***	***-0.3***	***0.6***	***0.7***
	9	0.0	***1.5***	***0.2***	0.5	0.5	0.0	1.6	***0.2***	0.6	0.6	0.0	***1.5***	0.3	***0.4***	***0.5***
	10	0.0	***1.9***	-0.7	0.7	***0.9***	0.0	2.2	-0.7	0.7	1.0	0.0	***1.9***	-0.7	***0.6***	1.0
	11	0.0	***1.2***	0.3	***0.5***	***0.5***	0.0	1.5	0.0	0.7	0.7	0.0	***1.2***	***0.0***	0.7	0.7
N	**5**	0.0	***1.5***	-0.4	***0.6***	0.7	0.0	1.6	***-0.3***	0.6	***0.6***	0.0	4.2	-0.4	1.0	1.1
	7	0.0	***2.7***	***-0.9***	***0.7***	***1.1***	0.0	2.9	***-0.9***	0.7	***1.1***	0.0	4.1	-1.1	0.9	1.4
	8	0.0	***3.1***	***-0.3***	0.9	1.0	0.0	3.2	-0.4	***0.9***	1.0	0.0	***3.1***	-0.8	0.9	1.2
	9	0.0	2.0	0.2	0.8	0.8	0.0	2.0	0.2	0.8	0.8	0.0	***1.4***	***0.1***	***0.7***	***0.7***
	10	0.1	3.5	-0.5	1.6	1.7	0.0	3.5	-0.3	***1.5***	***1.5***	0.0	***3.4***	***-0.2***	1.6	1.6
	11	0.0	***2.4***	***-1.1***	***0.6***	***1.3***	0.0	3.2	-1.5	0.9	1.7	0.0	3.1	-1.5	0.9	1.7
U	**5**	0.0	3.4	***-0.4***	1.1	1.2	0.0	3.6	-0.5	1.1	1.2	0.0	***3.0***	-0.5	***1.1***	***1.2***
	7	0.1	3.1	0.7	1.1	1.3	0.0	***2.7***	0.7	1.1	1.3	0.0	***2.7***	0.7	***1.0***	***1.2***
	8	0.0	7.1	0.3	2.6	2.6	0.0	6.1	***0.1***	2.4	2.4	0.0	5.9	***0.1***	***2.4***	***2.3***
	9	0.0	3.4	***0.1***	***0.8***	***0.9***	0.0	***3.0***	***0.1***	1.0	1.0	0.0	3.1	0.2	0.9	0.9
	10	0.0	5.5	***-0.4***	2.5	2.6	0.0	***5.1***	-0.5	***2.4***	***2.4***	0.0	5.7	***-0.4***	2.5	2.5
	11	0.0	***2.6***	-0.6	1.1	1.2	0.0	3.1	-0.6	1.0	1.2	0.0	2.7	-0.6	***0.9***	***1.1***

6.3.3 MKF: Estimated Accuracy vs. Absolute Accuracy

Just as important as understanding the absolute accuracy of modified Kalman filter, is understanding whether or not the VCV matrix of the estimated states is properly scaled to produce realistic accuracy estimates. In this section, similar to Section 6.2.5, 95% CI error ellipses are formed from the VCV matrix using each of the three processing styles: MKF, RTK, and Static. Theoretically, if the error distribution is normal (see Section 6.3.2) and the VCV is properly scaled, then the 95% CI error ellipses should contain the true coordinates within their bounds 95% of the time. Figures 6.20 through 6.22 show an example of the horizontal error ellipses analyzed in this section for each processing style. Error ellipses plotted in green contain the true coordinates, marked as a triangle. Error ellipses plotted in red fail to contain the true coordinates within their boundary. The scattered points plotted in black represent the estimated coordinates over which the error ellipses are centered.

Figure 6.20 shows the 95% CI error ellipses produced for Pt. 10, located underneath a tree canopy, during Job 2 using the modified Kalman filter. The error ellipses are properly scaled, with a few of the error ellipses barely containing the true coordinates. Compare this to Figure 6.21, produced using the RTK processing style, and Figure 6.22, produced using the Static processing style. While using the RTK processing style, where process noise is added to the filter to allow for kinematic movement, the horizontal error ellipses are so large they can be considered over-pessimistic. On the other hand, the Static processing style, where very little process noise is added within the filter, produces error ellipses that are over-optimistic, as reflected in the large number of error ellipses that fail to contain the true coordinates.

Table 6.9 shows the percentage of 95% CI horizontal error ellipses that contain the truth coordinates within their bounds. In the case of vertical accuracy, Table 6.9 shows the

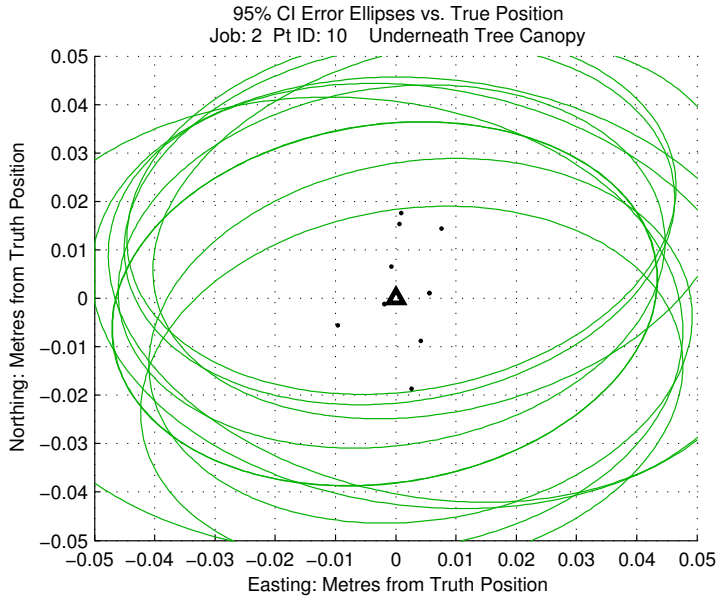

Figure 6.21: Horizontal error ellipses (95% CI) produced using the RTK processing style. Green error ellipses contain the true coordinates (Marked as a triangle). Red error ellipses do not contain the true coordinates.

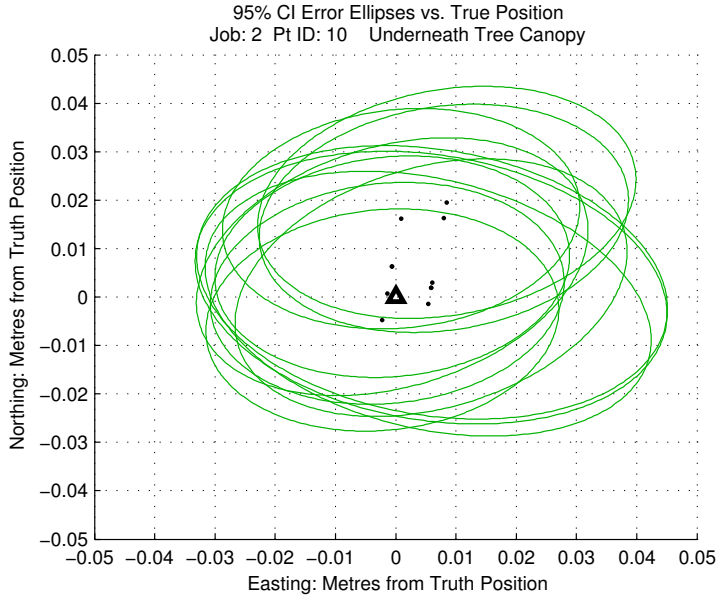

Figure 6.20: Horizontal error ellipses (95% CI) produced using the MKF. Green error ellipses contain the true coordinates (Marked as a triangle). Red error ellipses do not contain the true coordinates.

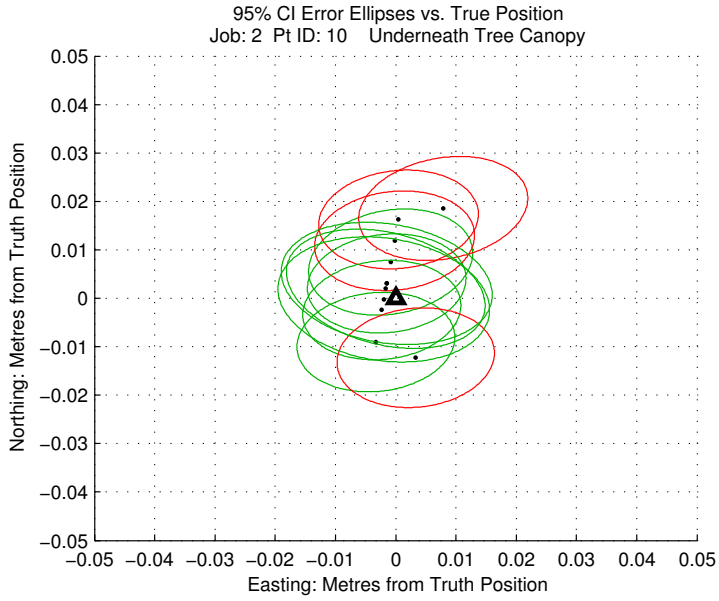

Figure 6.22: Horizontal error ellipses (95% CI) produced using the Static processing style. Green error ellipses contain the true coordinates (Marked as a triangle). Red error ellipses do not contain the true coordinates.

percentage of time that vertical error is less than the estimated vertical accuracy, scaled to 95% CI (1.96-σ). The results are filtered according to the Pt. ID, and baseline length.

As seen in Table 6.9, between the three processing styles, the modified Kalman filter produced the most realistically scaled VCV matrices. As a whole, the 95% CI horizontal error ellipses and 95% CI vertical sigmas contained the true horizontal and vertical coordinates approximately 94% of the time. This is compared to those produced using the RTK processing style which contained the true coordinates both horizontally and vertically between 99% and 100% of the time. The Static processing style produced drastically over-optimistic estimated accuracies which contained the true coordinates in the range of 60-75% of the time.

Table 6.9: Percentage of the 95% CI Error Ellipses and 95% CI vertical accuracy estimates that contain the absolute position, as established by the truth survey network, for the MKF, RTK, and Static processing styles.

Data Filter		Samples	95% CI Horz. Error Ellipses Containing True Position	95% CI Vertical Sigmas Containing True Position
MKF				
Pt ID	5	149	100.0%	100.0%
	7	144	97.9%	100.0%
	8	191	97.4%	93.7%
	9	124	100.0%	100.0%
	10	123	70.7%	69.1%
	11	107	92.5%	99.1%
Baseline	Short	453	93.4%	91.4%
	Med	398	91.5%	92.5%
	Long	110	93.6%	92.7%
Total		838	93.8%	93.9%
RTK				
Pt ID	5	182	100.0%	100.0%
	7	138	100.0%	100.0%
	8	215	100.0%	100.0%
	9	126	100.0%	100.0%
	10	104	99.0%	93.3%
	11	141	100.0%	100.0%
Baseline	Short	500	99.8%	100.0%
	Med	411	100.0%	98.3%
	Long	150	100.0%	95.3%
Total		906	99.9%	99.2%
Static				
Pt ID	*5*	182	78.6%	79.7%
	7	138	50.0%	72.5%
	8	215	73.0%	65.6%
	9	126	77.0%	92.9%
	10	97	34.0%	38.1%
	11	141	31.2%	83.0%
Baseline	*Short*	493	65.1%	68.2%
	Med	374	52.7%	77.0%
	Long	150	62.0%	53.3%
Total		899	60.4%	73.1%

Focusing on how the results varied according to Pt. ID, it is interesting to note that modified Kalman filter did not perform as well as expected during observations of Pt. 10. One possible explanation for this is based on the chosen length of temporal correlation. The same length of temporal correlation (T = 60 sec) was used regardless of the point being occupied. This chosen value is a generalization and will not always accurately reflect the specific signal characteristics observed at each point. In the case of Pt. 10, the length of temporal correlation may have been longer than estimated, while in the case of Pt. 5, located in an open field where little multipath is expected, the selected length of temporal correlation may have been too long, as seen in the over-pessimistic error ellipses.

During the field work, the roving receiver would remain motionless for up to 15 minutes while centered over each point. The receiver was physically static during these observations and no process noise should be necessary to allow for kinematic movement. When using a static rover to collect data, the static processing style should be an ideal choice. As seen in Table 6.9, this is not the case as the static mode fails to model the temporal correlation found within the observations. If temporal correlation in GPS ceased to exist, then the static processing style would likely produce the most realistic error ellipses, and would be identical to the modified Kalman filter using a correlation time of zero seconds.

The RTK processing style reveals an alternative method for dealing with the temporal correlations found within the GPS observations. By simply adding process noise to the VCV matrix in the Kalman filter, the VCV matrix can be inflated to a point that the estimated accuracies are no longer over-optimistic. In the case of the RTK processing style used in this research, so much process noise was added that the error ellipses became over-pessimistic. The method of enlarging the VCV matrix is a choice that RTK software manufacturers must make. The temporal correlation in the observations can be estimated using a generalized T value, and accounted for using the modified Kalman filter, or extra process noise can be

added to the VCV in an attempt to overcome the effect of ignoring the correlation.

6.3.4 MKF: Ambiguity Resolution

A critical part of RTK surveying is the correct identification of the integer ambiguities. Improper selection will result in a large positional error that is unaccounted for by the estimated accuracy. The probability of selecting the correct set of integer values can be estimated using the PCF, explained in detail within O'Keefe et al. (2006); Cao (2009). The positioning software written for this research, as well as commercial RTK software, will not attempt to fix the ambiguities until the PCF reaches a certain level. For reliability reasons, in commercial software, the confidence in successful ambiguity resolution must be very high (99.9%) before an attempt is made (Trimble Navigation Limited, 2009). Often, in addition to the PCF value, a ratio test must also be met (see Teunissen and Verhagen (2009)).

Figure 6.23 shows the estimated PCF value as a function of time, computed using the modified Kalman filter with different values for the length of temporal correlation, T. As the length of temporal correlation increases, it takes longer and longer to achieve a certain PCF value. This is also seen in Table 6.10, which shows the length of time it takes to reach a 95% PCF. Apart from the length of temporal correlation, T, the stochastic parameters chosen for the MKF are those found in Table 6.6. When no temporal correlation is included (0 sec), the PCF value quickly obtains 95% probability after only 5 seconds. By changing the length of correlation time to 1 second, the length of time required to reach 95% PCF doubles. Doubling the length of temporal correlation more than doubles the length of time required to meet a certain PCF.

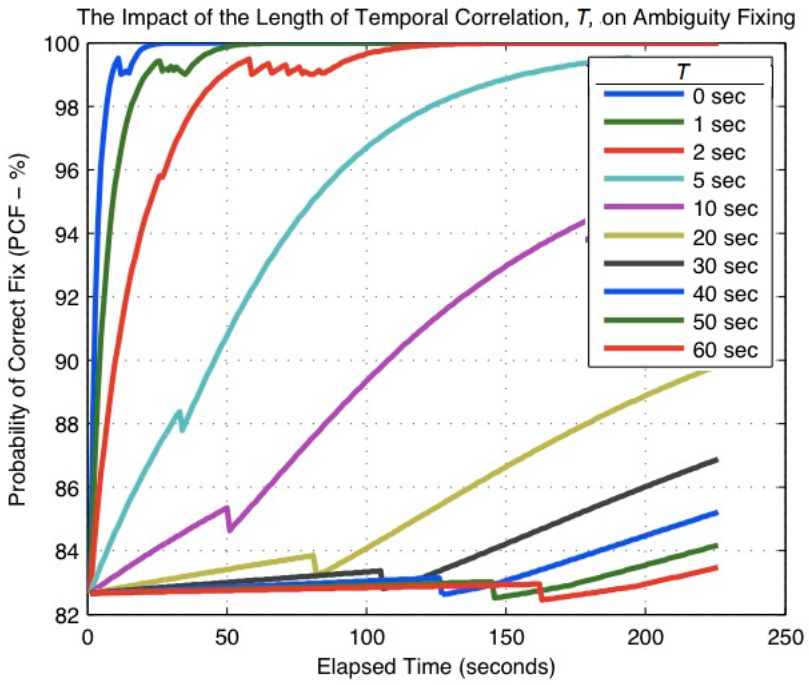

Figure 6.23: PCF vs. time, using different values for temporal correlation, *T*, for the modified Kalman filter.

As seen in Figure 6.23, as the length of temporal correlation reaches 10 seconds and beyond, a desirable (aka. high) PCF becomes harder and harder to obtain. With the relatively short 15-minute observation spans used within the field work of this research, a 99.9% PCF, or any value close to 99.9%, was not achievable. For this reason, all of the results shown in Section 6.3, pertaining to the MKF, RTK, and Static processing styles, were fixed ambiguity positions obtained using a very low PCF requirement of only 30%. This meant that there were a quite a few occasions where the integer ambiguities were incorrectly fixed. The samples which used incorrectly fixed ambiguities were removed from the dataset under

Table 6.10: Length of time it takes to obtain a PCF of 95%, using the modified Kalman filter with different temporal correlation values, *T*.

Length of Time to Obtain 95% PCF					
T (sec)	0	1	2	5	10
Elapsed Time (sec)	5	10	26	81	195

the assumption that they would not have occurred if a higher PCF requirement were used. These erroneous samples were detectable by large positional errors of 15 cm or greater in multiple position components. Tables 6.11 and 6.12 were created before the samples with incorrectly fixed ambiguities were removed from the dataset.

Table 6.11 shows the number of times the ambiguities were incorrectly fixed according to the processing style and Pt. ID. The modified Kalman filter experienced the lowest percentage of incorrect fixes, less than half that of the other two processing styles. Although the required PCF was very low, with temporal correlation accounted for in the Kalman filter, the estimated PCF is more realistic than it would be if temporal correlations were ignored due to an improperly scaled VCV matrix, see O'Keefe et al. (2006). Pt. 10, located underneath the tree canopy, experienced the greatest number of incorrect fixes, a further example of the risk involved when surveying in that type of environment. Without a knowledge of the absolute error or truth coordinates, an incorrect fix can be very difficult to detect, requiring a resurvey.

Table 6.12 shows the percentage of the 95% CI Error Ellipses and 95% CI vertical accuracy estimates that contain the absolute position, for the MKF, RTK, and Static processing styles, with the incorrect fixes remaining in the dataset. With the incorrectly fixed ambiguities included in the dataset, the RTK processing style becomes the ideal choice, with 95% of the horizontal and vertical accuracy estimates being greater than the true accuracy. With these errors remaining in the solution, the error ellipses generated using the MKF become over optimistic.

One of the greatest unsolved challenges in using the modified Kalman filter to account for temporal correlation, is being able to reliably resolve the ambiguities to their integer values. Using the equations shown in this research, when the length of temporal correlation exceeds 10 seconds, there is not enough observability in the remaining measurements to produce

Table 6.11: Number of times the ambiguities were incorrectly fixed (ICF) for each of the three processing styles, according to Pt. ID.

Process Style	Pt. ID						Total ICF / Total Samples	Percentage of Sample
	5	7	8	9	10	11		
MKF	1	4	1	1	7	2	**16** / 886	1.8%
RTK	1	4	3	0	28	4	**40** / 946	4.2%
Static	1	3	3	0	27	5	**39** / 945	4.1%

Table 6.12: Percentage of the 95% CI Error Ellipses and 95% CI vertical accuracy estimates that contain the absolute position, as established by the truth survey network, for the MKF, RTK, and Static processing styles. Positions established using incorrectly fixed ambiguities are included in this dataset.

	Total Samples	95% CI Horz. Error Ellipses Containing True Position	95% CI Vertical Sigmas Containing True Position
MKF	886	87.1%	92.7%
RTK	946	95.6%	95.0%
Static	945	56.6%	68.5%

reliable estimates for the float ambiguities and resolve them to their integer values with great confidence. Although the MKF outperformed the other two processing styles in terms of the percentage of incorrect fixes when only a 30% PCF value was required, the RTK and Static processing styles have enough observability to obtain a 99.9% PCF value before fixing, a requirement which would result in drastically fewer cases of incorrectly fixed ambiguities for these two processing styles. To become a viable option for commercial RTK software, the MKF must be capable of reliable ambiguity resolution 99.9% of the time.

6.3.5 MKF: Satellite Residuals

This Section shows the effect that the modified Kalman filter has on the satellite residuals. For this analysis, it is desirable to use a satellite pair that experienced some multipath, resulting in a dataset where the observations were sufficiently time correlated to see a difference in the residuals.

By subtracting the carrier phase observable from the pseudorange observable, multipath errors in the pseudorange observable can be detected. By differencing, errors that are common to both signals are eliminated, such as satellite and receiver clock errors, tropospheric error, and satellite position errors. Remaining errors include phase and code multipath, receiver noise, twice the ionospheric error, and the ambiguity term. Carrier phase multipath error is very small relative to pseudorange multipath so only pseudorange multipath is detectable using this method.

The observables from satellite PRN pair 3-7, observed during Job 3 on Pt. 11, were differenced, shown in Figure 6.24. The remaining errors show slow fluctuations in time, indicating that multipath error was observed in pseudorange observable, an indication that the carrier phase signal was effected by multipath as well and is temporally correlated.

Going back to Chapter 4, it was through an analysis of satellite residuals, using the autocorrelation function, that temporal correlation was detected. If the modified Kalman filter is properly implemented, then the temporally correlated errors should be mitigated through time differencing, resulting in residuals that are whiter in appearance.

Figure 6.25 shows the residuals from PRN pair 3-7, observed during Job 3 while the receiver was located on Pt. 11, using both the MKF and Static processing styles. Unlike the results shown in previous sections, the ambiguities in this dataset were not reinitialized every 15 seconds. The residuals from the MKF, shown in blue, appear to be random with

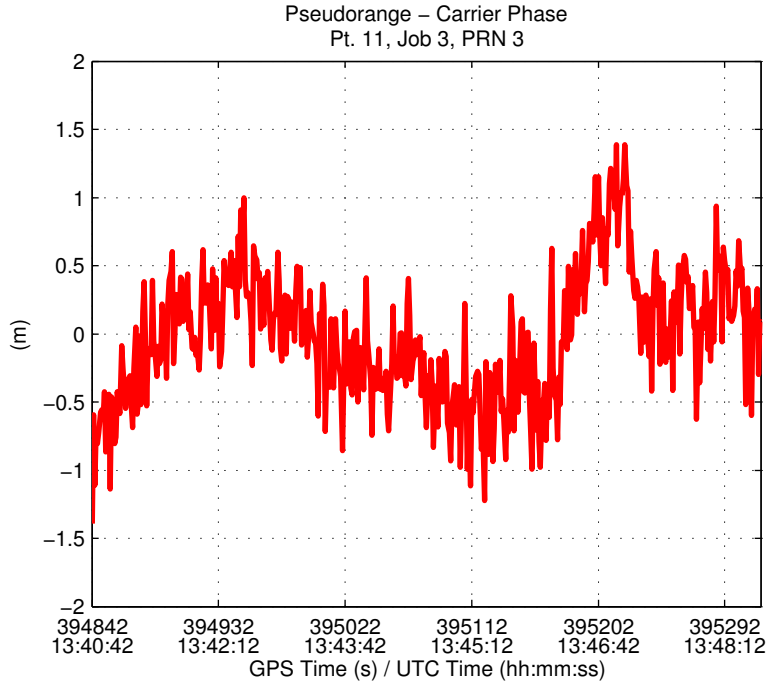

Figure 6.24: Pseudorange observable minus the carrier phase observable. PRN pair 3-7, from observation of Pt. 11, Job 3.

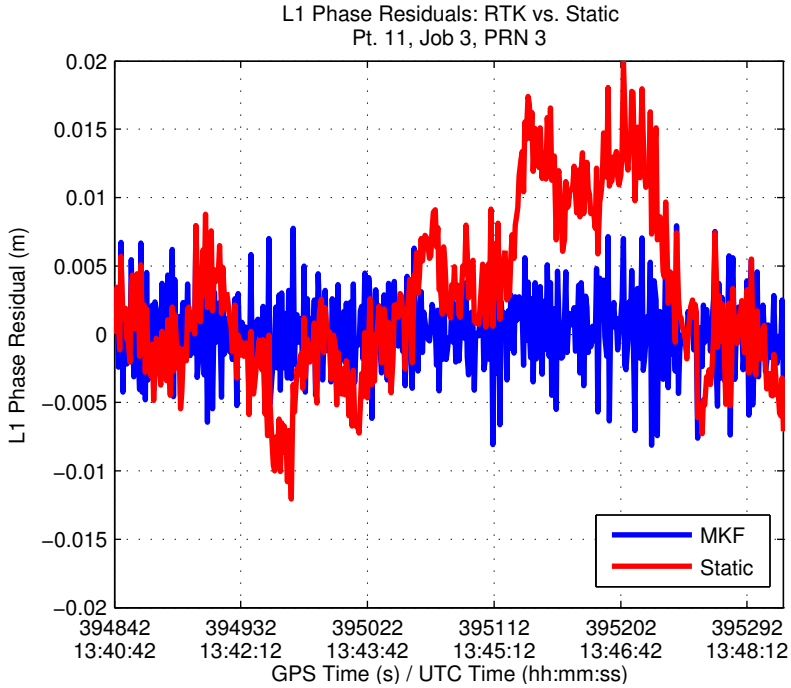

Figure 6.25: L1 carrier phase residuals using the MKF and static processing styles. PRN pair 3-7, from observation of Pt. 11, Job 3.

time but also appear to be noisy. The residuals from the Static processing style appear temporally correlated and less noisy than those produced using the MKF.

The additional noise can be attributed to the law of covariance propagation, Equation 2.8. Assuming that a correlation time, T, of 60 seconds, best models the temporal correlation in the observations, the estimated correlation coefficient is 0.983 (calculated using the exponential function in Equation 2.14) for a lag of 1 epoch. Assuming a random walk model, where the transition matrix is identity, the resulting difference operator, $\left(\frac{\delta f}{\delta \Phi}\right)$, used to difference the design matrix between epochs, is shown in Equation 6.10.

$$\left(\frac{\delta f}{\delta \Phi}\right) = \begin{bmatrix} 1 & -0.983 \end{bmatrix} \tag{6.10}$$

Applied to the law of covariance propagation results in Equation 6.11:

$$C_{MKF} = C_{\phi}^{1} + 0.966 \cdot C_{\phi}^{2} = \begin{bmatrix} 1 & -0.983 \end{bmatrix} \begin{bmatrix} C_{\phi}^{1} & 0 \\ 0 & C_{\phi}^{2} \end{bmatrix} \begin{bmatrix} 1 \\ -0.983 \end{bmatrix} \tag{6.11}$$

where C_{ϕ}^{1} and C_{ϕ}^{2} are the VCV matrices that stochastically model the double difference observations at epochs 1 and 2. Varying in magnitude with the estimated correlation time, T, when time-differencing observations, the observations become noisier, resulting in the residuals being noisier as well.

6.3.6 Slower data rate vs. Modified Kalman filter

A widely accepted method of dealing with temporal correlation in static surveying is slowing down the data rate. When selecting a data rate, the goal is to only update the Kalman filter with fully independent observations, observed after any temporal correlation from a previously used observation has passed. Theoretically, slowing down the data rate should produce the same results as those produced by the modified Kalman filter.

To repeat from Section 4.2.2.2, there is a key difference between the length of time between fully independent observations, used to determine an appropriate static surveying data rate, and the length of temporal correlation used in the modified Kalman filter, *T*. In this research, *T* is the variable used to create an exponential function, shown in Equation 2.14, which best models the autocorrelation results established from the L1 carrier phase residuals (see Chapter 4). It was shown in Figure 4.5 that using a temporal correlation time, *T*, of 5 seconds, assumes that independent data is not obtained until 20 seconds have elapsed, see Section 4.2.2.2.

Figure 6.26 compares the estimated 1-sigma accuracy for the latitude established using three different processing methods, all of which use the same amount of process noise: The modified Kalman filter, with a *T* value of 5 seconds, a static filter using a 0.05 Hz data rate, and a static filter using a 1 Hz data rate. The static filter with the 1 Hz data rate, which uses the incorrect assumption that the data is completely independent after only one second, produces a very small accuracy estimate that is likely over-optimistic. The modified Kalman filter, which eliminates information that is assumed to be redundant through time-differencing, produces a much larger estimated accuracy. The static filter with the 0.05 Hz data rate (the Kalman filter updates with new information every 20 seconds), produces a estimated accuracy that eventually converges to the same magnitude as that of the modified Kalman filter.

If by simply reducing the data rate the same results can be obtained, then why use the modified Kalman filter? It must be understood that the modified Kalman filter is not limited to surveying applications. The filter may be the most beneficial when used in other applications where the data rate is considered more critical. An example of such an application is (INS) GPS integration where it is essential to update the position solution as often as possible. When dealing with time-correlated observations by reducing the data rate, no

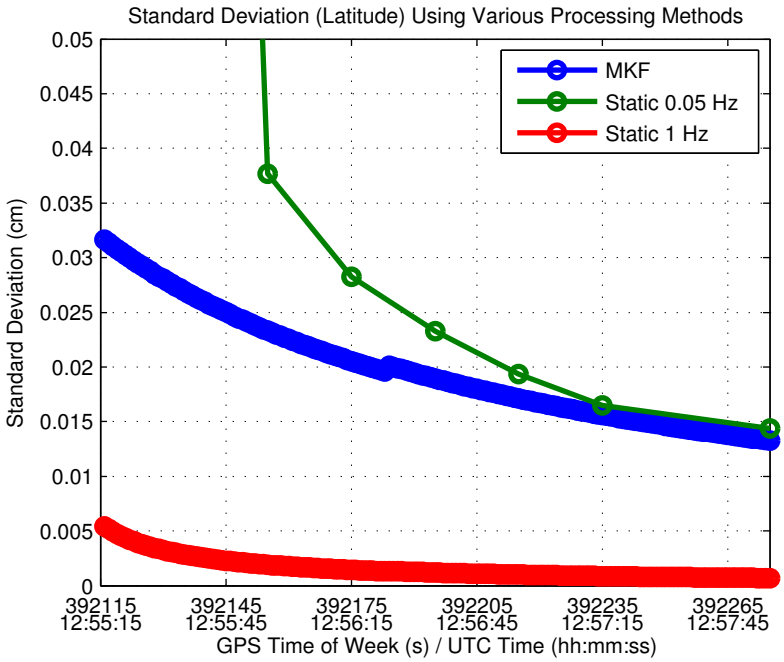

Figure 6.26: Estimated standard deviation for the latitude using three different processing methods: The modified Kalman filter (T = 5 seconds), Static (little process noise) with a 0.05 Hz data rate, and Static with a 1 Hz data rate.

new information is brought into the filter until enough time has elapsed to consider the observations fully independent. In the modified Kalman filter, the same results are obtained while utilizing the small amounts of new information that are available in each epoch. The position can be updated once a second instead of once every 20 seconds, a benefit in RTK surveying and other applications alike.

Chapter 7

Conclusions and Future Work

7.1 Key Findings and Conclusions

The drive behind this research was to accomplish two things: To analyze the accuracy of modern commercial RTK software and see if it is capable of producing realistic accuracy estimates regardless of ignoring the temporal correlation found within the GPS observables, and to test the time-differencing modified Kalman filter presented by Petovello et al. (2009) to see if it produces better results and performs well enough for use in everyday survey tasks. The following were key findings in the course of this research:

Key Findings

- In this research, commercial RTK software was used for positioning on a survey network of known coordinates. The advertised positional accuracy according to the manufacturer was 1 cm + 1 ppm horizontally and 2 cm + 1 ppm vertically. These accuracies were verified in this research using multiple observations of seven points.

The accuracy of RTK generated position depends on where the point is located. Points underneath tree canopies and adjacent to chain link fences are especially susceptible to poor accuracies.

- Commercial software, which generally does not model the temporal correlation found in the GPS observables, produced over-optimistic estimated accuracies. Only 77% of the 797 total samples produced 95% CI error ellipses that contained the true horizontal coordinates. The estimated vertical accuracy was more realistic. Surveyors should not rely on the estimated accuracy to reflect the absolute accuracy. VCV matrices produced using commercial software should be de-weighted/scaled.

- L1 carrier phase data was collected over baselines up to 10 km in length. Temporal correlation was detected in the residuals using the autocorrelation function. Baseline length, when kept under 10 km, did not play a factor in how long the observable was correlated, but the satellite elevation angle did. When using baselines of 10 km or less, the multipath error, due to the environment surrounding the receiver, was the largest contributor of temporal correlation.

- The modified Kalman filter eliminates temporally correlated errors by differencing the observations over time. Any redundant information within the consecutive observations is eliminated, leaving only new information to update the states. As the amount of temporal correlation increases, there is not enough new information contained within the consecutive epochs to update the states and allow the filter to converge. One of the byproducts of this lack of observability is that process noise cannot be added to the filter to facilitate kinematic movement.

- The time-differencing Kalman filter is shown to be a very accurate form of positioning. By time-differencing temporally correlated errors, the satellite residuals become

whiter, but also noisier. Regardless of the extra noise, the accuracy of the modified Kalman filter was on par with other data processing methods.

- By eliminating redundant information found within consecutive observations using the time-differencing modified Kalman filter, the VCV matrix, containing information regarding the statistical quality of the states, is more realistic. 94% of the 838 total samples produced 95% CI error ellipses that contained the true horizontal coordinates. The estimated vertical accuracy is equally as realistic. The modified Kalman filter produced more realistic VCV matrices than commercial RTK software, or other processing methods.

- It was found that as the length of temporal correlation increased, ambiguities became harder and harder to fix with great confidence. As T exceeds 10 seconds, there is not enough observability to obtain a high PCF (99.9%). Regardless of not being able to achieve a high PCF, the modified Kalman filter still experienced fewer incorrectly fixed ambiguities than other processing styles. These results may reveal that achieving a high PCF is not possible when the observations are correlated, again showing that confidence placed in the ambiguity resolution by commercial software is over-optimistic.

Conclusions

The time-differencing modified Kalman filter performed extremely well. It produced VCV matrices that realistically described the absolute error within the system. Despite its performance, there are a few key implementation issues that need to be resolved to make the filter practical for use by surveyors:

First and foremost, is the difficulty in obtaining a high confidence in the ambiguity resolution. Understanding the dramatic errors that occur when ambiguities are incorrectly fixed, it is a situation that surveyors cannot allow to occur often. They need to know that ambiguities will be resolved correctly 99.9% of the time. Another issue is that of state observability. When time-correlated errors are present, so much of the information is differenced that there is hardly any left to update the states. This makes performing RTK positioning, which uses process noise to allow for kinematic movement, impractical for the modified Kalman filter. Perhaps these two issues cannot be resolved but can be used as an awakening, that in reality, when the GPS observables are time-correlated, there isn't enough observability to update the states or obtain a high PCF. Assuming the observables are independent leads to false confidence in the solution.

The most practical application for the modified Kalman filter is not when the receiver is moving, but when the surveyor is occupying a point. When the receiver is located on a point, the surveyor could initiate the modified Kalman filter to account for any temporal correlation observed during the occupation. Understanding that the largest contributor is multipath, which is dependent on receiver position, it is likely that during moments of kinematic movement, there is very little time-correlation in the GPS observables and the modified Kalman filter isn't as critical during those periods. Moments that the receiver is static is when the modified Kalman filter is most beneficial.

7.2 Future Work

There is always more knowledge that can be obtained about a certain subject. This research topic is abundant with additional work that can be performed and the following are a few examples:

- An independent analysis was made on the L1 carrier phase signal to determine whether or not the signal was temporally correlated. An exponential function was fit to the autocorrelation results to estimate a value for the temporal correlation, T, to be used in the modified Kalman filter. A similar analysis could be made on the pseudorange observable, and the L2, and L3 (ionosphere-free) signals.

- The temporal correlation of the satellite residuals was only analyzed during periods that the receiver was static. The temporal correlation within satellite residuals generated using a receiver in motion could also be analyzed.

Bibliography

Bakula, M., Oszczak, S., and Pelc, R. (2009). Performance of RTK Positioning in Forest Conditions: Case Study. *Journal of Surveying Engineering*, 135(3):125–130.

Barnes, J., Ackroyd, N., and Cross, P. (1998). *Stochastic Modelling for very High Precision Real-Time Kinematic GPS in an Engineering Environment*. Proceedings of FIG XXI International Conference, Brighton, U.K. 19-25 July, 1998. pp. 61-76.

Boey, S., Coombe, L., Gerdan, G., and Hill, C. (1996). Assessing the Accuracy of Real Time Kinematic GPS Positions for the Purposes of Cadastral Surveying. *The Australian Surveyor*, 41(2):109–120.

Borre, K. and Tiberius, C. (2000). *Time Series Analysis of GPS Observables*. Proceedings 13th Int. Tech Meeting of the Satellite Division of the Institute of Navigation, ION-GPS 2000. Salt Lake City, 15-18, 19-22 September. pp. 1885-1894.

British Columbia (2008). *Province of British Columbia (BC) Guidelines for GPS RTK Surveys, Including Operating within a Municipal Active Control System Area, version 1.1*. Province of British Columbia, Ministry of Agriculture and Lands, Crown Registry and Geographic Base Branch. Victoria, BC. May 2008. pp. 1-19.

Brown, R. and Hwang, P. (1997). *Introduction to Random Signals and Applied Kalman Filtering, 3rd Edition*. John Wiley & Sons, Inc.

Bryson, Jr., A. and Henrikson, L. (1968). Estimation Using Sampled Data Containing Sequentially Correlated Noise. *Journal of Spacecraft and Rockets*, 5(6):662–665.

Cao, W. (2009). Multi-Frequency GPS and Galileo Kinematic Positioning with Partial Ambiguity Fixing. Master's thesis, Department of Geomatics Engineering, University of Calgary, Calgary, Alberta, Canada. pp. 142.

Correlation (2009). *Merriam-Webster Online Dictionary*. [Online] Retrieved August 10, 2009 from http://www.merriam-webster.com/dictionary/correlation.

Craymer, M., Wells, D., Vanicek, P., and Devlin, R. (1990). Specifications for Urban GPS Surveys. *Surveying and Land Information Systems*, 50(4):251–259.

Datta-Barua, S., Doherty, P., and Delay, S. (2003). *Ionospheric Scintillation Effects on Single and Dual Frequency GPS Positioning*. Proceedings of ION GPS/GNSS 2003. Portland, OR, September 9-12, 2003. pp. 336-346.

El-Mowafy, A. (2000). Performance Analysis of the RTK Technique in an Urban Environment. *The Australian Surveyor*, 45(1):47–54.

El-Rabbany, A. (1994). *The Effect of Physical Correlations on the Ambiguity Resolution and Accuracy Estimation in GPS Differential Positioning*. PhD thesis, Department of Geodesy and Geomatics Engineering Technical Report, No. 170, University of New Brunswick, Fredericton, New Brunswick, Canada, 161 pp.

El-Rabbany, A. and Kleusberg, A. (2003). Effect of Temporal Physical Correlation on Accuracy Estimation in GPS Relative Positioning. *Journal of Surveying Engineering*, 129(1):28–32.

El-Rabbany, A. and Kleusberg, A. (2004). Efficient Algorithm for Inverse of the Fully Populated Covariance Matrix in Global Positioning System Relative Positioning. *Journal of Surveying Engineering*, 130(1):29–35.

Featherstone, W. and Stewart, M. (2001). Combined Analysis of Real-Time Kinematic GPS Equipment and its Users for Height Determination. *Journal of Surveying Engineering*, 127(2):31–51.

Gao, Y. (2008). *Advanced Estimation Methods and Analysis, ENGO 629 Course Notes*. Department of Geomatics Engineering, University of Calgary, Canada.

Georgiadou, Y. and Doucet, K. (1990). Innovation: The Issue of Selective Availability. *GPS World*, 1(5):4–6.

Ghilani, C. and Wolf, P. (2006). *Adjustment Computations: Spatial Data Analysis, Fourth Edition*. John Wiley & Sons, Inc., Hoboken, N.J.

Han, S. and Rizos, C. (1995). Standardisation of the Variance-Covariance Matrix for GPS Rapid Static Positioning. *Geomatics Research Australasia*, (62):37–53.

Hofmann-Wellenhof, B., Lichtenegger, H., and Collins, J. (2001). *Global Positioning System : Theory and Practice, Fifth Edition*. Springer-Verlag, Wien ; New York.

Iliffe, J. and Lott, R. (2008). *Datums and Map Projections for Remote Sensing, GIS, and Surveying*. Whittles Pub. CRC Press, Scotland, UK Boca Raton, FL.

Iyiade, A. (2005). *Real Time Kinematic GPS in an Urban Canyon Environment*. [Online] Retrieved April 2010 from http://www.gisdevelopment.net/technology/gps/techgps_001.htm.

Jarroush, J., Adler, R., and Zeibak, M. (2005). *Cadastre Surveys with Real Time Kinematic GPS (RTK) as a Basis for Future Survey Regulations*. From Pharaohs to Geoinformatics, FIG Working Week 2005 and GSDI-8, Cairo, Egypt, April 16-21, 2005.

Kowoma (2009). *The GPS System: Transmitted GPS Signals*. [Online] Retreived May 20, 2010 from http://www.kowoma.de/en/gps/signals.htm. Last Updated April 19, 2009.

Kunches, J. (2007). GNSS and Space Weather: Making the Least Out of Solar Max. *InsideGNSS*, 2(8):30–36.

Lachapelle, G. (2008). *Advanced GNSS Theory and Applications, ENGO 625 Course Notes*. Department of Geomatics Engineering, University of Calgary, Canada.

Langley, R. (1998). RTK GPS. *GPS World*, 9(9):70–76.

Langley, R. (2000). GPS, the Ionosphere, and the Solar Maximum. *GPS World*, 11(7):44–49.

Lawrence, D., Langley, R., Kim, D., Chan, F., and Pervan, B. (2006). *Decorrelation of Troposphere Across Short Baselines*. Position, Location, And Navigation Symposium IEEE/ION 2006. 25-27 April, San Diego, CA. pp. 97-102.

Lee, I. and Ge, L. (2006). The Performance of RTK-GPS for Surveying under Challenging Environmental Conditions. *Earth, Planets, Space*, 58(5):515–522.

Leica Geosystems (2010). *Leica Instrument EDM Specifications*. [Online] Retrieved May 31, 2010 from http://www.docstoc.com/docs/35120618/LEICAInstrumentEDM-Specifications. Updated April 20, 2010.

Leick, A. (2004). *GPS Satellite Surveying*. John Wiley & Sons, Inc., Hoboken, NJ.

Lemmon, T. and Gerdan, G. (1999). The Influence of the Number of Satellites on the Accuracy of RTK GPS Positions. *The Australian Surveyor*, 44(1):64–70.

Mekik, C. (1997). *Troposphere Delay Models in GPS*. International Symposium on GIS/GPS, Istanbul, Turkey, September 15-18, 1997. pp. 156-170.

Mekik, C. and Arslanoglu, M. (2009). Investigation on accuracies of real time kinematic gps for gis applications. *Remote Sensing*, 1(1):22–35.

Misra, P. and Enge, P. (2001). *Global Positioning System: Signals, Measurements and Performance*. Ganga-Jamuna Press, Lincoln, MA.

Monteiro, L., Moore, T., and Hill, C. (2005). What is the Accuracy of DGPS? *The Journal of Navigation*, 58(2):207–225.

O'Keefe, K., Petovello, M., Lachapelle, G., and Cannon, M. (2006). Assessing Probability of Correct Ambiguity Resolution in the Presence of Time-Correlated Errors. *Journal of the Institute of Navigation*, 53(4):269–282.

Olynik, M. (2002). Temporal Characteristics of GPS Error Sources and Their Impact on Relative Positioning. Master's thesis, Department of Geomatics Engineering, University of Calgary, Calgary, Alberta, Canada. pp. 122.

Parkinson, B. and Spilker, J. (1996). *The Global Positioning System: Theory and Applications, Volume 1*. American Institute of Aeronautics and Astronautics, Inc., Washington, D.C.

Petovello, M., O'Keefe, K., Lachapelle, G., and Cannon, M. (2009). Consideration of Time-Correlated Errors in a Kalman Filter Applicable to GNSS. *Journal of Geodesy*, 83(1):51–56.

Pirti, A. (2007). Performance Analysis of the Real Time Kinematic GPS (RTK GPS) Technique in a Highway Project (Stake-Out). *Survey Review*, 39(303):43–53.

Pirti, A., Arslan, N., Deveci, B., Aydin, O., Erkaya, H., and Hosbas, R. (2009). Real-Time Kinematic GPS for Cadastral Surveying. *Survey Review*, 41(314):339–351.

Radovanovic, R. (2002). *Mitigation of GPS Code and Carrier Phase Multipath Effects using a Multi-Antenna System*. PhD thesis, Department of Geomatics Engineering, University of Calgary, Calgary, Alberta, Canada. pp. 260.

Ray, J. (2000). *Mitigation of GPS Code an Carrier Phase Multipath Effects using a Multi-Antenna System*. PhD thesis, Department of Geomatics Engineering, University of Calgary, Calgary, Alberta, Canada. pp. 260.

Raziq, N. and Collier, P. (2006). *High Precision GPS Deformation Monitoring using Single Receiver Carrier Phase Data*. Springer Berlin Heidelberg, Proceedings of the International Association of Geodesy Symposia 2006, Jaen, Spain. Volume 131:95-102.

Roberts, C. (2005). *GPS for Cadastral Surveying-Practical Considerations*. Proceedings of SSC Spatial Intelligence, Innovation and Praxis: The National Biennial Conference of the Spatial Sciences Institute, September 2005. Melbourne Australia.

Root Mean Square (2010). *Websters Online Dictionary*. [Online] Retrieved 7/25/2010 from http://www.websters dictionary-online.org/definitions/root+mean+square?cx=partnerpub093945 0753529744:v0qd01-tdlq&cof=FORID:9&ie=UTF8&q=root+mean+square&sa=Search#922.

Saghravani, S., Mustapha, S., Ibrahim, S., Yusoff, M., and Saghravani, S. (2009). *Performance of Real-Time Kinematic Global Positioning System and Automatic Level Surveying for Height Determination: A Comparison*. 2009 International Conference on Signal Acquisition and Processing, Malaysia, 2009. pp. 108-111.

Schofield, W. and Breach, M. (2007). *Engineering Surveying, Sixth Edition*. Butterworth-Heinemann.

Schon, S. and Brunner, F. (2006). *Modelling Physical Correlation of GPS Phase Observations: First Results*. Proceedings of 3rd Symp. Geodesy for Geotechnical and Structural Engineering/ 12th FIG Symp. Deform. Meas., Baden, Austria 2006.

Schon, S. and Brunner, F. (2008a). Atmospheric Turbulence Theory Applied to GPS Carrier-Phase Data. *Journal of Geodesy*, 82(1):47–57.

Schon, S. and Brunner, F. (2008b). A Proposal for Modelling Physical Correlations of GPS Phase Observations. *Journal of Geodesy*, 82(10):601–612.

Semmlow, J. (2005). *Circuits, Signals, and Systems for Bioengineers*. Elsevier Academic Press, Amsterdam.

Skone, S. and Shrestha, S. (2002). Limitations in DGPS Positioning Accuracies at Low Latitudes during Solar Maximum. *Geophysical Research Letters*, 29(10):pp. 81/1–4.

Teunissen, P. (1994). *A New Method for Fast Carrier Phase Ambiguity Resolution.* IEEE Position, Location, and Navigation Symposium PLANS'94, Las Vegas, NV, April 11-15, 1994. pp. 562-573.

Teunissen, P. and Kleusberg, A. (1998). *GPS for Geodesy, Chapter 8: GPS Carrier Phase Ambiguity Fixing Concepts*. Springer-Verlag Berlin and Heidelbery GmbH & Co. KG, Berlin.

Teunissen, P. and Verhagen, S. (2004). *On the Foundation of the Popular Ratio Test for GNSS Ambiguity Resolution*. ION GNSS 17th International Technical Meeting of the Satellite Division, Long Beach, CA, Sept. 21-24, 2004. pp. 2529-2540.

Teunissen, P. and Verhagen, S. (2009). The GNSS Ambiguity Ratio-Test Revisited: A Better Way of Using It. *Survey Review*, 41(312):138–151.

Trimble Navigation Limited (2001). *Trimble Survey Controller User Guide, Version 10.0, Revision A*. [Online] Retrieved October 1, 2009 from www.geoplane.com/./Survey/survey%20controller%20manual.pdf. pp. 478.

Trimble Navigation Limited (2009). *Trimble R8 GNSS Receiver Datasheet*. [Online] Retrieved 8/4/2010 from http://trl.trimble.com/dscgi/ds.py/Get/File140079/022543-079J_TrimbleR8GNSS_DS_1109_LR.pdf. Last updated 2009.

U.S. Naval Observatory (2010). *Current GPS Constellation*. [Online] Retrieved and last updated May 31, 2010 from http://tycho.usno.navy.mil/gpscurr.html.

Van Sickle, J. (2001). *GPS for Land Surveyors, Second Edition*. Ann Arbor Press, Chelsea, MI.

Wang, K., Li, Y., and and, Rizos, C. (2010). The Practical Approaches to kalman Filtering with Time-Correlated Measurement Errors. *Unpublished*, DOI 10.1.1.151.2550.

Wylde, G. and Featherstone, W. (1995). An Evaluation of some Stop-and-Go Kinematic GPS Survey Options. *The Australian Surveyor*, 40(3):205–212.

Yoshimura, T. and Hasegawa, H. (2003). Comparing the Precision and Accuracy of GPS Positioning in Forested Areas. *Journal of Forest Research*, 8(3):147–152.

Zhang, Z. (1997). Impact of rubidium clock aiding on gps augmented vehicular navigation. Master's thesis, Department of Geomatics Engineering, University of Calgary, Calgary, Alberta, Canada. pp. 135.

Appendix A

Photos of Occupied Pts

Figure A.1: Pt. 1, facing east.

Figure A.2: Pt. 2, facing northwest.

Figure A.3: Pt. 3, facing west.

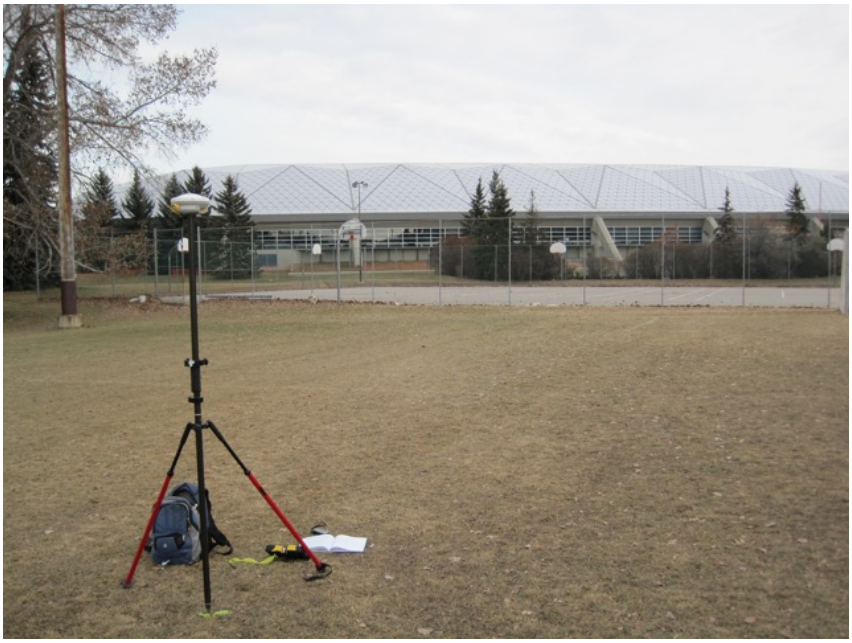

Figure A.4: Pt. 4, facing east.

Figure A.5: Pt. 5, facing west.

Figure A.6: Pt. 6, facing south.

Figure A.7: Pt. 7, facing north.

Figure A.8: Pt. 8, facing southeast.

Figure A.9: Pt. 9, facing north.

Figure A.10: Pt. 10, facing east.

Figure A.11: Pt. 11, facing west.

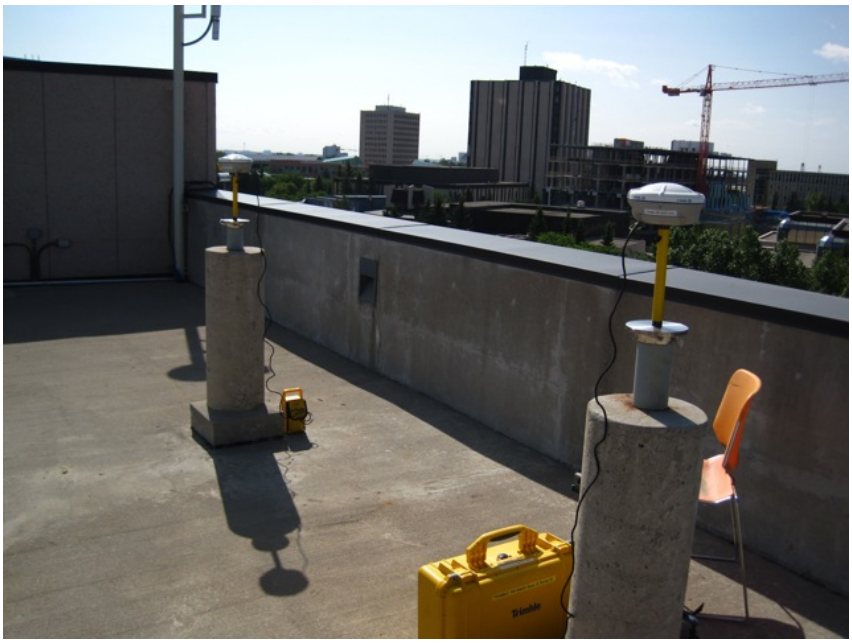

Figure A.12: Pt. 21, used as base station for short baseline, Job 2, facing southeast.

Figure A.13: Pt. 22, used as base station for 5 km baseline, Jobs 6 and 8.

Figure A.14: Pt. 23, used as base station for 5 km baseline, during Job 7, facing east.

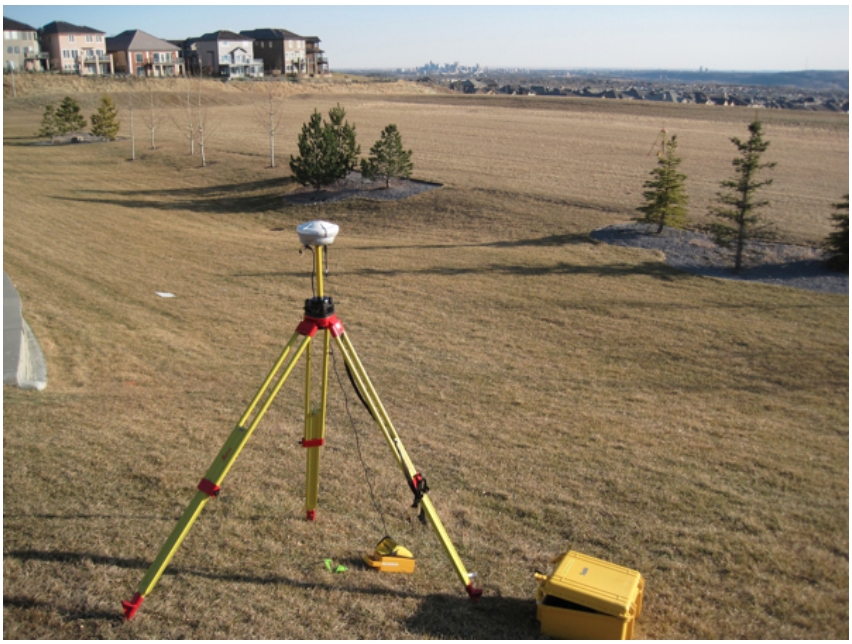

Figure A.15: Pt. 24, used as base station for 10 km baseline, Jobs 9 and 10, facing south-east.

Appendix B

Additional Tables

B.0.1 Localization Residuals and Estimated Parameters

Residuals from the 4 points used in the localization, resulting from the transformation from GPS coordinates in the ECEF coordinate system to the local coordinate system used in the survey network.

Table B.1: Job 1: Localization residuals (SF = scale factor).

Pt	Horizontal Residual	Vertical Residual
Pt. 1	0.005 m	-0.007 m
Pt. 2	0.004 m	0.008 m
Pt. 3	0.014 m	-0.008 m
Pt. 4	0.010 m	0.008 m
SF	-0.999987649	

Table B.2: Job 2: Localization residuals (SF = scale factor).

Pt	Horizontal Residual	Vertical Residual
Pt. 1	0.009 m	0.003 m
Pt. 2	0.004 m	-0.003 m
Pt. 3	0.006 m	0.003 m
Pt. 4	0.007 m	-0.003 m
SF	-0.99995576	

Table B.3: Job 3: Localization residuals (SF = scale factor).

Pt	Horizontal Residual	Vertical Residual
Pt. 1	0.011 m	-0.001 m
Pt. 2	0.007 m	0.001 m
Pt. 3	0.003 m	-0.001 m
Pt. 4	0.005 m	0.001 m
SF	-0.99999594	

Table B.4: Job 4: Localization residuals (SF = scale factor).

Pt	Horizontal Residual	Vertical Residual
Pt. 1	0.004 m	0.000 m
Pt. 2	0.006 m	0.000 m
Pt. 3	0.008 m	0.000 m
Pt. 4	0.003 m	0.000 m
SF	-0.999945685	

Table B.5: Job 5: Localization residuals (SF = scale factor).

Pt	Horizontal Residual	Vertical Residual
Pt. 1	0.009 m	-0.002 m
Pt. 2	0.005 m	0.002 m
Pt. 3	0.013 m	-0.002 m
Pt. 4	0.011 m	0.002 m
SF	-0.999915384	

Table B.6: Job 6: Localization residuals (SF = scale factor).

Pt	Horizontal Residual	Vertical Residual
Pt. 1	0.002 m	-0.002 m
Pt. 2	0.001 m	0.002 m
Pt. 3	0.005 m	-0.002 m
Pt. 4	0.004 m	0.002 m
SF	-0.999922907	

Table B.7: Job 7: Localization residuals (SF = scale factor).

Pt	Horizontal Residual	Vertical Residual
Pt. 1	0.005 m	0.000 m
Pt. 2	0.003 m	0.000 m
Pt. 3	0.008 m	0.000 m
Pt. 4	0.006 m	0.000 m
SF	-1.000042801	

Table B.8: Job 8: Localization residuals (SF = scale factor).

Pt	Horizontal Residual	Vertical Residual
Pt. 1	0.001 m	-0.003 m
Pt. 2	0.003 m	0.004 m
Pt. 3	0.008 m	-0.004 m
Pt. 4	0.006 m	0.004 m
SF	-0.99989908	

Table B.9: Job 9: Localization residuals (SF = scale factor).

Pt	Horizontal Residual	Vertical Residual
Pt. 1	0.004 m	0.000 m
Pt. 2	0.002 m	0.000 m
Pt. 3	0.005 m	0.000 m
Pt. 4	0.004 m	0.000 m
SF	-0.999953279	

Table B.10: Job 10: Localization residuals (SF = scale factor).

Pt	Horizontal Residual	Vertical Residual
Pt. 1	0.010 m	-0.004 m
Pt. 2	0.011 m	0.004 m
Pt. 3	0.007 m	-0.005 m
Pt. 4	0.003 m	0.004 m
SF	-1.00002972	

B.0.2 Network Adjustment Results Output from Microsurvey®

```
     **** MicroSurvey Least Square Adjustment Report ****

                ADJUSTMENT OPTION SUMMARY

Traverse Files Used          = TRAVERSE.TRV
Adjustment Mode              = Adjust Coordinates using LSA
Dimension of Adjustment      = 3D
Movement Allowance in 3D     = 3D
Linear Units                 = meters
Num. of Iterations           = 2
Convergence Limit            = 10 mm
Number of Total Observations = 69
Number of Unknowns           = 27

                ADJUSTMENT RESULT SUMMARY

Degrees of Freedom         = 42
Average angular  residual  = 5.1 seconds
Average zenith  residual   = 5.9 seconds
Average distance residual  = 0.002 meters
Confidence Level           = 95.0 Percent
Average network redundancy = 0.6

                DEFAULT INSTRUMENT STANDARD ERROR SETTINGS

Ang. & Dist. Instrument Used  = N/A (User Input for St. Dev's)
St. Dev for Angle             = 3.000 sec
St. Dev for Distance          = 2.000 mm
St. Dev for Zenith            = 3.000 sec


                ADJUSTMENT RESULTS (Adjusted Station Coordinates)

                                                  Station    Semi    Semi     Theta
 Station   Northing      Easting    Height Status     Major   Minor    (deg)

1    10000.000    10000.000 1100.000  Fixed     0.0000  0.0000      0.0
9     9912.311    10027.023 1097.697   3D       0.0051  0.0035    168.3
10     9887.551     9957.356 1097.999   3D       0.0075  0.0058     42.4
8     9985.990    10066.170 1099.486   3D       0.0052  0.0030     78.4
7    10056.402    10069.219 1100.321   3D       0.0050  0.0037     58.3
6    10015.624    10052.806 1099.336   3D       0.0045  0.0031     81.3
5    10040.847     9972.194 1099.835  Fixed     0.0000  0.0000      0.0
4     9951.102    10015.251 1098.987   3D       0.0033  0.0020    155.5
3    10089.909     9876.598 1100.623   3D       0.0073  0.0048    127.8
2     9917.514    10047.624 1098.499   3D       0.0056  0.0037    140.1
11     9960.366    10038.262 1098.288   3D       0.0034  0.0025    139.5

                INPUT & ADJUSTED OBSERVATIONS and RESIDUALS

  Type of     From  To   At   Input Obs.   Residual   Adj. Obs   Redund. Residual
Observation   Stn. Stn. Stn. ( dms / m )   (sec/mm)  (dms / m)   Number  Test(ABS)

Angle        10 1    50-46'03.0"      3      50-46'05.7"   0.2842     5.0
Angle         9 1    12-52'23.0"     -3      12-52'20.2"   0.5809     6.0
Angle         8 1   311-57'13.0"      3     311-57'15.6"   0.2592     5.0
Angle         7 1   260-49'19.0"     14     260-49'32.6"   0.5167     7.0 *
Angle         6 1   283-31'05.0"      1     283-31'05.7"   0.0656     3.0
Angle         5 1   175-45'12.0"      0     175-45'12.0"   0.0000     0.0
Angle         4 1    12-40'36.0"      4      12-40'39.8"   0.5504     7.0
Angle         3 1   156-04'21.0"     15     156-04'36.0"   0.7159     8.0 *
Angle       1 5 9   354-01'34.0"      1     354-01'34.9"   0.9476    10.0
Angle       1 4 9     0-14'47.0"     -2       0-14'45.0"   0.3582     5.0
Angle       1 2 9    92-57'22.0"     -1      92-57'21.2"   0.0157     0.0
Angle       1 10 9   267-33'44.0"     -2     267-33'42.1"   0.1130     2.0
Angle       1 7 8    80-31'32.0"     -4      80-31'28.5"   0.1894     3.0
Angle       1 6 8    53-46'16.0"      0      53-46'15.7"   0.0224     0.0
Angle       1 4 5     8-37'10.0"    -19       8-36'51.2"   0.8838     8.0 *
Angle       1 3 5   151-24'56.0"    -11     151-24'44.9"   0.4018     5.0 *
Angle       1 7 5   295-08'25.0"    -15     295-08'10.0"   0.5554     6.0 *
Angle       5 7 3   342-42'02.0"     -2     342-42'00.3"   0.7443     7.0
Angle       5 2 4   161-41'03.0"      3     161-41'06.3"   0.1512     4.0
Angle       4 11 1   333-20'03.0"     -9     333-19'54.1"   0.5907     7.0 *
Angle       1 2 11   211-40'00.0"     -2     211-39'57.9"   0.1027     2.0
Angle       1 4 11   292-03'44.0"     -1     292-03'42.6"   0.0361     1.0
Angle       1 8 11    91-26'04.0"     -4      91-26'00.3"   0.0725     2.0 *
Distance    1 10 1    120.285        -3      120.282      0.6428     7.0
Distance    1 9 1      91.788        -1       91.787      0.8274     8.0
Distance    1 8 1      67.638         3       67.641      0.8401     9.0
Distance    1 7 1      89.293        -5       89.288      0.8326     8.0
```

Distance	1 6 1	55.073	1	55.074	0.8646	9.0	
Distance	1 5 1	49.411	0	49.411	0.0000	0.0	
Distance	1 4 1	51.236	-2	51.234	0.9282	8.0	
Distance	1 3 1	152.681	2	152.683	0.6429	8.0	
Distance	9 5 9	139.753	-1	139.752	0.8301	8.0	
Distance	9 4 9	40.550	-1	40.549	0.8692	8.0	
Distance	9 2 9	21.249	4	21.253	0.8681	9.0	
Distance	9 10 9	73.939	-2	73.937	0.5995	7.0	
Distance	8 7 8	70.485	-5	70.480	0.8152	8.0	
Distance	8 6 8	32.507	4	32.511	0.8822	9.0	
Distance	5 4 5	99.544	1	99.545	0.9276	9.0	
Distance	5 3 5	107.452	1	107.453	0.6496	8.0	
Distance	5 7 5	98.270	-3	98.267	0.8430	8.0	
Distance	3 7 3	195.512	1	195.513	0.6250	8.0	
Distance	4 2 4	46.658	-2	46.656	0.8430	8.0	
Distance	1 11 1	55.116	-1	55.115	0.9220	8.0	
Distance	11 2 11	43.861	2	43.863	0.8360	9.0	
Distance	11 4 11	24.815	0	24.815	0.9674	10.0	
Distance	11 8 11	37.909	0	37.909	0.7915	9.0	
Zenith angle1	10 1	90∞59'50.0"	-4	90∞59'46.1"	0.6805	7.0	
Zenith angle1	9 1	91∞26'56.0"	-3	91∞26'53.3"	0.8528	8.0	
Zenith angle1	8 1	90∞34'48.0"	-4	90∞34'43.9"	0.7710	8.0	
Zenith angle1	7 1	89∞53'19.0"	-4	89∞53'14.9"	0.6965	7.0	
Zenith angle1	6 1	90∞47'36.0"	-12	90∞47'23.6"	0.5515	6.0 *	
Zenith angle1	5 1	90∞20'15.0"	0	90∞20'15.0"	0.0000	0.0	
Zenith angle1	4 1	91∞15'06.0"	4	91∞15'10.3"	0.6620	8.0	
Zenith angle1	3 1	89∞47'45.0"	-6	89∞47'39.5"	0.7215	7.0	
Zenith angle9	5 9	89∞15'24.0"	5	89∞15'29.3"	0.9365	9.0	
Zenith angle9	4 9	88∞38'28.0"	-6	88∞38'21.6"	0.5589	6.0	
Zenith angle9	2 9	88∞43'60.0"	-11	88∞43'48.9"	0.1607	3.0 *	
Zenith angle9	10 9	89∞47'01.0"	2	89∞47'02.9"	0.2571	5.0	
Zenith angle8	7 8	89∞33'21.0"	5	89∞33'26.1"	0.4899	7.0	
Zenith angle8	6 8	90∞46'15.0"	17	90∞46'32.2"	0.1922	4.0 *	
Zenith angle5	4 5	90∞38'42.0"	9	90∞38'50.7"	0.9104	9.0	
Zenith angle5	3 5	89∞43'35.0"	4	89∞43'38.9"	0.4377	6.0	
Zenith angle5	7 5	89∞28'09.0"	0	89∞28'09.4"	0.7494	8.0	
Zenith angle3	7 3	89∞55'56.0"	2	89∞55'58.4"	0.7881	9.0	
Zenith angle4	2 4	90∞56'47.0"	-2	90∞56'45.0"	0.6757	7.0	
Zenith angle1	11 1	91∞43'58.0"	14	91∞44'11.7"	0.7168	8.0 *	
Zenith angle11	2 11	90∞03'33.0"	-1	90∞03'32.3"	0.5786	6.0	
Zenith angle11	4 11	88∞25'07.0"	-1	88∞25'05.9"	0.2773	4.0	
Zenith angle11	8 11	88∞05'19.0"	14	88∞05'32.7"	0.3291	6.0 *	

B.0.3 Job Statistics

Performance According to Time

Figure B.1: Commercial RTK repeatability and true error statistics, from each of the 10 different Jobs. (EM = Early Morning, ~5am) (D = Daytime)

	Job	Time	Samples	Min (cm)	Max (cm)	Mean (cm)	σ (cm)	RMS (cm)
	1	D	39	0.0	1.3	-0.4	0.5	0.6
	2	D	60	0.0	0.9	-0.2	0.4	0.5
	3	EM	78	0.0	1.6	-0.2	0.6	0.7
	4	D	66	0.0	3.4	0.0	0.8	0.8
E	5	D	133	0.0	1.4	0.1	0.6	0.6
	6	D	78	0.0	4.5	-0.1	1.1	1.1
	7	EM	78	0.0	4.3	0.2	1.2	1.2
	8	D	78	0.0	1.7	0.1	0.9	0.9
	9	D	92	0.0	7.4	-0.1	1.2	1.2
	10	EM	95	0.0	3.0	0.1	1.0	1.0
	1	D	39	0.2	3.0	-1.6	1.0	1.8
	2	D	60	0.0	2.1	-0.3	0.7	0.7
	3	EM	78	0.0	2.3	0.0	0.8	0.8
	4	D	66	0.0	9.9	-0.9	1.7	1.9
N	5	D	133	0.0	2.1	-0.8	0.7	1.0
	6	D	78	0.0	3.4	-0.7	1.0	1.2
	7	EM	78	0.0	4.4	-0.4	1.2	1.3
	8	D	78	0.0	2.8	-0.3	1.0	1.0
	9	D	92	0.0	6.4	-0.3	1.7	1.7
	10	EM	95	0.0	4.1	-0.8	1.6	1.8
	1	D	39	0.0	4.0	0.7	1.6	1.8
	2	D	60	0.1	4.3	0.3	1.6	1.6
	3	EM	78	0.0	3.4	-0.3	1.5	1.5
	4	D	66	0.1	12.9	-1.2	2.6	2.8
U	5	D	133	0.0	5.5	-0.1	1.8	1.8
	6	D	78	0.0	12.8	-1.4	2.9	3.2
	7	EM	78	0.0	12.1	0.3	2.3	2.3
	8	D	78	0.0	4.4	0.4	1.3	1.4
	9	D	92	0.0	8.9	-0.7	2.7	2.8
	10	EM	95	0.0	7.5	0.4	2.5	2.5

Appendix C

Additional Plots

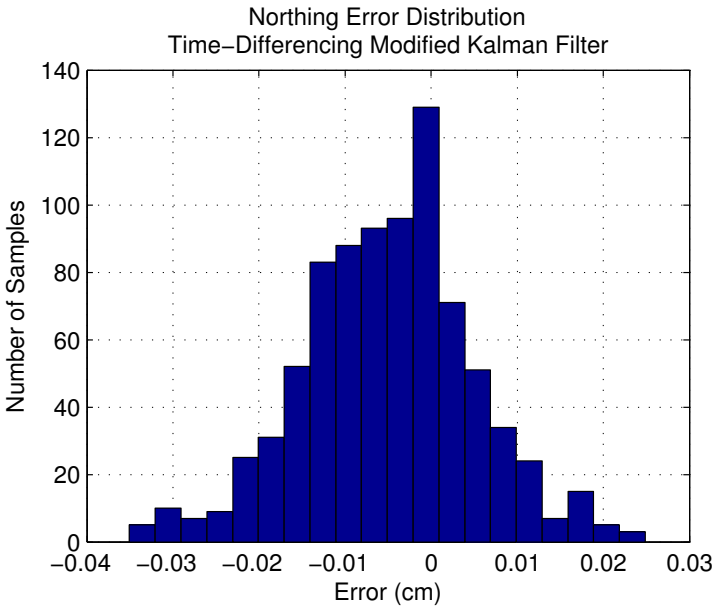

Figure C.1: North error distribution using the time-differencing modified Kalman filter.

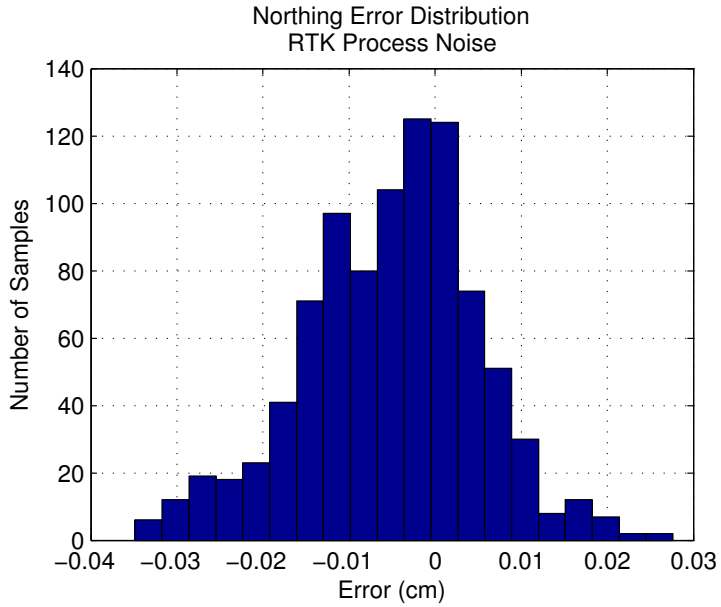

Figure C.2: North error distribution using the RTK processing style (Additional process noise).

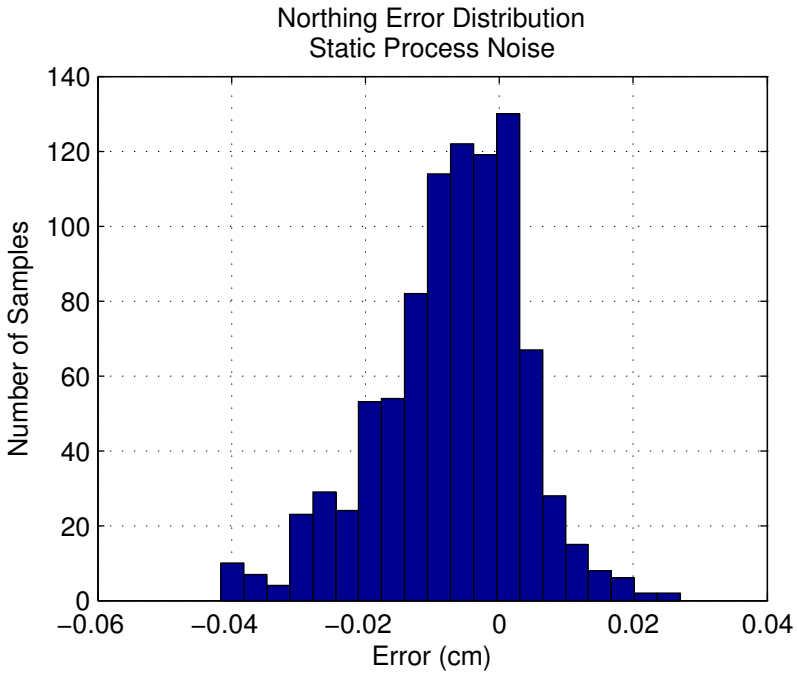

Figure C.3: North error distribution using the Static processing style (Minimal process noise).

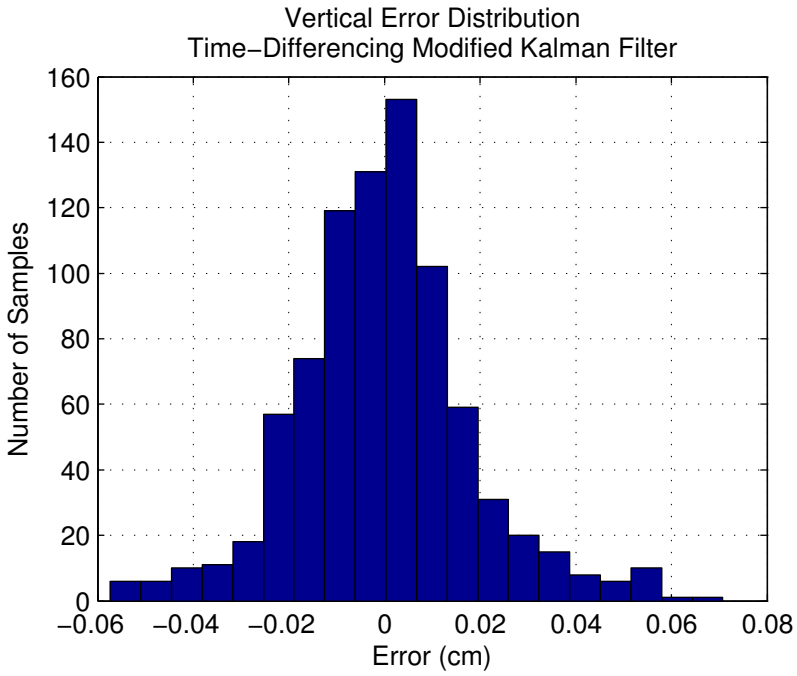

Figure C.4: Vertical error distribution using the time-differencing modified Kalman filter.

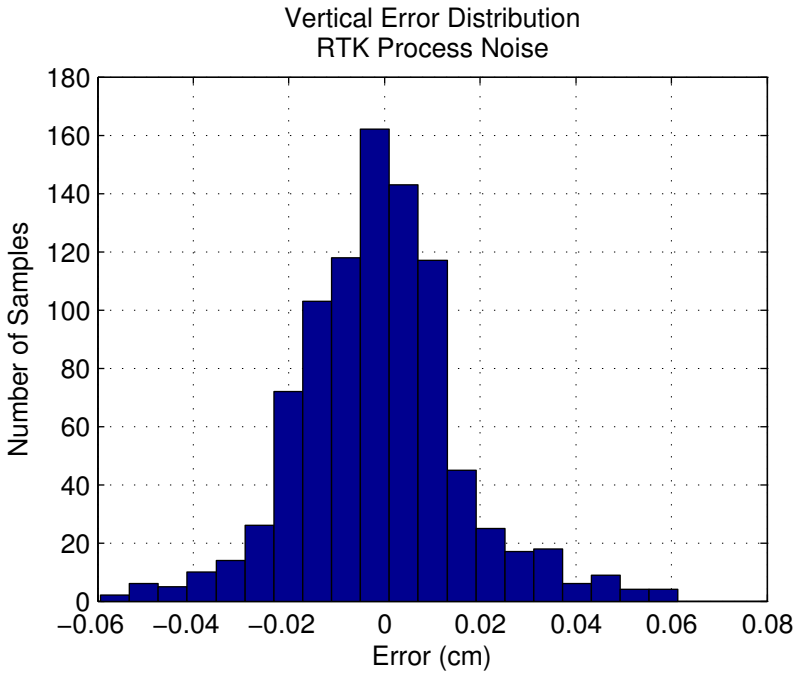

Figure C.5: Vertical error distribution using the RTK processing style (Additional process noise).

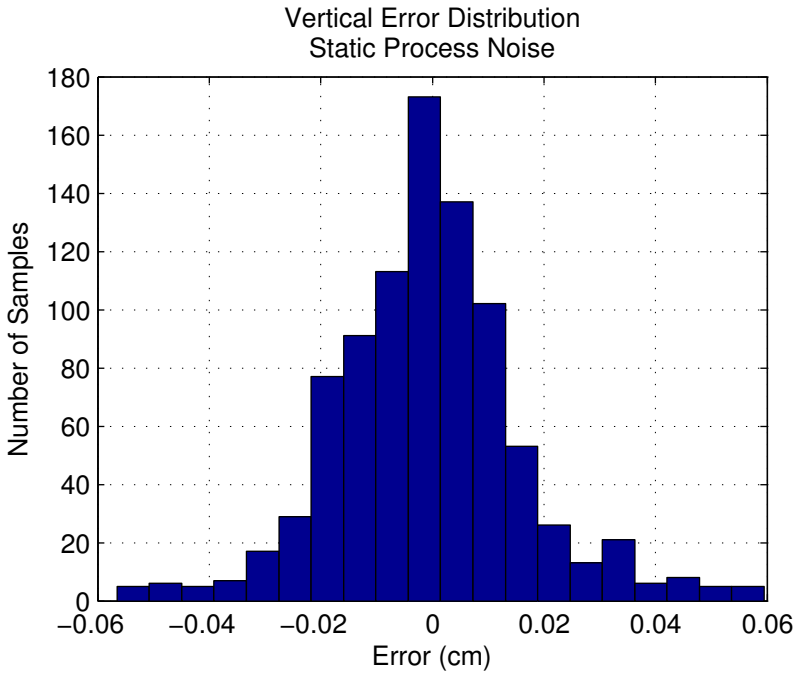

Figure C.6: Vertical error distribution using the Static processing style (Minimal process noise).

Appendix D

Additional Math

D.0.4 Seven Parameter Transformation

When GPS positions are first obtained, they are in an Earth-Centered, Earth-Fixed (ECEF) geodetic reference system, the World Geodetic System of 1984 (WGS 84). Surveyors often work within a local tangent plane coordinate system where the datum references a local point given arbitrary coordinates and the earth is assumed to be flat. In order to utilize GPS positions, the WGS 84 positions must be transformed into the local coordinate system. A 7 parameter transformation (3 translations, 3 rotations, 1 scale factor) is often used for this task and is described in in this Section. To perform a localization, GPS observations are made on 4 points with known local coordinates to determine their WGS 84 coordinates. With four points having both known WGS 84 and known local coordinate system coordinates, the 7 transformation parameters can be estimated, enabling other points to be surveyed and transformed into the local coordinate system in real-time. The issue is that if any of the four points used in the localization has bad local coordinates (often determined by traditional survey methods), or bad WGS 84 coordinates due to observed GPS

errors, the estimation of the transformation parameters will have large residuals and any RTK surveying performed using the localization will be affected. To mitigate issues with the localization, GPS observations of the selected localization points should be observed for as long as possible and should be free of potential multipath. For more on localization and the 7 parameter transformation, see Iliffe and Lott (2008) and Ghilani and Wolf (2006).

D.0.4.1 Mathematical Models

To rotate from one coordinate system to another, the following math models are used to rotate coordinates from the *uvw* coordinate system to the *XYZ* system: (Equations D.1 through D.3)

$$X = S(r_{11}u + r_{21}v + r_{31}w) + Tx \tag{D.1}$$
$$Y = S(r_{12}u + r_{22}v + r_{32}w) + Ty \tag{D.2}$$
$$Z = S(r_{13}u + r_{23}v + r_{33}w) + Tz \tag{D.3}$$

Within these math models, S is the scale factor, and Tx, Ty, and Tz are the translations in the X, Y, and Z directions. r_{11} through r_{33} are parameters of a rotation matrix, defined as follows.

$$\begin{aligned}
r_{11} &= cos\theta_2 \cdot cos\theta_3 \\
r_{12} &= sin\theta_1 \cdot sin\theta_2 \cdot cos\theta_3 + cos\theta_1 \cdot sin\theta_3 \\
r_{13} &= -cos\theta_1 \cdot sin\theta_2 \cdot cos\theta_3 + sin\theta_1 \cdot sin\theta_3 \\
r_{21} &= -cos\theta_2 \cdot sin\theta_3 \\
r_{22} &= -sin\theta_1 \cdot sin\theta_2 \cdot sin\theta_3 + cos\theta_1 \cdot cos\theta_3 \\
r_{23} &= cos\theta_1 \cdot sin\theta_2 \cdot sin\theta_3 + sin\theta_1 \cdot cos\theta_3 \\
r_{31} &= sin\theta_2 \\
r_{32} &= -sin\theta_1 \cdot cos\theta_2 \\
r_{33} &= cos\theta_1 \cdot cos\theta_2
\end{aligned}$$

Within these rotation parameters are 3 angles that must be estimated, θ_1, θ_2, and θ_3. These 7 parameters in total (S, Tx, Ty, Tz, θ_1, θ_2,θ_3) are estimated using iterative least squares. Iterative least squares, performed when the relationship between the states and the observations is not linear, requires initial values for each of the seven parameters.

Least squares is performed as follows (Equation D.4):

$$X = (A^T A)^{-1} A^T L \tag{D.4}$$

A is the design matrix relating the observations to the states. Each of the following derivatives are provided in Ghilani and Wolf (2006).

$$A = \begin{bmatrix} \left(\frac{\delta X}{\delta S}\right)_0 & 0 & \left(\frac{\delta X}{\delta \theta_2}\right)_0 & \left(\frac{\delta X}{\delta \theta_3}\right)_0 & 1 & 0 & 0 \\ \left(\frac{\delta Y}{\delta S}\right)_0 & \left(\frac{\delta Y}{\delta \theta_1}\right)_0 & \left(\frac{\delta Y}{\delta \theta_2}\right)_0 & \left(\frac{\delta Y}{\delta \theta_3}\right)_0 & 0 & 1 & 0 \\ \left(\frac{\delta Z}{\delta S}\right)_0 & \left(\frac{\delta Z}{\delta \theta_1}\right)_0 & \left(\frac{\delta Z}{\delta \theta_2}\right)_0 & \left(\frac{\delta Z}{\delta \theta_3}\right)_0 & 0 & 0 & 1 \end{bmatrix} \tag{D.5}$$

X is the calculated delta vector, which provides corrections to be applied to each of the initial values for the seven estimated parameters.

$$X = \begin{bmatrix} dS \\ d\theta_1 \\ d\theta_2 \\ d\theta_3 \\ dTx \\ dTy \\ dTz \end{bmatrix} \tag{D.6}$$

L is the vector containing the measurements. In this case of GPS localization, the coordinates of the four localization points (With coordinates known in both systems) will be applied to the above math models.

D.0.5 Error Ellipses

An error ellipse is a good way to gain an understanding regarding the accuracy of a position graphically. The error ellipse is calculated using the VCV matrix of the estimated states, P. An ellipse is produced using a semi-major and semi-minor axes, sa and sb, and a rotation angle a. An example of an ellipse in shown in Figure D.1

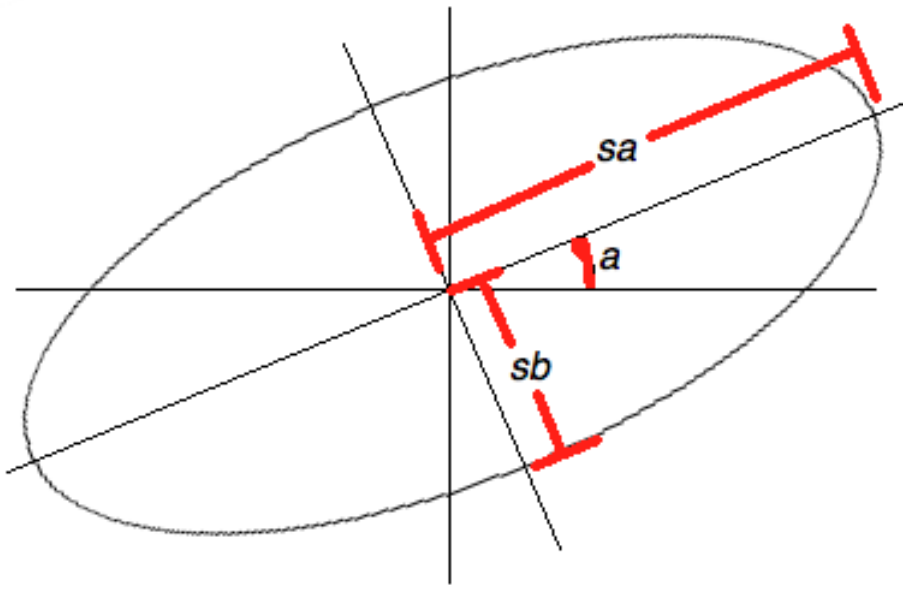

Figure D.1: Parameters used to define an error ellipse. sa = semi-major axis, sb = semi-minor axis, a = rotation angle of semi-major axis.

D.0.5.1 Rotating the VCV Matrix to the Local Coordinate System

Since GPS positions are obtained in the ECEF XYZ coordinate system, the VCV matrix, P, originally contains statistical information for that system. This would work fine if surveyors were interested in ECEF XYZ coordinates, but that is generally not the case. To understand the accuracy in a local coordinate system, the VCV must be rotated using the law of covariance propagation. Equation D.7 shows the contents of the VCV in the ECEF

XYZ coordinate system, which is rotated using Equation D.8 to the local ENU coordinate system.

$$P_{XYZ} = \begin{bmatrix} \sigma_X^2 & \sigma_{XY} & \sigma_{XZ} \\ \sigma_{XY} & \sigma_Y^2 & \sigma_{YZ} \\ \sigma_{XZ} & \sigma_{YZ} & \sigma_Z^2 \end{bmatrix} \tag{D.7}$$

$$P_{ENU} = R \cdot P_{XYZ} \cdot R^T = \begin{bmatrix} \sigma_E^2 & \sigma_{EN} & \sigma_{EU} \\ \sigma_{EN} & \sigma_N^2 & \sigma_{NU} \\ \sigma_{EU} & \sigma_{NU} & \sigma_U^2 \end{bmatrix} \tag{D.8}$$

In this case, the rotation matrix is calculated using the latitude, ϕ, and the longitude, λ, of the surveyed location.

$$R = \begin{bmatrix} -sin(\phi) & cos(\lambda) & 0 \\ -sin(\phi) \cdot cos(\lambda) & -sin(\phi) \cdot sin(\lambda) & cos(\phi) \\ cos(\phi) \cdot cos(\lambda) & cos(\phi) \cdot sin(\lambda) & sin(\phi) \end{bmatrix} \tag{D.9}$$

This process is also performed when rotating the cofactor matrix to the local coordinate system to calculate the HDOP and VDOP.

D.0.5.2 Ellipse Orientation

Using the information found in the rotated VCV matrix, the ellipse orientation can be calculated using Equation D.10.

$$tan2a = \frac{2\sigma_{EN}}{\sigma_N^2 - \sigma_E^2} + C \tag{D.10}$$

In the above equation, C is dependent upon the numerical signs of the numerator and denominator (Ghilani and Wolf, 2006). Solve for a to determine the rotation angle of the semi-major axis.

Quadrant	Numerator (+/-)	Denominator (+/-)	C
I	+	+	0^o
II	+	-	180^o
III	-	+	180^o
IV	-	-	360^o

Table D.1: Determination of C value. See Ghilani and Wolf (2006)

D.0.5.3 Ellipse Semi-major and Semi-minor Axis

The size of the error ellipse is dependent upon the semi-major and semi-minor axis, calculated in Equations D.11 and D.12 (Schofield and Breach, 2007).

$$\sigma_{sa}^2 = \frac{1}{2}\left[\sigma_N^2 + \sigma_E^2 + \left\{\left(\sigma_N^2 - \sigma_E^2\right)^2 + 4\sigma_{EN}^2\right\}^{\frac{1}{2}}\right] \tag{D.11}$$

$$\sigma_{sb}^2 = \frac{1}{2}\left[\sigma_N^2 + \sigma_E^2 - \left\{\left(\sigma_N^2 - \sigma_E^2\right)^2 + 4\sigma_{EN}^2\right\}^{\frac{1}{2}}\right] \tag{D.12}$$

For more on the calculation of error ellipses, see Ghilani and Wolf (2006); Schofield and Breach (2007).

D.0.6 Equations from El-Rabbany (1994)

The following equations are from El-Rabbany (1994), referenced throughout this research. A fully populated VCV matrix is formed to account for the temporal correlations within the observations. For more, see El-Rabbany (1994); El-Rabbany and Kleusberg (2003, 2004).

Equation D.13: Double differencing: In order to perform double differencing, an operator must be applied to the observations to do the differencing.

$$DD = f(\Phi) \tag{D.13}$$

Equation D.14: Mathematical correlation: By applying a double difference operator to the GPS observations, the observations become mathematically correlated which must be taken into account in the VCV matrix of the observations.

$$M = C_{DD} = \left(\frac{\delta f}{\delta \Phi}\right) C_{\Phi} \left(\frac{\delta f}{\delta \Phi}\right)^{T} \tag{D.14}$$

Equation D.15: Exponential equation for determining the correlation coefficient. Accepted for use by most reviewed literature. El-Rabbany (1994), using autocorrelation data from 47 baselines, found the exponential function to be the closest fitting function. T is the correlation time, and τ is the lag, essentially the data rate.

$$f = e^{-|\tau|/T} \tag{D.15}$$

Equation D.16: The VCV matrix of the observations. M is the mathematical correlation matrix determined by Equation D.14 and f is the correlation coefficient determined by Equation D.15. Each new epoch results in an additional row and column.

$$C_l = \begin{bmatrix} M & fM & f^2M & f^3M & \dots & f^{n-1}M \\ fM & M & fM & f^2M & \dots & f^{n-2}M \\ f^2M & fM & M & fM & \dots & f^{n-3}M \\ f^3M & f^2M & fM & M & \dots & f^{n-4}M \\ \dots & \dots & \dots & \dots & \dots & \dots \\ f^{n-1}M & f^{n-2}M & f^{n-3}M & f^{n-4}M & \dots & M \end{bmatrix} \tag{D.16}$$

Equation D.17: In order to simplify the inverse of such a large VCV matrix, a variable P is created using the mathematical correlation, M, and the correlation coefficient, f.

$$P = \frac{1}{1-f^2} M^{-1} \tag{D.17}$$

Equation D.18: The inverse of the VCV Matrix of the observations. A block diagonal matrix where P is from Equation D.17 and f is from Equation D.15.

$$C_l^{-1} = \begin{bmatrix} P & -fP & 0 & ... & 0 & 0 \\ -fP & (1+f^2)P & -fP & ... & 0 & 0 \\ 0 & -fP & (1+f^2)P & ... & 0 & 0 \\ ... & ... & ... & ... & ... & ... \\ 0 & 0 & 0 & ... & (1+f^2)P & -fP \\ 0 & 0 & 0 & ... & -fP & P \end{bmatrix} \tag{D.18}$$

Equation D.19: With a change in the number of satellites, Equation D.18 is modified to accommodate the change with the introduction of Q.

$$C_l^{-1} = \begin{bmatrix} P & -fP & ... & 0 & 0 & 0 \\ -fP & (1+f^2)P & ... & 0 & 0 & 0 \\ ... & ... & ... & ... & ... & ... \\ 0 & 0 & ... & (1+f^2)P & -fP & 0 \\ 0 & 0 & ... & -fP & Q_{11} & Q_{21}^T \\ 0 & 0 & ... & 0 & Q_{21} & Q_{22} \end{bmatrix} \tag{D.19}$$

Equations D.20: Used in the inverse of the VCV matrix of the observations when there is a change in the number of satellites visible to the receiver.

$$Q_{11} = P - fM^{-1}M_{n+1,n}^T Q_{21} \tag{D.20}$$

$$Q_{21} = fQ_{22}M_{n+1,n}M^{-1} \tag{D.21}$$

$$Q_{22} = M_{n+1,n+1} - f^2 M_{n+1,n}M^{-1}M_{n+1,n}^T \tag{D.22}$$

Equation D.23: Solving for Delta: To accommodate the large VCV matrix, the sequential solution for delta must be modified.

$$\hat{\delta}_i = \hat{\delta}_{i-1} + N_{i-1}^{-1}A_i^{*T}[P_{i,i}^{-1} + A_i^* N_{i-1}^{-1}A_i^{*T}]^{-1}[W_i^* - A_i^*\hat{\delta}_{i-1}] \tag{D.23}$$

Equation D.24: The normal equation matrix. From this, the accuracy is obtained, which theoretically should be larger than it otherwise would be without the temporal correlation accounted for.

$$N_i^{-1} = N_{i-1}^{-1} - N_{i-1}^{-1} A_i^{*T} [P_{i,i}^{-1} + A_i^* N_{i-1}^{-1} A_i^{*T}]^{-1} A_i^* N_{i-1}^{-1} \tag{D.24}$$

Equation D.25: The design matrix:

$$A_i^* = A_i - C_{i,i-1} C_{i-1,i-1}^{-1} A_{i-1} \tag{D.25}$$

Equation D.26: The measurement vector:

$$W_i^* = W_i - C_{i,i-1} C_{i-1,i-1}^{-1} W_{i-1} \tag{D.26}$$